

การตรวจวัดการเปลี่ยนแปลงตามระดับความเครียดของโมดูลัสเฉือนของดินอ่อน
โดยใช้เบนเดอริอิลิเมนต์



นาย กฤษอย ชาน

สถาบันวิทยบริการ

วิทยานิพนธ์นี้เป็นส่วนหนึ่งของการศึกษาตามหลักสูตรปริญญาวิศวกรรมศาสตรดุษฎีบัณฑิต

สาขาวิชาวิศวกรรมโยธา ภาควิชาวิศวกรรมโยธา

คณะวิศวกรรมศาสตร์ จุฬาลงกรณ์มหาวิทยาลัย

ปีการศึกษา 2550

ลิขสิทธิ์ของจุฬาลงกรณ์มหาวิทยาลัย

DETERMINATION OF STRAIN DEPENDENCY OF SHEAR MODULUS
OF SOFT CLAYS USING BENDER ELEMENT



Mr. Kok-Hooi Chan

สถาบันวิทยบริการ
จุฬาลงกรณ์มหาวิทยาลัย

A Dissertation Submitted in Partial Fulfillment of the Requirements
for the Degree of Doctor of Philosophy Program in Civil Engineering

Department of Civil Engineering

Faculty of Engineering

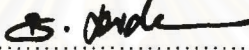
Chulalongkorn University

Academic year 2007

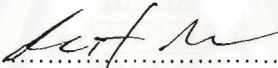
Copyright of Chulalongkorn University


Thesis Title	DETERMINATION OF STRAIN DEPENDENCY OF SHEAR MODULUS OF SOFT CLAYS USING BENDER ELEMENT
By	Mr. Kok-Hooi Chan
Field of Study	Civil Engineering
Thesis Advisor	Associate Professor Tirawat Boonyatee, D. Eng.
Thesis Co-advisor	Professor Toshiyuki Mitachi, D. Eng.


Accepted by the Faculty of Engineering, Chulalongkorn University in Partial
Fulfillment of the Requirements for the Doctoral Degree

 Dean of the Faculty of Engineering
(Associate Professor Boonsom Lerdkhironwong, Dr. Ing.)


THESIS COMMITTEE

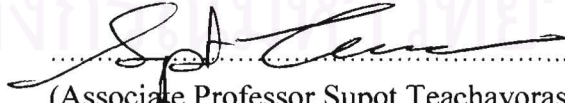
 Chairman
(Assistant Professor Thavee Thanacharoengit, Dr. Ing.)

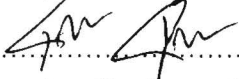
 Thesis Advisor
(Associate Professor Tirawat Boonyatee, D. Eng.)

 Thesis Co-advisor
(Professor Toshiyuki Mitachi, D. Eng.)

 External Member
(Tian Ho Seah, Sc. D.)

 Member
(Associate Professor Boonsom Lerdkhironwong, Dr. Ing.)

 Member
(Associate Professor Supot Teachavorasinskun, D. Eng.)

 Member
(Associate Professor Boonchai Ukritchon, Sc. D.)

ก๊กชอย ชาน : การตรวจวัดการเปลี่ยนแปลงตามระดับความเครียดของโมดูลัสเฉือนของดินอ่อนโดยใช้เบนเคอร์อิลิเมนต์ (DETERMINATION OF STRAIN DEPENDENCY OF SHEAR MODULUS OF SOFT CLAYS USING BENDER ELEMENT) อ. ที่ปรึกษา : รศ.ดร. จูริวัตร บุญญะรัฐ, อ.ที่ปรึกษาร่วม : PROF. TOSHIYUKI MITACHI, 149 หน้า

เนื่องจากความสัมพันธ์ระหว่างแรงกระทำและการเสียรูปของดินแตกต่างจากความสัมพันธ์เชิงเส้นเป็นอย่างมาก ความรู้ความเข้าใจเรื่องพฤติกรรมการรับแรงของดินจึงเป็นสิ่งจำเป็นสำหรับการออกแบบทางวิศวกรรม งานวิจัยนี้มุ่งศึกษาพฤติกรรมการเปลี่ยนแปลงโมดูลัสเฉือนของดินที่ผันแปรตามระดับความเครียดที่เกิดขึ้นเนื่องจากแรงกระทำภายนอก การศึกษากระทำโดยใช้เครื่องทดสอบแรงอัดสามแกนและเครื่องทดสอบอัดตัวคาน้ำที่มีติดตั้งเบนเคอร์อิลิเมนต์เพื่อใช้ในการวัดความเร็วคลื่นเฉือนที่เดินทางผ่านตัวอย่างดิน ทั้งนี้ตัวอย่างดินที่ใช้ในการศึกษาประกอบด้วยตัวอย่างดินเหนียวสร้างใหม่และตัวอย่างดินเหนียวสภาพรบกวนต่ำ

จากการศึกษาพบว่าค่าโมดูลัสเฉือนที่วัดได้จากการทดสอบด้วยเบนเคอร์อิลิเมนต์มีการเปลี่ยนแปลงตามระดับความเครียดและ ได้เสนอสมการความสัมพันธ์ระหว่างค่าโมดูลัสที่วัดได้จากการทดสอบด้วยเบนเคอร์อิลิเมนต์กับค่าโมดูลัสที่วัดได้จากการทดสอบด้วยเครื่องทดสอบแรงอัดสามแกน กระบวนการวัดแบบใหม่สองชนิดได้ถูกพัฒนาขึ้นในการศึกษานี้ซึ่งได้แก่ เทคนิคการวัดความเร็วเฟสของคลื่นแรงเฉือน และการใช้สัญญาณคลื่นเชิงรีปเพื่อเพิ่มความแม่นยำในการวัดความเร็วกลุ่มของคลื่นแรงเฉือน เทคนิคที่ได้พัฒนาขึ้นใหม่ทำให้สามารถวัดได้ทั้งความเร็วเฟสและความเร็วกลุ่มของคลื่นเฉือนในดิน การใช้สัญญาณคลื่นเชิงรีปยังทำให้สามารถวัดผลตอบสนองเชิงความถี่ของตัวอย่างดินได้ โดยพิสูจน์ความถูกต้องได้จากความสอดคล้องกันระหว่างสัญญาณที่สังเคราะห์ขึ้นจากผลตอบสนองดังกล่าวกับสัญญาณคลื่นที่วัดได้จริง จากการศึกษาพบว่าความเครียดที่เกิดขึ้นในการทดสอบด้วยเบนเคอร์อิลิเมนต์มีค่าประมาณ 10^{-4} % และการติดตั้งอุปกรณ์เข้ากับตัวอย่างดินไม่ได้ส่งผลกระทบต่ออย่างมีนัยสำคัญต่อผลการวัดค่าโมดูลัสเฉือนของตัวอย่างดิน

ภาควิชา วิศวกรรมโยธา ลายมือชื่อนิสิต *C. Keey*
 สาขาวิชา วิศวกรรมโยธา ลายมือชื่ออาจารย์ที่ปรึกษา *T. P.*
 ปีการศึกษา 2550 ลายมือชื่ออาจารย์ที่ปรึกษาร่วม *Mitachi*

4871832321: MAJOR CIVIL ENGINEERING

KEYWORDS: BENDER ELEMENT / CLAY / LABORATORY TESTS / SHEAR MODULUS / SHEAR WAVE VELOCITY

KOK-HOOI CHAN: DETERMINATION OF STRAIN DEPENDENCY OF SHEAR MODULUS OF SOFT CLAYS USING BENDER ELEMENT. THESIS ADVISOR: ASSOC. PROF. TIRAWAT BOONYATEE, D. Eng. THESIS CO-ADVISOR: PROF. TOSHIYUKI MITACHI, D. Eng. 149 pp.

The relationship between modulus and strain of soil is extremely non-linear so the profound knowledge of this relationship is essential for standard design of construction. In this research, to elucidate this relationship, a series of laboratory tests is performed to determine the shear modulus degradation curve for reconstituted and undisturbed clay samples by using the bender elements tests. The tests are performed by using a modified triaxial apparatus and a consolidometer each of which is equipped with a pair of bender elements. The research results show that shear modulus determined from the bender elements test has relationships with shear strain and shear modulus calculated from a conventional triaxial test. The relationships are proposed. Besides, the shape of the normalised shear modulus degradation curve determined by bender elements test is not affected by the plasticity index. This research yields two novel findings. Firstly the variable-path length and continuous wave method is used to determine phase velocity of shear wave. The proposed method combined with the conventional time domain method gives the explicit picture of the relationship between phase and group velocities. The other finding is swept wave and cross-correlation technique can be used to compute the travel time based on time domain method. By also using swept signal, frequency response of soil sample can be computed and frequency response determined is used to regenerate received signal. The study also reveals that the installation of bender elements into the clay sample generates almost no disturbance and the magnitude of shear strain generated from bender elements tests is $10^{-4}\%$.

Department	Civil Engineering.....	Student's signature	<i>L. Hui</i>
Field of study	Civil Engineering.....	Advisor's signature	<i>T. Boonyatee</i>
Academic year	2007.....	Co-advisor's signature	<i>T. Mitachi</i>

ACKNOWLEDGEMENTS

I would like to express my deep gratitude to my advisor, Associate Professor Tirawat Boonyatee, and co-advisor, Professor Toshiyuki Mitachi, for their extensive and valuable advice, generosity of their time and support during my doctoral program at Chulalongkorn University and Hokkaido University.

I am deeply indebted to ASEAN University Network / Southeast Asia Engineering Education Development Network (AUN/SEED-Net JICA) for granting the scholarship of my doctoral study and the 90th Years Anniversary of Chulalongkorn University (Ratchadphiseksomphot Endowment Fund) for awarding a research fund for my research study.

Many thanks also go to several people: the geotechnical research group at Chulalongkorn University, soil mechanic research group at Hokkaido University and the Center of Excellence in Earthquake Engineering and Vibration research group for their helpful assistance and suggestion. To Bouygues-Thai Co., Ltd. for all possible assistance provided at the excavation construction site. To Dr. Toshihiro Oginno for performing a collaborative research study. To Dr. Tamrakar for his useful advice and suggestion about embankment construction. To Dr. Sangrawee for her editorial contribution to my publications and thesis.

I would like to thank my friends, to name a few, Mr. Tatwachai, Mr. Wasin, Ms. Pamila and many more who provide me with guidance and care during my stay at Chulalongkorn University. Please accept my sincere gratitude.

Last but not least, special thanks are due to my wife and family. Without their continuous support, encouragement and love, I could not have successfully gone through all the difficulty I faced.

TABLE OF CONTENTS

		Page
Abstract (in Thai)		iv
Abstract (in English)		v
Acknowledgements		vi
Table of contents		vii
List of tables		xi
List of figures		xii
List of abbreviations		xviii
Chapter I	Introduction	1
	1.1 General	1
	1.2 Objectives	2
	1.3 Organisation of thesis	2
Chapter II	Literature review	4
	2.1 Background	4
	2.2 Techniques to determine shear modulus in the field	4
	2.2.1 Down-hole test	4
	2.2.2 Cross-hole test	6
	2.2.3 Seismic cone penetration test	7
	2.3 Techniques to determine shear modulus in the laboratory	8
	2.3.1 Bender elements test (BEs test)	8
	2.3.2 Cyclic triaxial test	11
	2.3.3 Resonant column test	12
	2.3.4 Torsional shear test	12
	2.3.5 Conventional triaxial testing	14
	2.3.6 Local axial displacement gauge	15
	2.4 Factor affecting the normalised shear modulus degradation curve of cohesive soil	16

Chapter III	Determination of phase velocity of shear wave	17
3.1	Overview	17
3.2	Testing equipment	17
3.2.1	Preparation of BEs	17
3.2.2	Modification of triaxial apparatus and equipment used for BEs test	20
3.3	Properties of reconstituted and undisturbed samples	24
3.4	The method of variable-path length by using continuous sinusoidal wave	26
3.4.1	Background	26
3.4.2	Variable-path length method	27
3.4.3	Methodology	29
3.4.4	Analyses and discussion	31
3.4.5	Summary	34
3.5	The effects of the BE installation on shear wave velocity measurement	34
3.5.1	Background	34
3.5.2	Methodology	34
3.5.3	Study of the disturbance	37
3.5.3.1	Penetration test	37
3.5.3.2	Parametric study: Penetration rate	37
3.5.3.3	Parametric study: Sample size ...	38
3.5.3.4	Parametric study: Isotropic consolidation pressure	38
3.5.4	Summary	38
3.6	The magnitude of shear strain generated by the BEs test	41
3.6.1	Background	41
3.6.2	Concept of shear strain calculation	41
3.6.3	Calibration of BEs displacement	42
3.6.4	Methodology	46

	3.6.5	Calculation of shear wave velocity	46
	3.6.6	Calculation of particle velocity	47
	3.6.7	Calculation of shear strain	49
	3.6.8	Summary	51
Chapter IV		Shear wave velocity determination based on time domain method	52
	4.1	Shear wave velocity determination based on swept signal	52
	4.1.1	Background	52
	4.1.2	Swept signal theory	54
	4.1.3	Methodology	56
	4.1.4	Analyses and discussion	57
	4.1.5	Summary	59
	4.2	Regeneration of received signal based on the BEs test by using the swept signal	60
	4.2.1	Background	60
	4.2.2	System of the BEs test	60
	4.2.3	Identification of frequency response function	61
	4.2.4	Methodology and soil properties	63
	4.2.5	Input/output characteristics of the testing system	64
	4.2.6	Frequency response and impulse response obtained from the swept signal	66
	4.2.7	Comparison between regenerated and observed received signals	70
	4.2.8	Shear wave velocity obtained from calculated wave	74
	4.2.9	Summary	75
Chapter V		Strain dependency of shear modulus	76
	5.1	Background	76
	5.2	Testing equipment and soil properties	77

5.3	Determination of soil parameters from triaxial testing	79
5.3.1	The undrained Poisson's ratio	79
5.3.2	Determination of G	81
5.3.3	Determination of γ	82
5.4	Methodology	83
5.4.1	Consistency of proposed methodology	87
5.4.2	The effects of the proposed methodology on the critical stress path	87
5.5	G_{bender} degradation curve	90
5.6	G degradation curve	97
5.7	Relationship between G determined from the BEs test, G_{bender} , and G determined from conventional triaxial test	102
5.8	Summary	110
Chapter VI	Conclusions	111
References	115
Appendices	122
Appendix A	Bender element preparation	123
Appendix B	Testing equipment	126
Appendix C	Consolidation and swelling tests results ...	129
Appendix D	Stress path and stress strain curves	142
Biography	149

LIST OF TABLES

Tables	Page
3.1 Properties of reconstituted samples	25
3.2 Properties of undisturbed samples	25
3.3 Results from time domain and variable-path length methods	32
3.4 Test conditions	36
3.5 The gradient of slope calculated from linear line fitting of BEs displacement calibration process	43
4.1 Description of tested soils	56
4.2 Testing apparatuses, samples and test conditions	64
5.1 Description of soil samples and testing conditions	78
5.2 Condition of the axial monotonic loading test with the BEs test	86



 สถาบันวิทยบริการ
 จุฬาลงกรณ์มหาวิทยาลัย

LIST OF FIGURES

Figures	Page
2.1 Application of down-hole test	6
2.2 Application of cross-hole test	7
2.3 Seismic cone penetration apparatus (after Tanaka <i>et al.</i> , 1994)	7
2.4 Application of seismic cone penetration test	8
2.5 Generation of shear wave by using bender element	9
2.6 BEs installed in the soil testing apparatus (after Dyvik and Madshus, 1985)	10
2.7 Typical transmitted and received signals for single sine signal from the BEs test	10
2.8 Improved cyclic triaxial test apparatus with inner load cell and high sensitivity proximity sensors (after Kokusho, 2004)	11
2.9 Two types of torsional vibration method for resonant column test (a) base stimulation, (b) top stimulation	13
2.10 Angular strain distributions (a) cylindrical sample, (b) hollow cylindrical sample	13
2.11 Hollow cylindrical torsional test apparatus (soil mechanic laboratory, Hokkaido University)	14
2.12 Local deformation transducer (LDT) (after Tatsuoka <i>et al.</i> , 1993) ...	15
2.13 Normalised shear modulus degradation curves for normally and overconsolidated soils with the effect of plasticity index (after Vucetic and Dobry, 1991)	16
3.1 A BE (a) schematic position of material, (b) parallel type, (c) series type	18
3.2 The connection of a parallel type BE with its electrode shallow cut at both sides and wired to operate as a self-monitoring circuit	19
3.3 Schematic view of an arrangement for the BEs test using triaxial apparatus	21
3.4 System of triaxial apparatus completed with BEs test	22
3.5 Attachment of the receiver BE to the penetration rod	23
3.6 Modification of the gap between receiver BE and bottom cap	23

Figures	Page
3.7 The slurry is preconsolidated under vertical pressure in preconsolidation cell	26
3.8 Explanation of wave propagation theory by using continuous sinusoidal wave (a) wave generated at transmitter and captured by a receiver at different positions, (b) signals motion with time for transmitted and received signals	30
3.9 Testing procedure for variable-path length method	31
3.10 Recorded signals of transmitted and received at different positions for 7 kHz of frequency	32
3.11 Variation of the time lag with positions of receiver determined by variable-path length method	33
3.12 Variation of V_s with positions of receiver determined by time domain method	33
3.13 Installation of BEs (a) installation of transmitter and receiver BEs at both ends of the sample, (b) penetration of receiver BE into the sample to study the disturbance effects	35
3.14 Variation of V_s with penetration positions (a) varying the penetration rate, (b) varying the sample size, (c) varying the consolidation pressure	39
3.15 Transmitted and received signals for sample 4 (a) transmitted signal, (b) received signals at different positions	40
3.16 Movement of soil continuum forced by vibration energy (a) one element, (b) continuum elements	42
3.17 Measurement method to determine the displacement of BEs by using a laser displacement gauge (a) transmitter, (b) receiver	44
3.18 Plot of laser beam displacement measurement versus BE self-monitoring voltage (a) transmitter, (b) receiver	45
3.19 Variation of V_s versus input voltage (a) 100 kPa of isotropic consolidation pressure, (b) 300 kPa of isotropic consolidation pressure	47

Figures	Page
3.20 Derivation of $V_{particle}$ from transmitted self-monitoring signal for ± 50 V input voltage and 5 kHz of frequency at 100 kPa of isotropic consolidation pressure	48
3.21 Variation of γ versus input voltage (a) 100 kPa of isotropic consolidation pressure, (b) 300 kPa of isotropic consolidation pressure	50
4.1 Typical transmitted and received signals for (a) single sine wave, (b) step wave	53
4.2 Typical transmitted and received signals for a swept wave	55
4.3 Cross-correlation between transmitted and received signals for a swept wave ($f_o = 500$ Hz, $\Delta f = 1.5$ kHz and $t_{target} = 10$ ms) and single sine wave ($f = 2$ kHz)	55
4.4 Typical cross-correlation signals from the transmitted and received swept wave shown in Figure 4.2	57
4.5 Variation of shear wave velocity with bandwidth for the swept wave at different initial frequency (a) sample 1, (b) sample 2, (c) sample 3	58
4.6 Variation of shear wave velocity with frequency for the single sine wave and step wave calculated based on different travel time (a) sample 1, (b) sample 2, (c) sample 3	59
4.7 TSP and LSSP in time and frequency domain (TSP: $m_f = 150$, $N = 2048$; LSSP: $f_o = 0.5$ kHz, $\Delta f = 10$ kHz and $t_{target} = 10$ ms)	63
4.8 Amplitude spectra of TSP and LSSP given by self-monitoring signals	65
4.9 Coherence for four times swept signal inputs	66
4.10 Coherence for various signal inputs	67
4.11 Typical transmitted and received signals for TSP and LSSP	67
4.12 Typical frequency responses restored by (a) TSP, (b) LSSP	68
4.13 Relationship of resonant frequency versus consolidation pressure	69
4.14 Comparison between (a) impulse response, (b) received signal for step wave input	70

Figures	Page
4.15 Comparison between observed and calculated received waves for various frequencies of single sine wave inputs (Kasaoka clay, triaxial apparatus, consolidation stress: 100kPa, initial height: 100mm)	72
4.16 Comparison of arrival times at characteristic points (a) Akita peat, (b) NSF clay	73
4.17 Comparison of shear wave velocities between observed and calculated waves	74
5.1 Shear modulus degradation curve for soil (after Atkinson and Sallfors, 1991)	76
5.2 Cylinder sample in orthogonal space	80
5.3 Definition of Young's and shear moduli	82
5.4 Flowchart of the axial monotonic loading test with the BEs test	85
5.5 (a) Plot of G_{bender} versus γ , (b) normalised G degradation curve	88
5.6 Plot of $p' - q$ (a) reconstituted samples, (b) undisturbed samples	89
5.7 Test results for reconstituted samples (a) G_{bender} versus γ curve, (b) normalised G degradation curve	91
5.8 Test results for undisturbed samples (a) G_{bender} versus γ curve, (b) normalised G degradation curve	92
5.9 Test results for samples in Figures 5.7 and 5.8 (a) G_{bender} versus γ curve, (b) normalised G degradation curve	93
5.10 Curve fitting and the plot of normalised G_{bender} versus γ	94
5.11 Curves for G_{bender} normalised with p' versus γ	95
5.12 Curves for (G_{bender} / p') normalised with $(G_{bender} / p')_{max}$ versus γ ...	96
5.13 G degradation curves based on the calculation of G_{bender} , G_{secant} and $G_{tangent}$ (continue)	98
5.13 G degradation curves based on the calculation of G_{bender} , G_{secant} and $G_{tangent}$	99
5.14 Normalised G degradation curves for samples in Figure 5.13 (continue)	100
5.14 Normalised G degradation curves for samples in Figure 5.13	101

Figures	Page	
5.15	Diagram showing the relationship among $G_{max,bender}$, G_{bender} , G_{secant} and $G_{tangent}$	104
5.16	Curve fitting and the plot of α versus γ	105
5.17	Curve fitting and the plot of θ versus γ	106
5.18	G degradation curves based on the calculation of G_{secant} and $G_{tangent}$ for (a) Kasaoka 3, (b) Bangkok 14(3)	107
5.19	Plot of calculated G_{bender} for Kasaoka 3 and Bangkok 14(3) based on G_{secant} (a) G_{bender} versus γ curve, (b) normalised G_{bender} degradation curve	108
5.20	Plot of calculated G_{bender} for Kasaoka 3 and Bangkok 14(3) based on $G_{tangent}$ (a) G_{bender} versus γ curve, (b) normalised G_{bender} degradation curve	109
A.1	Equipment and material used for preparing a waterproof BE transducer	123
A.2	Preparation of transmitter BE at the top cap	124
A.3	Preparation of receiver BE at the penetration rod	125
B.1	Testing equipment	126
B.2	Modified triaxial apparatus	127
B.3	Detail “A” - Thrust system completed with stepping motor	127
B.4	National Instruments NI 6120 card	128
B.5	Connection cable and box	128
C.1	Results of consolidation test for (Kasaoka 1) sample	129
C.2	Results of consolidation test for (Kasaoka 2) sample	130
C.3	Results of consolidation test for (Kasaoka 3) sample	131
C.4	Results of consolidation test for Fujinomori sample	132
C.5	Results of consolidation test for NSF sample	133
C.6	Results of consolidation test for Mihara sample	134
C.7	Results of consolidation and swelling tests for (Bangkok 6) sample ..	135
C.8	Results of consolidation and swelling tests for (Bangkok 8) sample ..	136
C.9	Results of consolidation and swelling tests for (Bangkok 10) sample.	137
C.10	Results of consolidation and swelling tests for (Bangkok 12) sample.	138

Figures	Page
C.11 Results of consolidation and swelling tests for (Bangkok 14(1)) sample	139
C.12 Results of consolidation and swelling tests for (Bangkok 14(2)) sample	140
C.13 Results of consolidation and swelling tests for (Bangkok 14(3)) sample	141
D.1 Stress path and stress strain curves for (Kasaoka 1) sample	142
D.2 Stress path and stress strain curves for (Kasaoka 2) sample	142
D.3 Stress path and stress strain curves for (Kasaoka 3) sample	143
D.4 Stress path and stress strain curves for Fujinomori sample	143
D.5 Stress path and stress strain curves for NSF sample	144
D.6 Stress path and stress strain curves for Mihara sample	144
D.7 Stress path and stress strain curves for (Bangkok 6) sample	145
D.8 Stress path and stress strain curves for (Bangkok 8) sample	145
D.9 Stress path and stress strain curves for (Bangkok 10) sample	146
D.10 Stress path and stress strain curves for (Bangkok 12) sample	146
D.11 Stress path and stress strain curves for (Bangkok 14(1)) sample	147
D.12 Stress path and stress strain curves for (Bangkok 14(2)) sample	147
D.13 Stress path and stress strain curves for (Bangkok 14(3)) sample	148

LIST OF ABBREVIATIONS

A	The maximum transverse displacement from an equilibrium point
BE	Bender element
d_{31}	Piezoelectric constant
d_{tip}	Tip displacement of BE
D	Diameter of sample before consolidation process
E'	Drained Young's modulus
E	Elastic Young's modulus
E_{max}	Maximum Young's modulus
E_{secant}	Secant Young's modulus
$E_{tangent}$	Tangent Young's modulus
E_u	Undrained Young's modulus
f	Frequency
f_0	Initial frequency
f_r	Resonant frequency
Δf	Frequency bandwidth
G'	Drained shear modulus
G	Shear modulus
G_{bender}	G calculated from BEs test
G_{HH}	G which shear wave propagate in horizontal direction and soil particle movement is in the horizontal direction
G_{HV}	G which shear wave propagate in horizontal direction and soil particle movement is in the vertical direction
G_{max}	Maximum shear modulus
$G_{max,bender}$	Maximum G_{bender}
G_{secant}	Secant shear modulus
$G_{tangent}$	Tangent shear modulus
G_u	Undrained shear modulus
G_{VH}	G which shear wave propagate in vertical direction and soil particle movement is in the horizontal direction
H	Height of sample before consolidation process
i	Complex number

k	Wave number ($=2\pi/\lambda$)
k_f	Discrete frequency
K'	Effective bulk modulus
L	Travel distance (tip-to-tip distance between the BEs)
L_{bender}	Free length of BE
LSSP	Linearly swept sine pulse
m	Gradient of the graph laser displacement measurement versus self-monitoring signal
m_f	Integer number
$m_{lag,x}$	Gradient of the graph t_{lag} versus x
m_r	m for receiver BE
m_t	m for transmitter BE
M	Critical stress ratio
N	Integer number
OCR	Overconsolidation ratio
\overline{OCR}	Mean overconsolidation ratio $\left(\frac{\sigma'_{mo}}{\sigma'_c}\right)$
p'	Mean effective stress
P_{xx}	Mean amplitude of spectrum for transmitted signal
P_{xy}	Cross spectrum of the received signal with transmitted signal
P_{yy}	Mean amplitude of spectrum for received signal
q	Deviatoric stress
q_0	Initial deviatoric stress
R^2	Coherence function
s	Parameter
t	Time
t_{lag}	Time lag
$t_{(swept)}$	Travel time for swept signal
t_{target}	Target time
t_{travel}	Travel time (time for wave to propagate from transmitter to receiver)
T	Period
T_{bender}	Thickness of BE

TSP	Time stretched pulse
v_{group}	Group velocity
v_{phase}	Phase velocity
V	Input voltage
V_c	Compression wave velocity
$V_{max,particle}$	Maximum particle velocity
$V_{particle}$	Particle velocity
V_s	Shear wave velocity
x	The position in the direction of wave propagation
$x(t)$	Input of the system
$X(f)$	Fourier transform of $x(t)$
$X(k_f)$	Fourier transform of TSP
y	The transverse displacement of an oscillating particle at x
$y(t)$	Output of the system
$Y(f)$	Fourier transform of $y(t)$
$z(t)$	Impulse response of the system
$Z(f)$	Frequency response function which is equivalent to Fourier transform of $z(t)$
α	Function of shear strain
γ	Shear strain
ϵ_a	Axial strain
ϵ_r	Radius strain
ϵ_v	Volumetric strain
θ	Function of shear strain
λ	Wavelength
ν'	Drained Poisson's ratio
ν	Poisson's ratio
ν_u	Undrained Poisson's ratio
ρ	Total density of soil
ρ_{depth}	Bulk density of soil at reference depth
σ'_a	Target axial pressure
σ'_c	Effective isotropic consolidation pressure in triaxial apparatus

σ'_i	Present insitu overburden pressure
σ'_{mo}	Mean preconsolidation pressure $\left(\frac{\sigma'_{pc} + 2K_0\sigma'_{pc}}{3} \right)$, assume $K_0 = 0.5$
σ'_{pc}	Vertical preconsolidation pressure
τ	Shear stress
ϕ_{phase}	Phase difference
ω	Angular frequency ($=2\pi f$)
*	Complex conjugate



สถาบันวิทยบริการ
จุฬาลงกรณ์มหาวิทยาลัย

CHAPTER I

INTRODUCTION

1.1 General

Most of the civil engineering structures such as building, road, bridge, dam, etc. are built on soil and rock. Soil is originated from weathering of rock. In natural state, the void between the soil particles is filled with water and air. Soil provides both sustaining force and destabilising force to structures. For example, the internal friction and cohesion of soil provide stabilising force, whereas the weight of soil leads to destabilising force. For earthwork like cutting and filling, the stability of the cut and fill is essential. In excavation and tunnel works, the force induced by soil may cause excessive deformation in the structure and lead to failure. Hence, geotechnical engineers have to evaluate such forces and design a retaining wall or tunnel linings under specified deformation. Atkinson (1993) mentioned that “Engineers are really applied scientists and very skilled and inventive ones at design”. Nearly all the conventional geotechnical design is based on simplified theory and empirical formula obtained from laboratory testing.

For a soil mass, the changes of applying force or stress result in deformation or strain. The change of stress must be in equilibrium and the induced strain must be compatible. The relationship between stress and strain is normally represented by stiffness of the soil. Two common types of stiffness used in soil mechanics are bulk and shear modulus. The bulk modulus is the ratio between hydrostatic stress and induced volumetric strain. The shear modulus is calculated from the relationship between shear stress and induced shear strain. Normally, both kinds of stiffness are required by designers since soil experiences both confining and shearing at the same time.

It is recognised that stiffness of soil is strain dependent (Atkinson, 2000; Kokusho *et al.*, 1982). Soil is most stiff when induced strain is very small and becomes weak when the strain increases. The relationship between stiffness and strain is extremely non-linear. Mair (1993) pointed out that the knowledge of this relationship is essential for standard design of retaining wall, excavation and foundation works.

1.2 Objectives

The objectives of the thesis are:

1. To study and improve the techniques of shear wave velocity determination by using the bender elements test.
2. To investigate the effects of the bender element installation on shear wave velocity measurement.
3. To evaluate the magnitude of shear strain induced by the bender elements test.
4. To propose a testing methodology in determining shear modulus degradation curve by using bender elements test.

1.3 Organisation of Thesis

The thesis is divided into six chapters and four appendices. The research methodology, findings and summary for each study is described in each chapter.

In chapter I, the general idea about soil mechanic and soil stiffness is discussed. The objectives and organisation of the thesis are mentioned.

In chapter II, the literature review of the method used to determine the shear modulus at the field and laboratory is described. The testing methods used at the field are the down-hole test, cross-hole test and seismic cone penetration test. The bender elements test, cyclic triaxial test, resonant column test, torsional shear test, conventional triaxial testing and local axial displacement gauge are among the methods used in the laboratory to determine shear modulus. The factors affecting the normalised shear modulus degradation curve for cohesive soil are examined.

In chapter III, novel method to determine phase velocity of shear wave is described. The proposed method is based on variable-path length method by using continuous sinusoidal signal. The study of the effect of the bender element installation on shear wave velocity measurement is performed. The study is carried out by penetrating the receiver bender element into the triaxial sample. The magnitude of shear strain induced by the bender elements test is evaluated. The evaluation is based on the calibration process of the output signal of self-monitoring circuit with a laser displacement gauge. The calibration process gives a direct measurement of the tip displacement of bender elements.

In chapter IV, an alternative transmitted signal which is the swept signal is proposed. The travel time needed for shear wave velocity calculation in time domain method is produced from the analysis of transmitted and received signals by using

cross-correlation technique. The usage of the swept signal to determine frequency response of the testing system also discussed. The frequency response obtained is used to regenerate the received signal and compared with the observed received signal.

In chapter V, the testing methodology to generate the G_{bender} (shear modulus determined from bender elements test) degradation curve is reported. The plot of shear modulus degradation curves for shear modulus determined from the bender elements test and conventional triaxial test is presented. The relationship of G_{bender} with shear modulus determined from the conventional triaxial test is examined.

In chapter VI, the conclusions of the research works are presented.

In appendix A, the equipment and material used to prepare a waterproof bender element transducer is described. Preparations of transmitter and receiver bender elements are mentioned.

In appendix B, the modified triaxial apparatus completed with penetration system is shown. National Instruments NI 6120 card and connection cable and box are presented.

In appendix C, the consolidation and swelling tests results for samples tested in chapter V are showed.

In appendix D, the stress path and stress strain curves for samples tested in chapter V are presented.

CHAPTER II

LITERATURE REVIEW

2.1 Background

Over the past few decades, many researchers have performed research to study the non-linear behaviour of soil stiffness in the field and laboratory. The non-linear behaviour of soil stiffness was noticed by Wroth (1975) and Burland (1979) when the back-calculated stiffness result obtained from ground deformation was different from the one measured in the laboratory testing.

Shear modulus, G , degradation curves for sand and cohesive soil have been studied in detail by many researchers (Kokusho, 1980; Hardin and Drnevich, 1972(a); (b); Seed and Idriss, 1970; Sun *et al.*, 1988; Vucetic and Dobry, 1991 and among others). Some researchers proposed an empirical equation to obtain the G degradation curve with only the information of G determined in very small strain regions or usually named maximum shear modulus, G_{max} . Hence, with the information of G_{max} determined from the field or laboratory, the degradation curve can be generated without the need of complicated testing procedure.

There are many testing methods presented to determine G_{max} in the field and laboratory. Some of the methods used in the laboratory can also be used to calculate G at wider strain such as the use of local axial displacement gauge. The detail of the testing method used to determine G in the field and laboratory is discussed in the next section.

2.2 Techniques to Determine Shear Modulus in the Field

2.2.1 Down-hole Test

The down-hole test is one of the popular methods to determine compression and shear wave velocities in the field because it is economic (Luna and Jardi, 2000; Hight *et al.*, 1997). In this test, only one borehole is required to install a geophone into the ground. The source of shear wave is generated by hitting a plank on the ground surface with the direction of hitting to be parallel to the ground surface as shown in Figure 2.1. To distinguish between compression and shear wave, difference polarised of shear wave

is produced by hitting the plank in the opposite direction and parallel to the ground surface. The compression wave can be produced by hitting on top of the plank.

When the plank is hit, the data logger is triggered and records the signal picked up at the plank and receiver geophone in the ground. The elastic Young's modulus, E , and G can be calculated from compression, V_c , and shear wave velocities, V_s , using the following equations (Prakash, 1981):

$$E = \rho_{depth} V_c^2 \left[\frac{(1+\nu)(1-2\nu)}{(1-\nu)} \right] \quad (2.1)$$

$$G = \rho_{depth} V_s^2 \quad (2.2)$$

where ρ_{depth} is the bulk density of soil at reference depth and ν is Poisson's ratio. The relation of E and G is given by the following equation:

$$G = \frac{E}{2(1+\nu)} \quad (2.3)$$

Hence, by substituting equations (2.1) and (2.2) into equation (2.3), the Poisson's ratio can be derived from V_c and V_s shown below:

$$\nu = \frac{[0.5 (V_c/V_s)^2] - 1}{(V_c/V_s)^2 - 1} \quad (2.4)$$

In the down-hole test, the G calculated is G_{VH} . This means that the wave propagates in vertical direction and the movement of soil particle is in the horizontal direction.

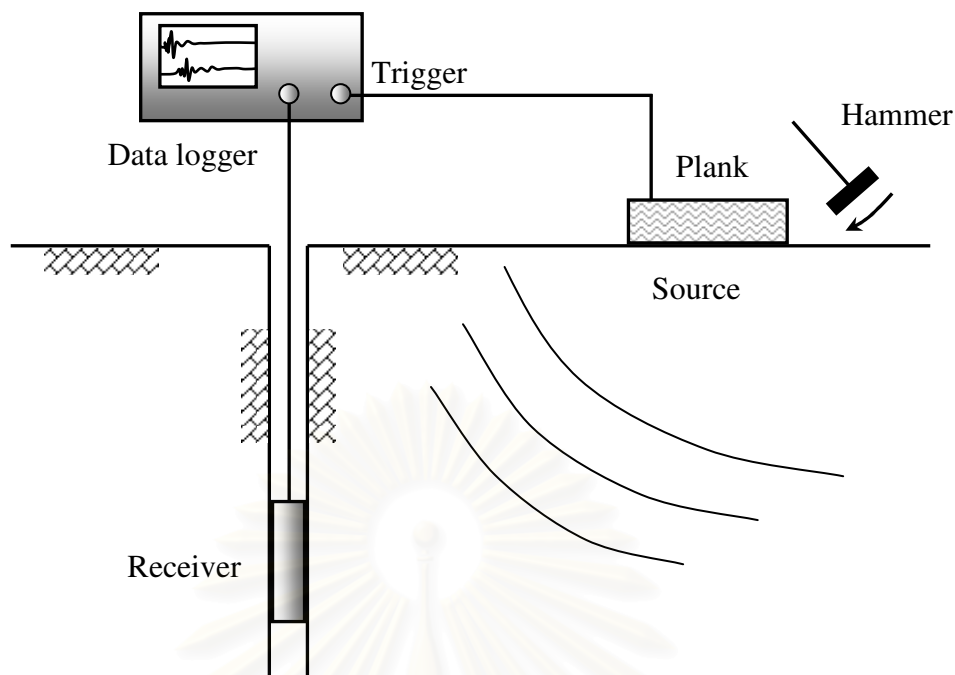


Figure 2.1 Application of down-hole test.

2.2.2 Cross-hole Test

The cross-hole test can be performed by using at least 2 boreholes (Stokoe and Woods, 1972; Salgado *et al.*, 1997; Hight *et al.*, 1997). One borehole is used to generate the shear wave and the other or more boreholes are used to capture the propagating wave shown in Figure 2.2. The G can be computed by using equation (2.2). Two types of G can be calculated from this test which is G_{HH} and G_{HV} . The first and second subscripts mean the direction of the wave propagation and the direction of soil particle movement, respectively. Hence, by combining cross-hole test and down-hole test, the anisotropic behaviour of soil can be studied (Sully and Campanella, 1995; Hope, 1996; Butcher and Powell, 1996).

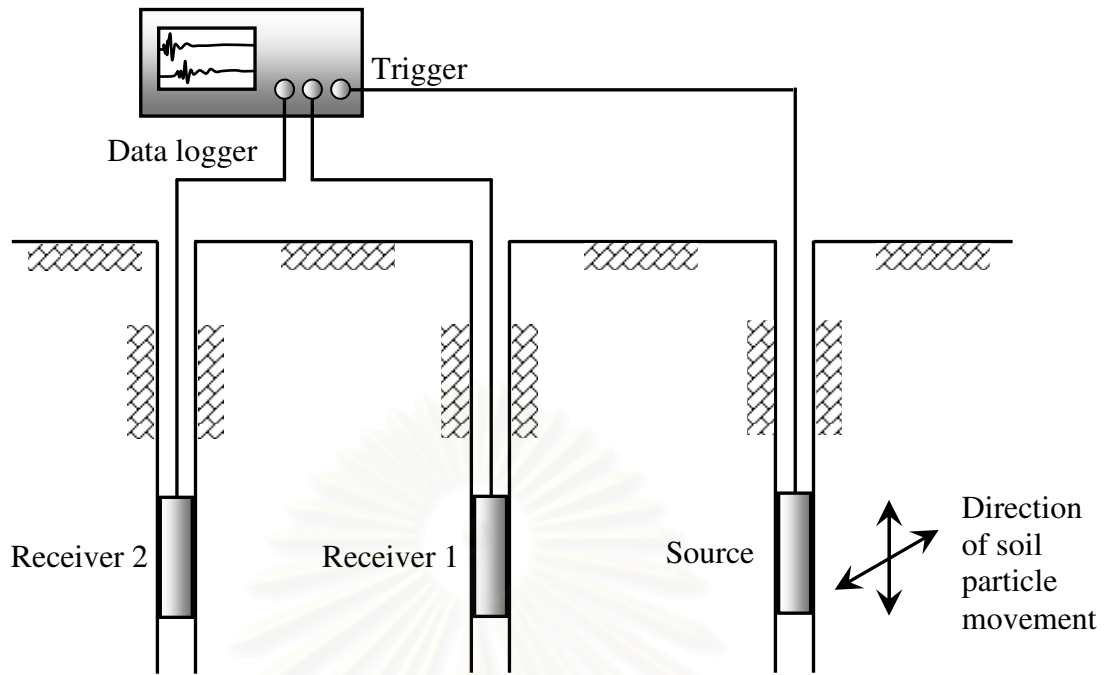


Figure 2.2 Application of cross-hole test.

2.2.3 Seismic Cone Penetration Test

The seismic cone penetration apparatus composes of a piezocone unit (similar to standard cone penetration test) and two accelerometers which are 1 meter apart as shown in Figure 2.3 (Tanaka *et al.*, 1994). The generation of the source of vibration is the same as that of the down-hole test (Figure 2.4). The test is performed when the seismic cone penetration apparatus stopped at a particular depth. The V_s can be calculated by dividing the fixed distance apart with the determined difference of travel time between receivers 1 and 2. The benefit of this test is while performing a seismic test, other properties of soil can be determined such as pore water pressure and density at a particular depth (Luna and Jadi, 2000).

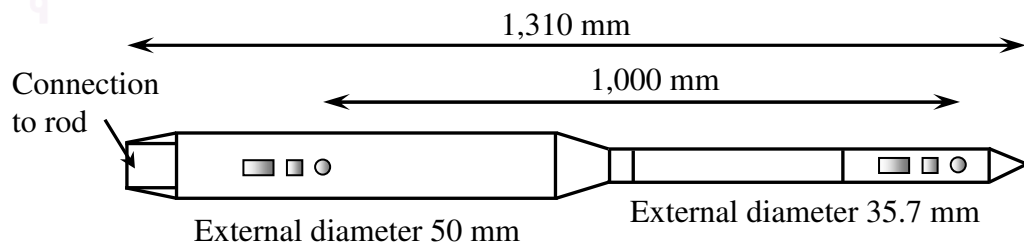


Figure 2.3 Seismic cone penetration apparatus (after Tanaka *et al.*, 1994).

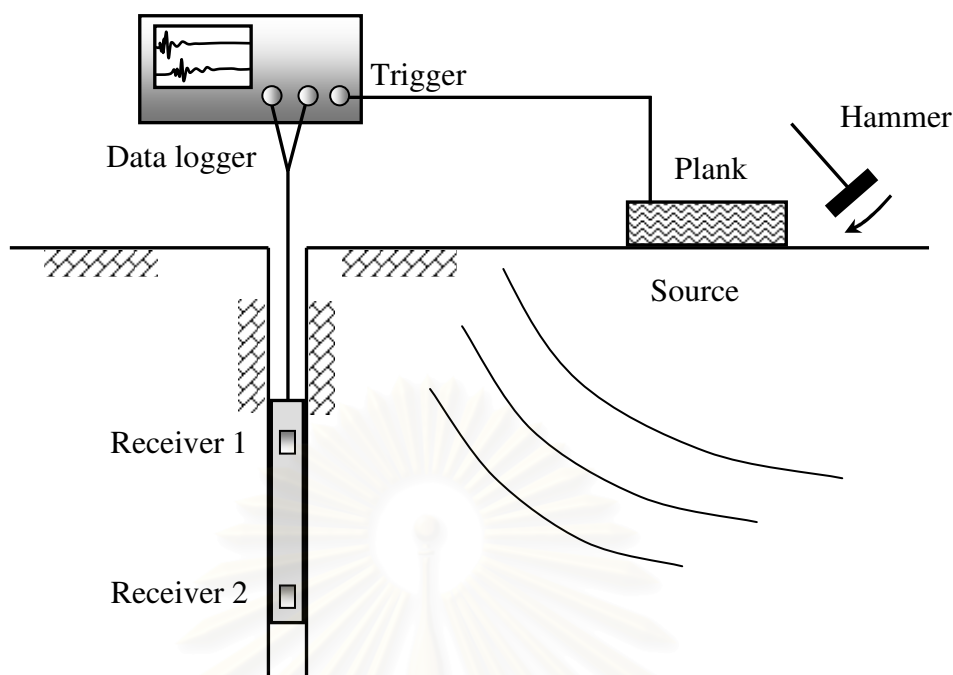


Figure 2.4 Application of seismic cone penetration test.

2.3 Techniques to Determine Shear Modulus in the Laboratory

2.3.1 Bender Elements Test (BEs Test)

The BE is a transducer made from two layers of piezoceramic material, a central metal shim and two layers of outer conductive electrode. The BE deforms when electricity passes through it or electricity is generated when it deformed. Hence, BE is suitable to be used as a transmitter (source) and receiver for a wave propagation test. Figure 2.5 shows the generation of shear wave by a BE and the direction of the wave propagation and the direction of soil particle movement. Figure 2.6 illustrates the BE installation in soil testing apparatus by Dyvik and Madshus (1985). Many researchers have used the BE to determine V_s of soil sample in the laboratory (Fioravante and Capoferri, 2001; Zeng and Grolewski, 2005; Teachavorasinskun and Amornwithayalax, 2002; Teachavorasinskun and Akkarakun, 2004). Step (Dyvik and Madshus, 1985) and single sine waves (Viggiani and Atkinson, 1995) are the typical driving signal used in BEs test. The transmitted signal is generated by using a function generator and the propagation wave is caught at the receiver. The typical transmitted and received signals for single sine wave measured by an oscilloscope are

shown in Figure 2.7. The recorded signals are used in the determination of travel time, t_{travel} .

The calculation of t_{travel} is still controversial. Previous researchers proposed the t_{travel} was between A-D, A-E, A-F, B-G and C-H in Figure 2.7. Viggiani and Atkinson (1995) proposed cross-power spectrum and cross-correlation methods to determine the t_{travel} . The travel distance, L , of the propagation wave is taken as the distance between the tips of BEs (Dyvik and Madshus, 1985; Viggiani and Atkinson, 1995; Chan *et al.*, 2007). Hence, the V_s of soil sample can be calculated by using equation (2.5).

$$V_s = \frac{L}{t_{travel}} \quad (2.5)$$

G can be determined from V_s with the following relation:

$$G = \rho V_s^2 \quad (2.6)$$

where ρ is the total density of soil sample. The BEs test is also used to study the anisotropy behaviour of soil sample (Pennington *et al.*, 1997; Pennington *et al.*, 2001; Zeng and Ni, 1999).

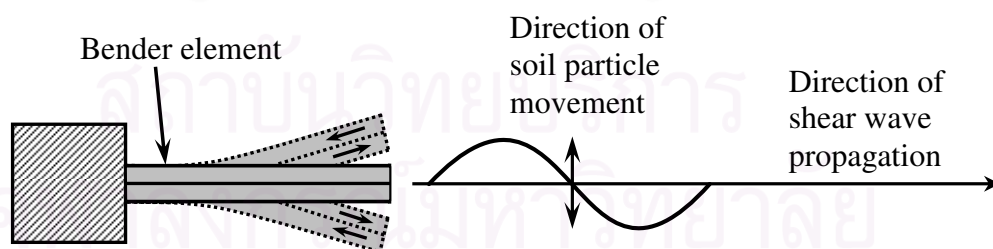


Figure 2.5 Generation of shear wave by using bender element.

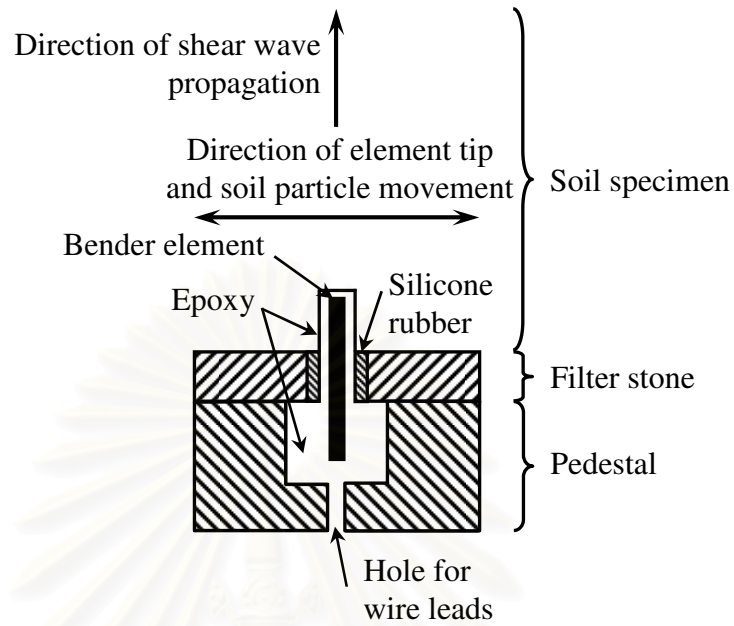


Figure 2.6 BEs installed in the soil testing apparatus (after Dyvik and Madshus, 1985).

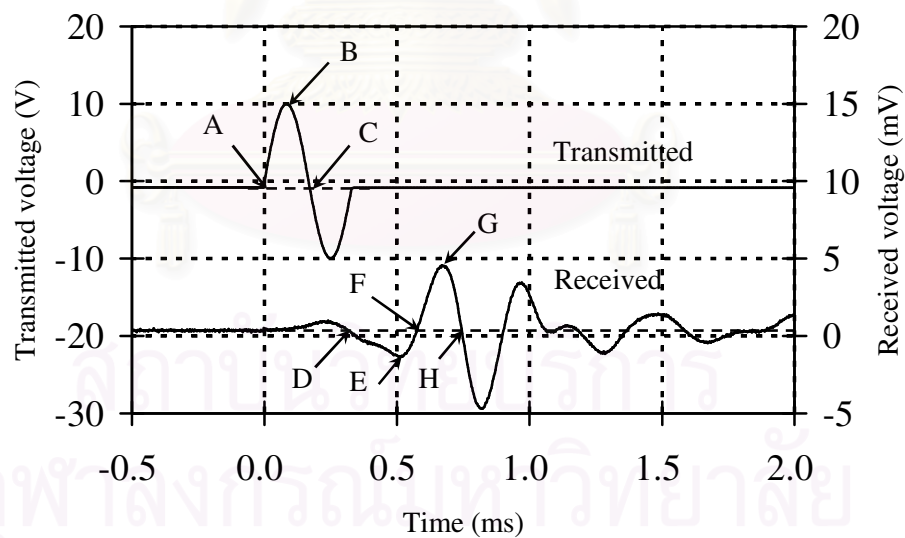


Figure 2.7 Typical transmitted and received signals for single sine signal from the BEs test.

2.3.2 Cyclic Triaxial Test

Kokusho (2004) showed the improved cyclic triaxial test apparatus as shown in Figure 2.8. The improvement of the apparatus is by using an inner load cell and a high sensitive gap sensor which eliminate the mechanical friction effect. The displacement gap sensor measurement concept is based on the inductance changes. Each sensor installed as shown in Figure 2.8 consists of electromagnetic coil. When one of the sensor moves the measurement inductance of the sensor changes and this change is converted to displacement. The improvement allows G to be measured in a wider strains range which is from 10^{-6} to 10^{-2} (Kokusho, 2004).

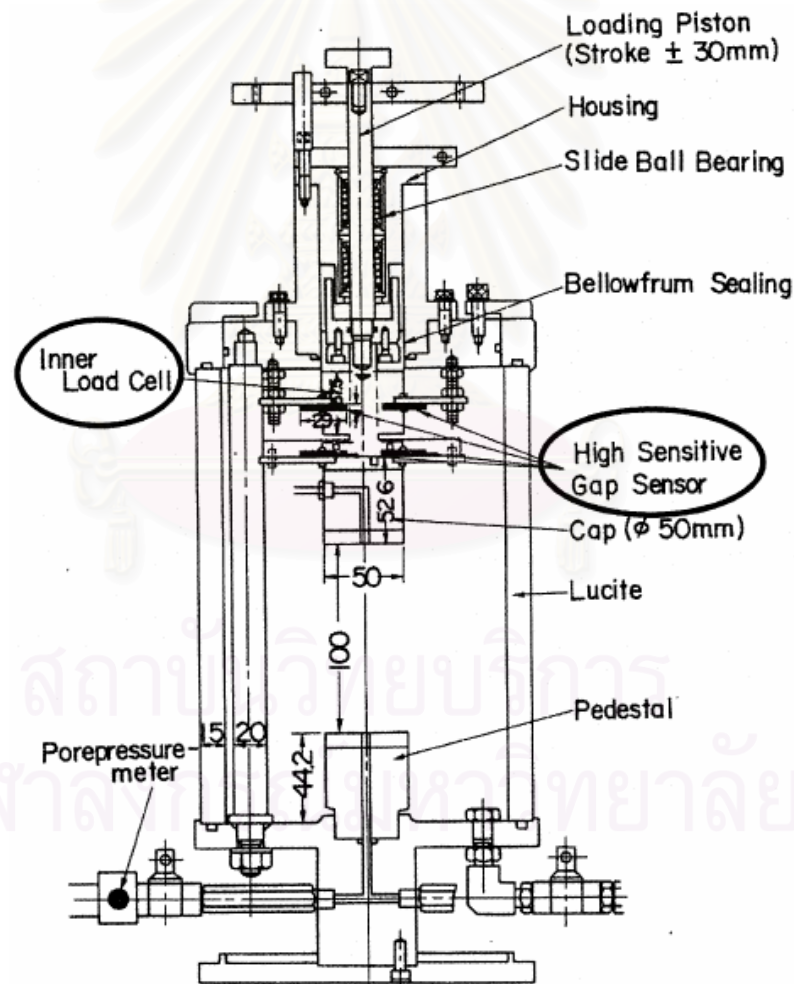


Figure 2.8 Improved cyclic triaxial test apparatus with inner load cell and high sensitivity proximity sensors (after Kokusho, 2004).

2.3.3 Resonant Column Test

Solid or hollow cylindrical samples can be used in the resonant column test (Shannon *et al.*, 1959; Drnevich, 1972; Kuribayashi *et al.*, 1974). The sample is prepared in the triaxial apparatus and consolidated. Then, axial or torsional vibration method is applied on the sample by using the electromagnetic driving system. The frequency of the driving system is increased until the natural frequency of the sample obtained. Based on the natural frequency and dimension of the sample, the wave propagation velocity can be back-calculated. After acquiring the natural frequency, the system is stopped and the free vibration of the sample is observed so that the damping behaviour of the soil can be obtained. The test is repeated with higher driving force and this means the stiffness of soil is decreased and also causes the natural frequency to reduce.

Figure 2.9 shows two types of torsional vibration method for the resonant column test. By referring to Figure 2.9(a), the vibration is stimulated at the base and the reaction is picked up at the top by using an accelerometer. For the top stimulation type shown in Figure 2.9(b), the reaction is also collected at the top, but in this method the moment inertia of the driving system has to be considered in the back-calculation.

Ishihara (1996) stated the limitation of resonant column test. The limitation is the result that has to be based on back-calculation to be obtained. Therefore, great attention is paid on the response of the testing system used because the testing system is the combination between the soil sample and testing apparatus. The apparatus is appropriate for the study of the dynamic behaviour of soil under the shear strain of about 5×10^{-4} .

2.3.4 Torsional Shear Test

According to Figure 2.10, when the sample is subjected to torsion the strain distribution in the angular direction for hollow cylindrical sample is assumed to be consistent compared to the cylindrical sample. Hence, the hollow cylindrical sample is preferred to be used in this testing compared to cylindrical sample. Figure 2.11 shows the hollow cylindrical torsional test apparatus developed at the soil mechanic laboratory in Hokkaido University. The testing apparatus is controlled by a computer. Four types of stresses can be applied to the sample such as the axial stress, torsional stress, outer and inner stresses. These combinations of stresses can be used to rotate

the directions of principal stress axes (Ishihara and Towhata, 1983; Towhata and Ishihara, 1985). Ishihara (1996) mentioned that torsional shear test can be used to study the deformation behaviour of soil but this testing is not suit for a practical work.

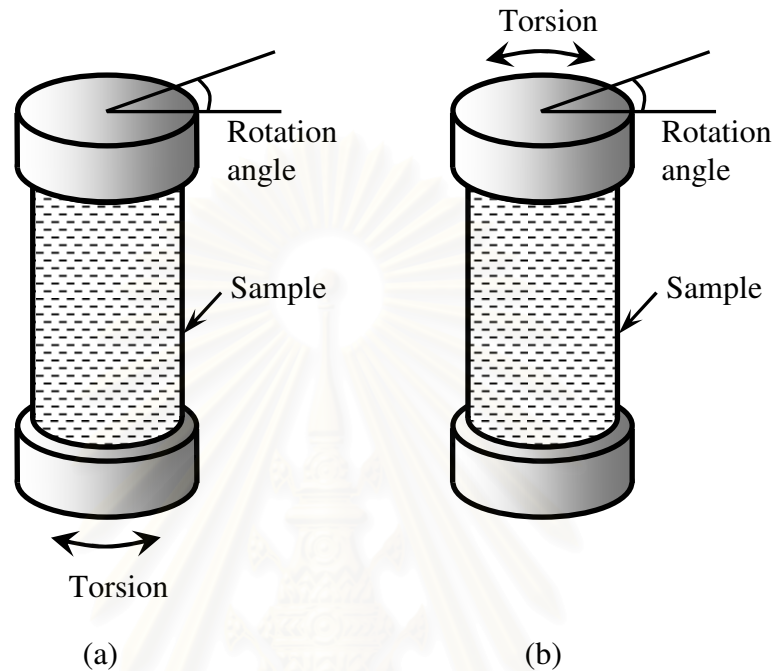


Figure 2.9 Two types of torsional vibration method for resonant column test (a) base stimulation, (b) top stimulation.

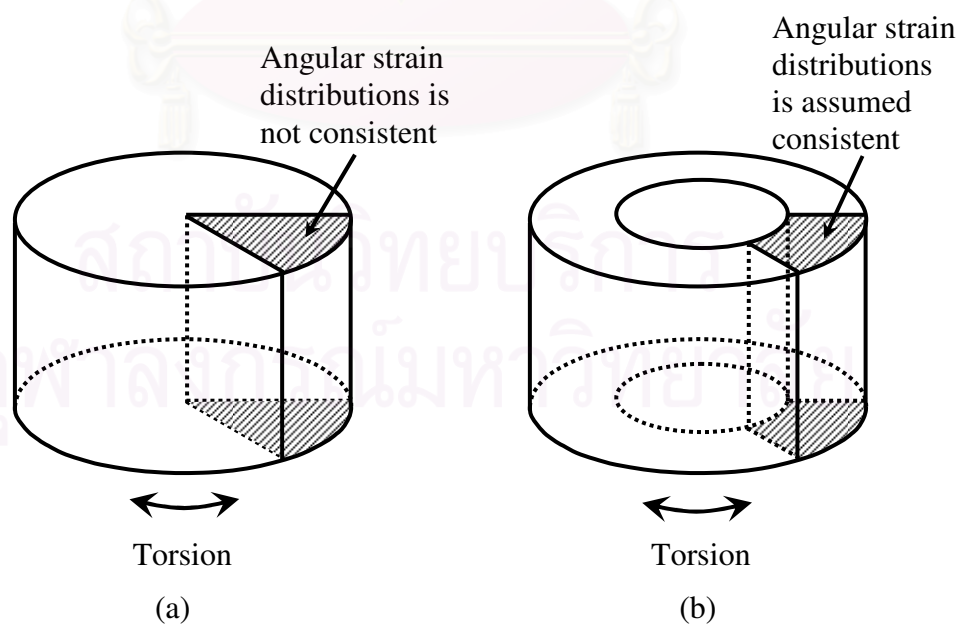


Figure 2.10 Angular strain distributions (a) cylindrical sample, (b) hollow cylindrical sample.

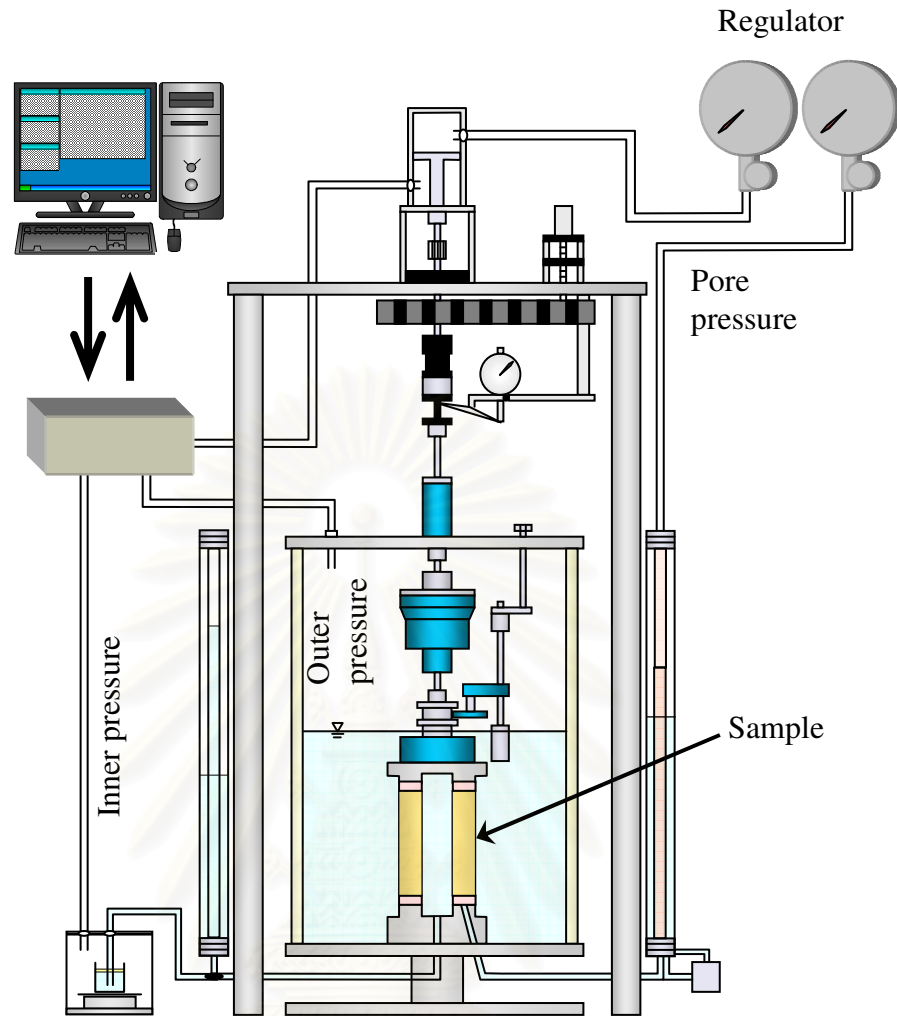


Figure 2.11 Hollow cylindrical torsional test apparatus (soil mechanic laboratory, Hokkaido University).

2.3.5 Conventional Triaxial Testing

The conventional triaxial test can be used to calculate G based on the relation shown in equation (2.3). For the undrained triaxial test, Poisson's ratio is equal to 0.5 for saturated sample. Then, G is equal to $E_u/3$, where E_u is the undrained Young's modulus. E_u can be obtained based on the gradient calculation of the graph showing deviatoric stress versus axial strain. The shear strain is equal to axial strain for an undrained test condition. Atkinson and Salfors (1991) reported that the conventional test is suitable to determine G in the strain level more than 10^{-3} . This means conventional triaxial testing is not reliable to calculate G_{max} .

2.3.6 Local Axial Displacement Gauge

The external axial displacement gauge may give some error readings when measuring small strains. This error is caused by the effects of bedding error which the error is caused by an imperfect contact between the sample and the top cap and pedestal. Hence, local axial displacement gauge (Jardine *et al.*, 1984) is proposed to measure the small strains stiffness. However, it can also be used to determine G from a small strains region to a large strains region. Few local gauges have been proposed such as strain gauge local deformation transducer (LDT) (Goto *et al.*, 1991; Kim *et al.*, 1994; Tatsuoka *et al.*, 1993) and linear variable differential transformers (LVDT) (Costa Filho, 1985; Cuccovillo and Coop, 1997). Figure 2.12 shows the arrangement of LDT in the triaxial test. Tatsuoka and Shibuya (1991) reported that the bedding error effect might not be significant for soft clays, but the effect is strong when stiff soil is tested such as stiff clays and soft rocks.

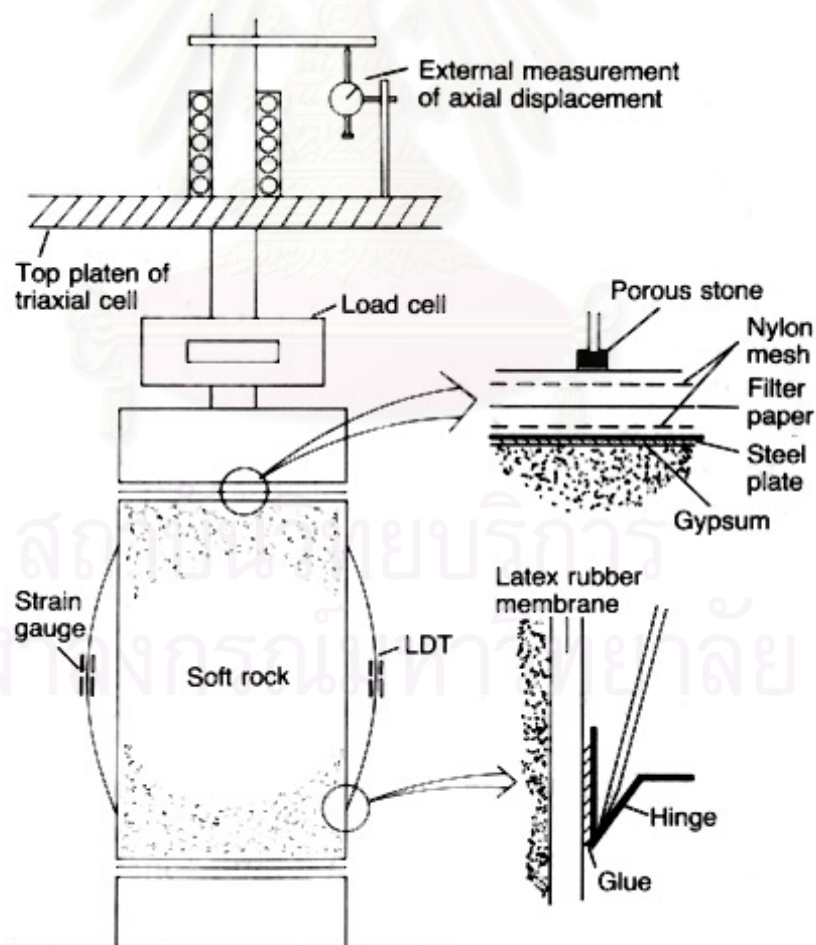


Figure 2.12 Local deformation transducer (LDT) (after Tatsuoka *et al.*, 1993).

2.4 Factor Affecting the Normalised Shear Modulus Degradation Curve of Cohesive Soil

Vucetic and Dobry (1991) have proposed normalised G degradation curves for cohesive soils as shown in Figure 2.13. The normalised G degradation curve depends on the cohesive soil plasticity index. When the plasticity index is higher, the curve is shifted to the right and this means the curve starts to behave in a nonlinear way at a higher strains level. Normalised G degradation curve for saturated cohesionless nonplastic soils also shown in Figure 2.13 in which the plasticity index is equal to zero. The research finding of Sun *et al.* (1988) and Kokusho (2004) supported that the normalised G degradation curves for cohesive soils depend on the plasticity index.

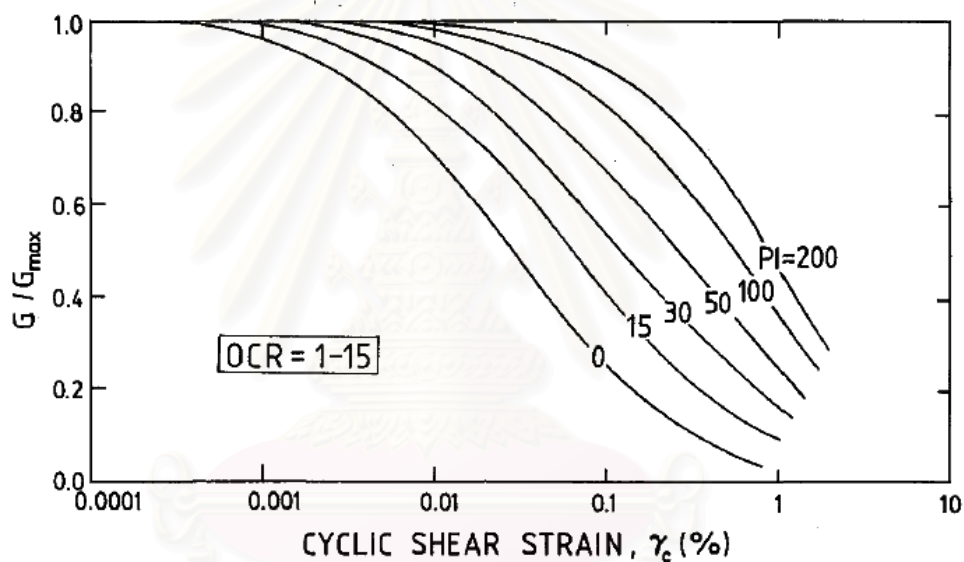


Figure 2.13 Normalised shear modulus degradation curves for normally and overconsolidated soils with the effect of plasticity index (after Vucetic and Dobry, 1991).

CHAPTER III

DETERMINATION OF PHASE VELOCITY OF SHEAR WAVE

3.1 Overview

The credit of the BEs test is usually given to Shirley and Hampton (1978). Since the BE is small, handy, durable and easy to operate, it has been adopted widely in geotechnical laboratory for determining V_s in soils and installed into various standard apparatus such as a consolidometer (Jamiolkowski *et al.*, 1995; Lee and Santamarina, 2005; Shibuya *et al.*, 1997 and among others) and triaxial apparatus (Viggiani and Atkinson, 1995; Jovicic *et al.*, 1996; Hwang *et al.*, 1998 and among others). The fact that V_s is related to the G_{max} and G_{max} is useful for a design that the nonlinear soil behaviour is considered (Atkinson, 2000). The V_s of a specimen is also used as an indicator for the quality of a soil sample (Landon *et al.*, 2007) and to study the consolidation process (Fam and Santamarina, 1997). Hence, V_s is an essential parameter in geotechnical engineering.

3.2 Testing Equipment

3.2.1 Preparation of BEs

A BE is a piezoceramic material composed of two layers of an outer conductive electrode, a conductive metal shim at the centre and two layers of piezoelectric sheets as shown in Figure 3.1(a). Typical materials used to produce BEs are also shown in this figure. The BE bends when electricity passes through it or generates electricity when it is bended. There are two types of BEs available in the market, the parallel and series types. For the parallel type, two layers of piezoelectric material have the same pole direction as shown in Figure 3.1(b) and a three-wire connection is required to create a bending movement. For the series type, the direction of a pole for piezoelectric layers is different and a two-wire connection is required to generate a bending movement as shown in Figure 3.1(c).

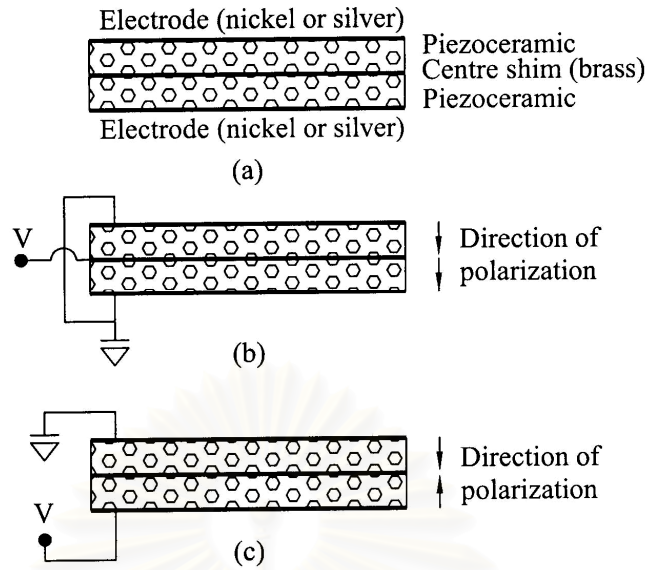


Figure 3.1 A BE (a) schematic position of material, (b) parallel type, (c) series type.

For a cantilever BE, the tip displacement, d_{tip} , for the parallel and series types BEs in free air is given by

$$d_{tip} = 4d_{31} \frac{L_{bender}^2 V}{T_{bender}^2} \quad (\text{parallel type BE}) \quad (3.1)$$

$$d_{tip} = 2d_{31} \frac{L_{bender}^2 V}{T_{bender}^2} \quad (\text{series type BE}) \quad (3.2)$$

where, d_{31} , V , L_{bender} , T_{bender} are the piezoelectric constant, input voltage, free length and thickness of the BE, respectively (Piezo Systems, Inc., 2004).

From equations (3.1) and (3.2), the parallel type BE can deform two times more than series type BE when it experiences the same input voltage. However, when comparing the two types, the series type BE can generate voltage two times more than the counterpart when they undergo the same deformation. Hence, the parallel and series types BEs are suitably utilised as the transmitter and receiver, respectively (Schultheiss, 1982).

As suggested by Lee and Santamarina (2005), the parallel type BE could be used to avoid the problem from a cross-talk effect. The cross-talk effect is an electromagnetic coupling between a transmitter and receiver exhibiting as an output signal that is concurrent with the input signal. The parallel type BEs were used in this

research. The signal generated by the parallel type BE receiver becomes half compared to the series type BE, but the cross-talk effect problem can be avoided.

When BEs are inserted into soil samples, the input voltage does not produce the same displacement calculated by equations (3.1) and (3.2) due to restraints from various factors such as the stiffness of the epoxy coating, the stiffness of the soil, the method of installation of BEs to the base, etc. To overcome this problem, self-monitoring circuit proposed by (Schultheiss, 1982) is used. Figure 3.2 shows the preparation and connection process for the parallel type BE equipped with a self-monitoring circuit. A three-core shielded cable was used. Both sides of the electrode surface are shallow cut to isolate the surface. The cuts are made before the BEs are coated. By isolating the electrode surface into three bands, the two side bands are used to drive the BE while the centre band is used to generate the self-monitoring signal which develops when the BE is bent. Transmitter and receiver BEs are equipped with self-monitoring circuits.

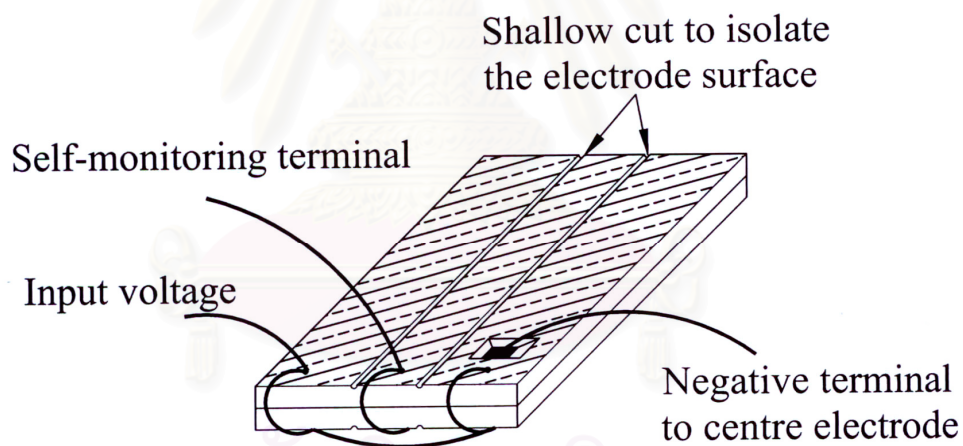


Figure 3.2 The connection of a parallel type BE with its electrode shallow cut at both sides and wired to operate as a self-monitoring circuit.

To prevent electrical short circuits when BEs are used in saturated soil, the BEs are coated with epoxy as described by Dyvik and Madshus (1985) and Chang (2005). Chang (2005) mentioned that the stiffness of the epoxy coating was important because the vibration energy of the BEs could not transfer to the soil particle if the coating was too soft. However, the deformation of the BEs is minimised if the coating is too stiff. If the coating of the BEs is too brittle, it may crack. It is also important that the BEs

should be coated with equal thickness to facilitate uniform deformation. Hence, a mould and an epoxy product shown in Appendix A are used in the coating process. The epoxy has a low setting time, low viscosity and flexible. Low viscosity is needed so that the epoxy can flow into the mould. The mould is used to reduce the preparation time and provides the smooth and equally thickness coating.

The dimensions of BEs for each study are different. In Section 3.4, 3.6 and Chapter V a wider transmitter BE was used in order to generate higher vibration energy and increase the signal to noise ratio of the received signal. It is difficult to make a spare BE with the same free length as the broken one.

3.2.2 Modification of Triaxial Apparatus and Equipment Used for BEs Test

Figure 3.3 shows a schematic view of an arrangement of a triaxial apparatus for the BEs test. A consolidometer apparatus is also used in the research (Chapter IV) and the schematic view of an arrangement of the consolidometer for the BEs test is the same as shown in Figure 3.3 except that the triaxial apparatus is replaced with the consolidometer apparatus. The details of the triaxial apparatus system (Shibuya and Mitachi, 1997) are shown in Figure 3.4. The triaxial apparatus was modified by drilling the centre of the bottom pedestal. Then, a penetration rod equipped with a receiver BE as shown in Figure 3.5 was inserted through this hole from the bottom. After that, the penetration rod was driven into the hole in axial direction by a thrust system completed with a stepping motor. The stepping motor was used to gradually penetrate the rod and also the receiver BE into the sample. The penetration position of the receiver BE was determined by measuring the movement of the penetration rod with a displacement transducer.

To prevent the soil from moving into the gap between the receiver BE and bottom cap, a one mm thick rubber membrane with thin slit at the centre was placed over the pedestal as shown in Figure 3.6. The flexibility of the rubber membrane allowed the BE to bend with a minimum constraint. In addition, a piece of filter paper was placed on top of the rubber membrane to close the remaining small gap.

Few precaution steps had been performed to reduce the noise level in the testing system. The essential precaution was to provide an isolation system by using isolation transformer in between the power supply and the testing system. The power supply was heavily contaminated with electrical noise generated by digital motor from other testing equipment in the laboratory. Therefore, the isolation transformer could filter

the electrical noise from the power supply before going into the system. Besides, the isolation system guaranteed that all equipment in the system had the same electric ground.

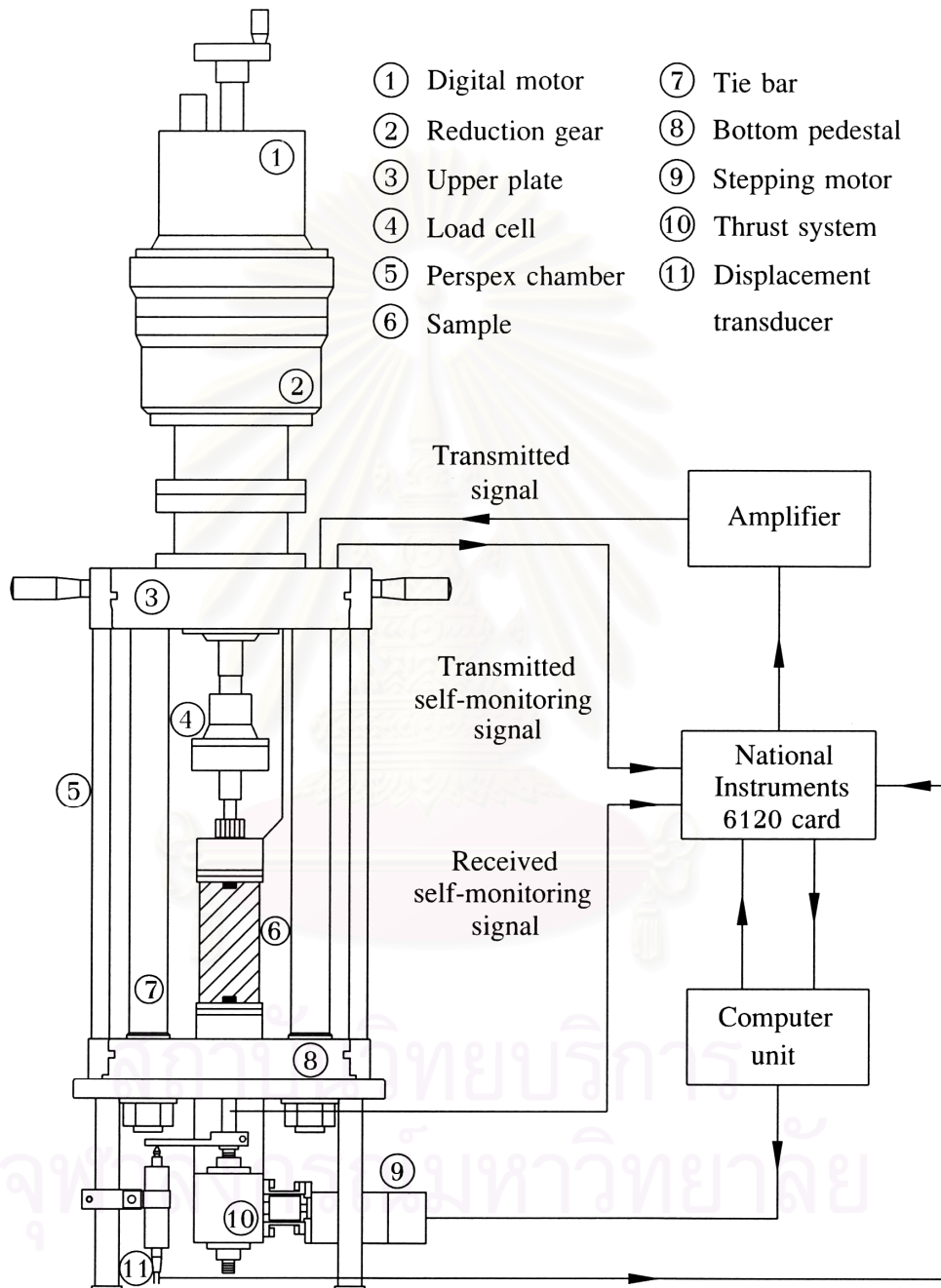
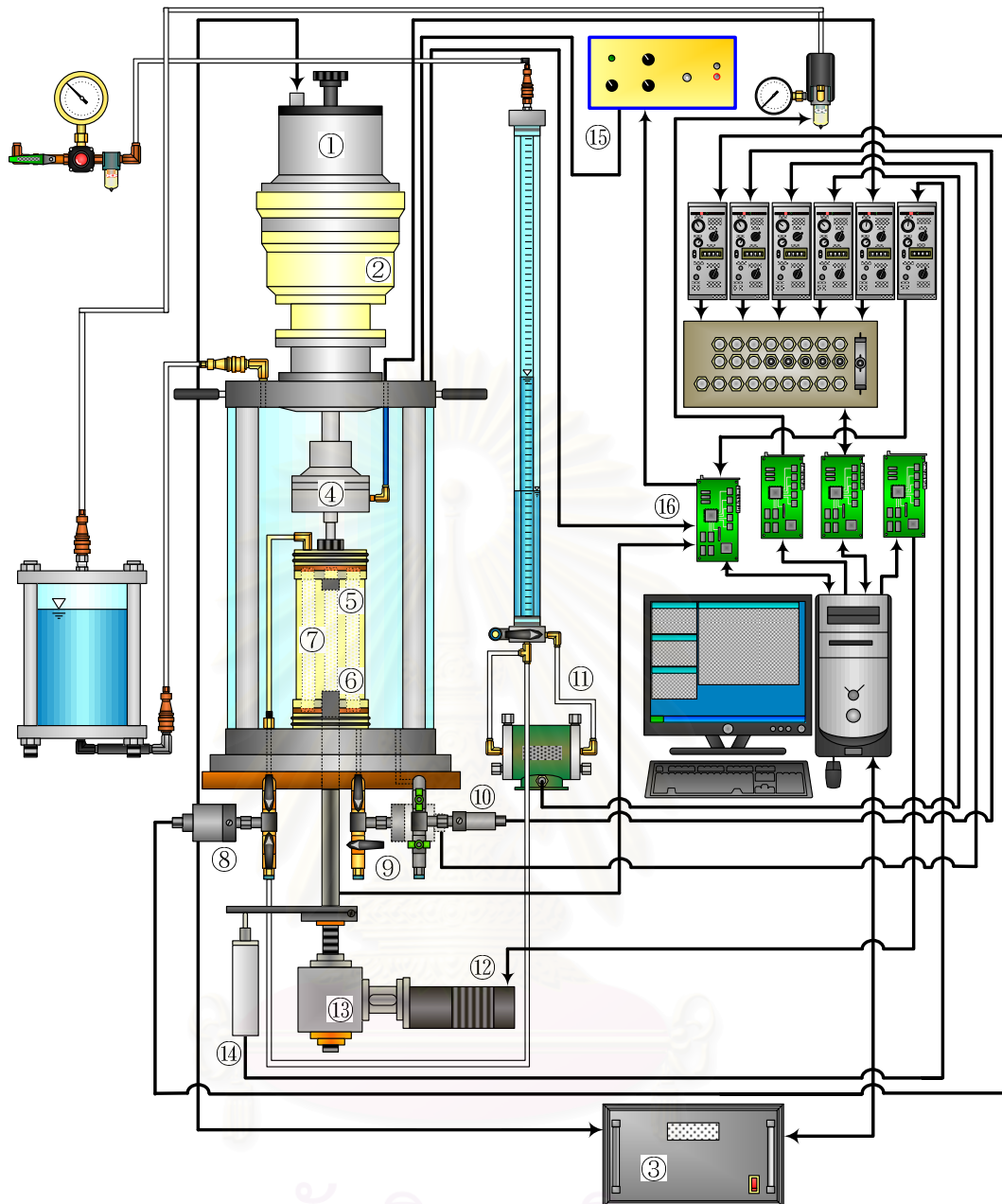


Figure 3.3 Schematic view of an arrangement for the BEs test using triaxial apparatus.



- | | |
|-----------------------------------|-------------------------------------|
| 1. Digital motor. | 9. Pore pressure transducer. |
| 2. Reduction gear. | 10. Cell pressure transducer. |
| 3. Control box for digital motor. | 11. Volumetric transducer. |
| 4. Load cell. | 12. Stepping motor. |
| 5. Transmitter BE. | 13. Thrust system. |
| 6. Receiver BE. | 14. Displacement transducer. |
| 7. Sample. | 15. Amplifier. |
| 8. Back pressure transducer. | 16. National Instruments 6120 card. |

Figure 3.4 System of triaxial apparatus completed with BEs test.

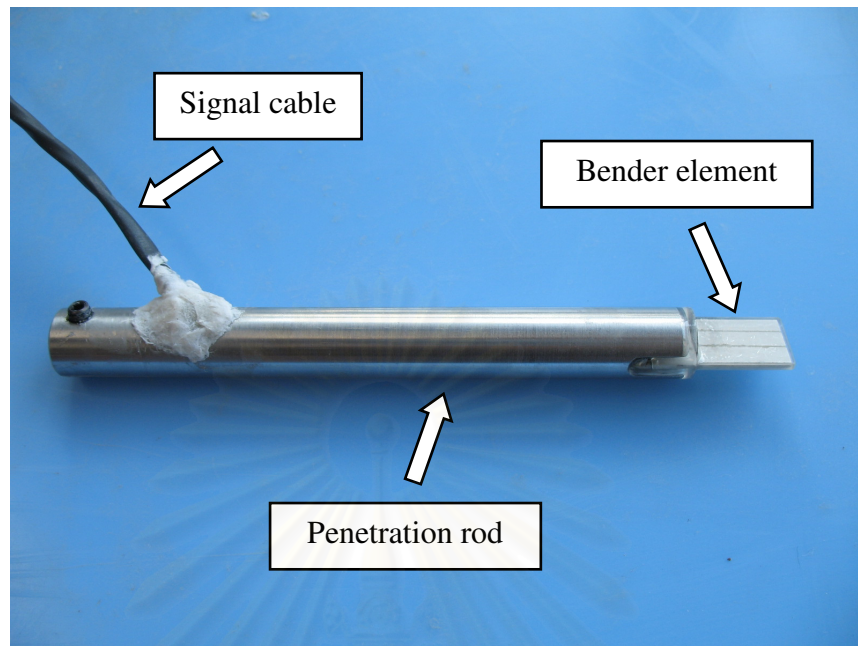


Figure 3.5 Attachment of the receiver BE to the penetration rod.

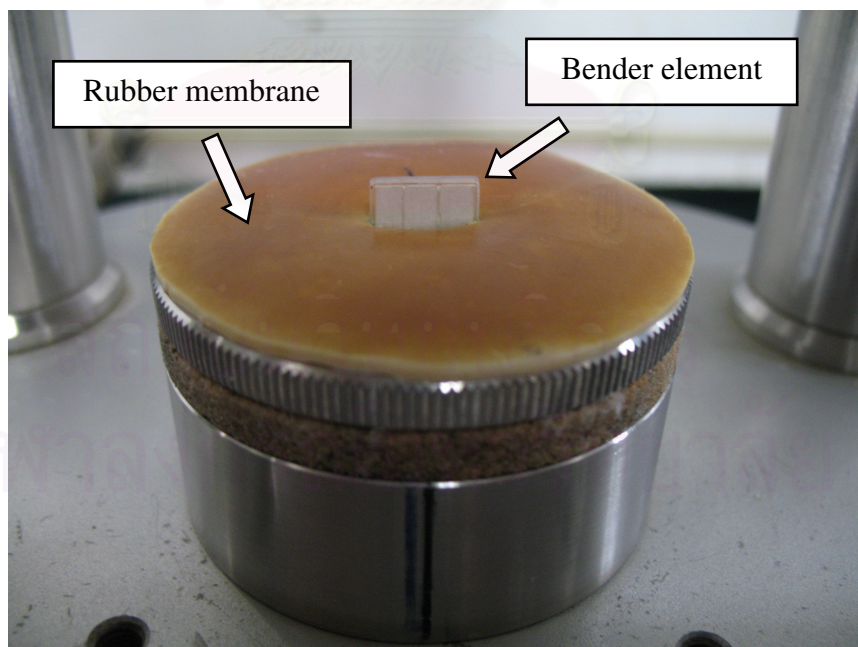


Figure 3.6 Modification of the gap between receiver BE and bottom cap.

The triaxial apparatus in the system could act as an antenna that gathered electromagnetic noise and establishes a different ground potential in the system. This problem could be eliminated by grounding the triaxial apparatus to the measurement system (in this study, personal computer based system is used). For the system shown in Figure 3.4, the best grounding method for the BE shielded cable was to shield ground at one end only. The control box for digital motor created a very high level of noise in the system. To solve this problem, the control box was switched off when the BEs test was conducted.

To generate and acquire the signals, a National Instruments (NI 6120) card was used. NI 6120 consists of two output and four input channels. One of the output channels was used to generate transmitted signal and two input channels were utilised to acquire the transmitted and received self-monitoring signals. The voltage of the displacement transducer shown in Figure 3.3 was sent to the third input channel. By using this card, any types of wave could be generated such as single sine, step, continuous sine, swept waves, etc. The signal generated was sent through an amplifier to the transmitter BE. The maximum output voltage of NI 6120 card was ± 10 V and the amplifier could amplify the output voltage 10 times. This means that the maximum input voltage to which the transmitter was subjected was ± 100 V.

3.3 Properties of Reconstituted and Undisturbed Samples

Four types of reconstituted samples were used in the research and they were Kasaoka clay, Fujinomori clay, NSF clay and Akita peat. Kasaoka clay, Fujinomori clay and NSF clay are commercially available in a powder state. The soil properties of the reconstituted samples are shown in Table 3.1. Reconstituted samples are used because the uniformity of the sample is more controllable than the natural soil. However, undisturbed samples are also used in Section 4.1 and Chapter V and the soil properties of undisturbed clay are shown in Table 3.2.

Reconstituted samples were made by adding distilled water of which the water content was about twice the liquid limit and stirred in the soil mixer. Akita peat was taken from peat layer spreading two meters below the ground surface in the suburb of Akita city, Japan. The sample was reconstituted to a paste by adding distilled water of which water content was about 800% and stirred. Particle density of the sample was 1640 kg/m^3 , ignition loss was 76.5% and degree of decomposition was 75.5%.

For a reconstituted sample used in the triaxial test, the slurry of the sample was preconsolidated one dimensionally by transferring the slurry from the soil mixer to the preconsolidation cell shown in Figure 3.7. The transferring process was done to the cell by applying vacuum pressure in the cell. The value of vertical preconsolidated pressure, σ'_{pc} , for each type of soil is shown in Table 3.1. For a reconstituted sample used for consolidometer, the slurry did not undergo preconsolidation process but it was directly transferred to the consolidometer and consolidated in the apparatus. The consolidation pressure used in consolidometer testing is shown in Table 4.2.

Table 3.1 Properties of reconstituted samples.

Reconstituted sample	Vertical preconsolidation pressure, σ'_{pc} # (kPa)	Liquid limit (%)	Plastic index
Kasaoka clay	70, 150	62	25
Fujinomori clay	70	62	33
NSF clay	150	55	26
Akita peat	40	-	-

#for samples used in triaxial test.

Table 3.2 Properties of undisturbed samples.

Undisturbed sample	Typical liquid limit (%)	Typical plastic index
Bangkok clay	80	52
Mihara clay	52	28



Figure 3.7 The slurry is preconsolidated under vertical pressure in preconsolidation cell.

3.4 The Method of Variable-path Length by Using Continuous Sinusoidal Wave

3.4.1 Background

The phase and group velocities are the same for nondispersive medium; they are unequal and depend on the frequency of the wave when the propagating medium is dispersive such as a soil sample. Brillouin (1960) showed that a pulse being a superposition of waves with its mean amplitude propagates with a group velocity, v_{group} . The relation between v_{group} , the wave number and angular frequency is given by

$$v_{group} = \frac{d\omega}{dk} \quad (3.3)$$

where $\omega (=2\pi f)$ is the angular frequency, $k (=2\pi/\lambda)$ represents the wave number, f and λ are frequency and wavelength, respectively.

Due to the fact that the wave travels one λ per period, T , the phase velocity, v_{phase} , of shear wave can be expressed as the product of the f and λ (Pain, 1999):

$$v_{phase} = f \lambda = \frac{\omega}{k} \quad (3.4)$$

Therefore, the relationship between the phase and group velocities can be obtained from equations (3.3) and (3.4) as

$$v_{group} = \frac{d(v_{phase}k)}{dk} = v_{phase} + k \left(\frac{dv_{phase}}{dk} \right) \quad (3.5)$$

By adopting π -point phase technique (Sachse and Pao, 1978), Greening and Nash (2004) reported that v_{group} of shear wave is higher than v_{phase} when it propagates through Gault clay specimen. Their work implies that G can be overestimated when it is derived from v_{group} .

The travel distance for the V_s calculation is usually set to the tip-to-tip distance as supported by Dyvik and Madshus (1985) and Viggiani and Atkinson (1995). The distance is obtained by deducting the length of the sample with the embedded length of BEs at each end of the sample. However, uncertainty occurs whether the sample length is still the same as measured after the sample has been installed in the apparatus, especially when a soft clay specimen is tested.

3.4.2 Variable-path Length Method

To circumvent the uncertainty of the travel time and travel distance, a new approach to determine the V_s is introduced. The idea of variable-path length method by using continuous sinusoidal signal is originated from the work of Lynnworth *et al.* (1981) and is adopted for soil testing by the author (Chan and Boonyatee, 2005). The advantage of proposed method is the ability to determine v_{phase} of shear wave at arbitrary frequency. It also yields high signal recovery which is preferable for highly damped soil. By the proposed method, the travel distance can also be determined directly without ambiguity.

The fundamental of variable path-continuous wave method can be stated as “The reached velocity of a wave is connected with the phase difference between the vibrations observed at two different points during the propagation of the wave”. A plane wave propagates in an undamped medium can be written as

$$y = A \sin(\omega t - \phi_{phase}) = A \sin(\omega t - kx) \quad (3.6)$$

where x is the position in propagation direction, y represents the transverse displacement of an oscillating particle at x , A refers to the maximum transverse displacement from an equilibrium point, t is the time and ϕ_{phase} is phase difference .

Shown in Figure 3.8, a change in x of λ causes a change in ϕ_{phase} of 2π or a change in time lag, t_{lag} , of an oscillation period, $T (=1/f)$. Every full period of t_{lag} change as x is changed demonstrates an increment of path length which is equal to λ . Hence, λ can be calculated using the following equation:

$$\frac{\Delta x}{\lambda} = \frac{\Delta \phi_{phase}}{2\pi} = \frac{\Delta t_{lag}}{T} \quad \text{where} \begin{cases} \Delta x \in [0, \lambda] \\ \Delta \phi_{phase} \in [0, 2\pi] \\ \Delta t_{lag} \in [0, T] \end{cases} \quad (3.7)$$

$$\lambda = \frac{\Delta x}{\Delta t_{lag}} T = \frac{\Delta x}{\Delta \phi_{phase}} 2\pi \quad (3.8)$$

Figure 3.8(a) shows a continuous sine wave signal generated at a transmitter and captured by a receiver at a different position and Figure 3.8(b) illustrates the signal motion with time for transmitted and received signals. When the receiver is located at position x_1 , the time lag is $t_{lag,1}$. After the receiver is located at a new position x_2 , the value of time lag is $t_{lag,2}$. Hence, the value of Δt_{lag} is equal to the difference between $t_{lag,1}$ and $t_{lag,2}$ because both received signals refer to the same transmitted signal. Based on equation (3.8), if the t_{lag} of the receiver at a different position, x , is measured and with the information of $T (=1/f)$, λ can be calculated.

By using equations (3.4) and (3.8) the v_{phase} can be calculated by

$$v_{phase} = f\lambda = f \left(\frac{\Delta x}{\Delta t_{lag}} T \right) = \frac{\Delta x}{\Delta t_{lag}} \quad (3.9)$$

In order to minimise the artefacts from the test, the graph t_{lag} versus x as shown in Figure 3.11 is plotted and fitted by linear relation. Then, the v_{phase} is determined from the plot by using

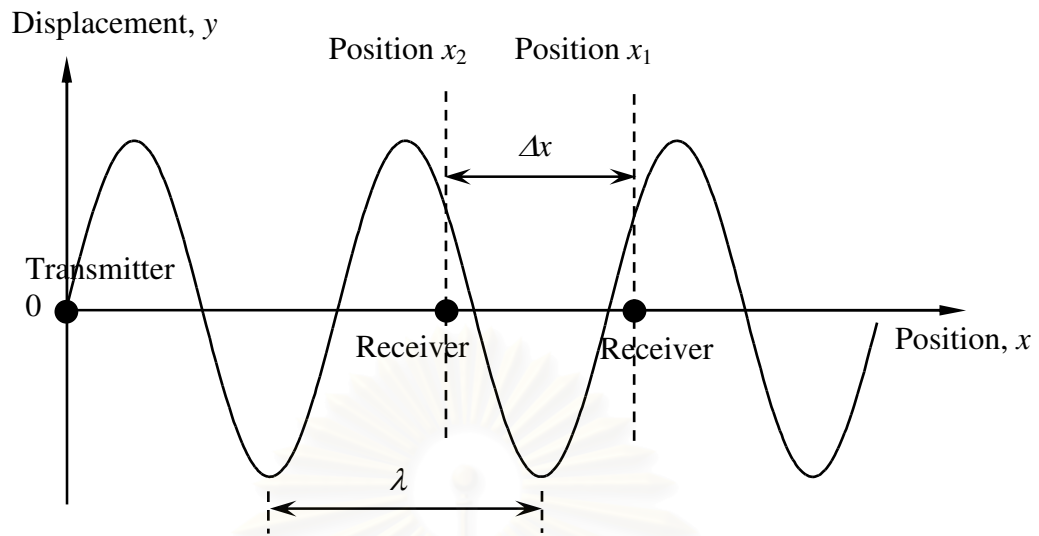
$$v_{phase} = \frac{1}{m_{lag,x}} \quad (3.10)$$

where $m_{lag,x}$ is the gradient of the graph t_{lag} versus x .

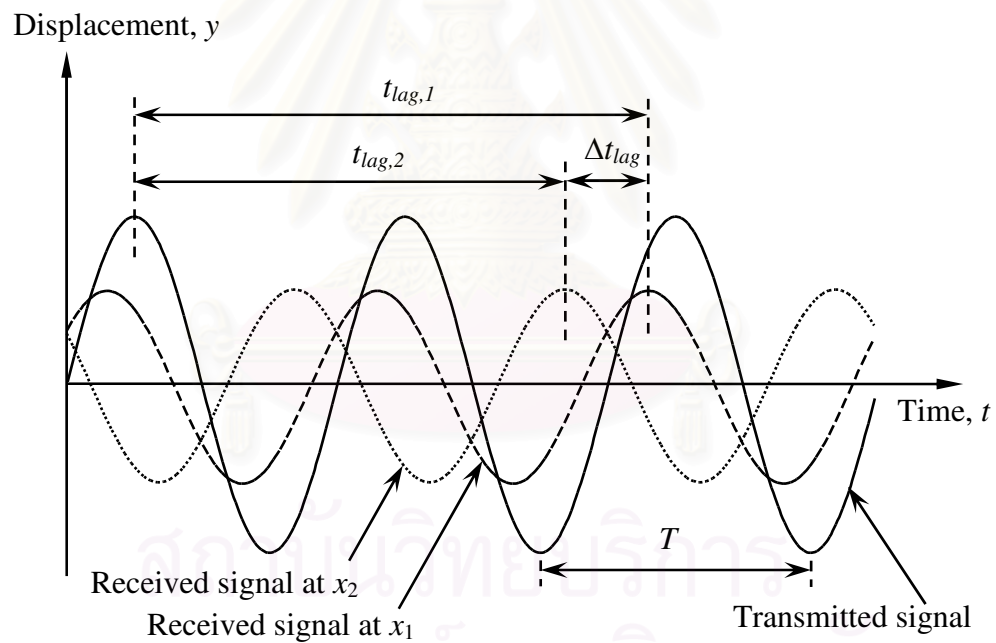
3.4.3 Methodology

To demonstrate the new methodology, a series of experiment was carried out on the reconstituted Kasaoka clay sample. The slurry of Kasaoka clay was preconsolidated under a vertical stress of 70 kPa. The specimen for the BEs test was prepared to be tested in a triaxial apparatus shown in Figure 3.3. The diameter and height of the specimen were 50 and 100 mm, respectively. Prior to the BEs test, the specimen was isotropically consolidated in triaxial apparatus with 300 kPa of cell pressure and 200 kPa of back pressure. The widths of the transmitter and receiver after coating were 21 and 11 mm, respectively. The free lengths of transmitter and receiver after coating and fixing were 9.5 and 15 mm, respectively. The initial embedded lengths of transmitter and receiver BEs into the sample were 9.5 and 5 mm, respectively.

According to Figure 3.9, at position zero, the displacement transducer reading was reset to zero. Then, BEs test was performed using single sine (time domain method) and continuous sine signals (proposed method). After that, the receiver BE was penetrated into the soil sample with a constant rate (0.5 mm/minute) and stopped when it reached the next position. The BEs test was conducted again and followed by the penetration of the BE to the next position. The procedures were repeated until the final position of the receiver BE reached approximately 6 mm. For each position, frequencies of 5, 6 and 7 kHz were employed for both signals. The amplitude of the signal after amplification was ± 50 V. The penetration position of the receiver BE was determined by measuring the movement of the penetration rod with a displacement transducer. During the testing process, the drainage valve was kept open so that no excess pore water pressure would be generated.



(a)



(b)

Figure 3.8 Explanation of wave propagation theory by using continuous sinusoidal wave (a) wave generated at transmitter and captured by a receiver at different positions, (b) signals motion with time for transmitted and received signals.

It is noted that the frequencies of 5, 6 and 7 kHz were used. The frequency combined with the results of V_s determined in the test (Presented in Table 3.3) led to the ratio L/λ to be greater than two. Hence, the near-field effect can be reduced (Arroyo *et al.*, 2003; Sanchez-Salineró *et al.*, 1986).

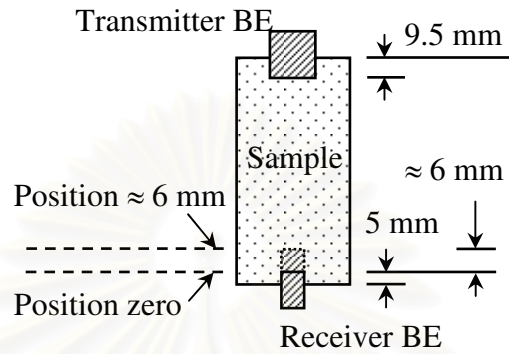


Figure 3.9 Testing procedure for variable-path length method.

3.4.4 Analyses and Discussion

For the proposed method, the primary results which are penetration position and time lag are used to calculate the v_{phase} based on equation (3.10). The acquired signals of transmitted and received at the different position for 7 kHz of frequency are shown in Figure 3.10. To get rid of high frequency noise, the acquired signal is least square fitted with the clean sinusoidal wave. Then, the time lag of each test position is determined.

The time lag obtained from all test positions using frequencies 5, 6 and 7 kHz are plotted in Figure 3.11. The linear fitting line and gradient for each frequency is also shown in this figure. By using the linear line gradient and equation (3.10) the v_{phase} is calculated and shown in Table 3.3.

For time domain method, the V_s is calculated using equation (2.5). The travel distance is based on the tip-to-tip distance and the initial tip-to-tip distance is 83.53 mm. The subsequent tip-to-tip distance when the receiver penetrates to the new position is the difference between the initial reading and the reading of the new position. The travel time is computed using the cross-correlation technique (Viggiani and Atkinson, 1995). Figure 3.12 shows the variations of V_s with the position of receiver. The average V_s calculated for frequencies 5, 6 and 7 kHz are shown in Table 3.3.

By comparing the V_s , the V_s determined by proposed method may not as consistent as compare to the time domain method. The reason is due to the frequency dependency of the v_{phase} . For each frequency, it is noticeable that the v_{phase} is less than the V_s calculated from the time domain method. The reason can be explained using equation (3.5), where the V_s determined from the time domain method is v_{group} . Hence, if the value of dv_{phase}/dk is positive, the v_{phase} should be less than the v_{group} .

Table 3.3 Results from time domain and variable-path length methods.

Frequency (kHz)	Time domain method	Variable-path length method		
	V_s (Average) (m/s)	$m_{lag,x}$ (μ s/mm)	V_s (m/s)	L/λ^*
5	84.6	12.15	82.3	4.7
6	84.2	12.90	77.5	6.0
7	83.9	12.43	80.5	6.7

* L is the tip-to-tip distance when the receiver BE at position 6.006 mm

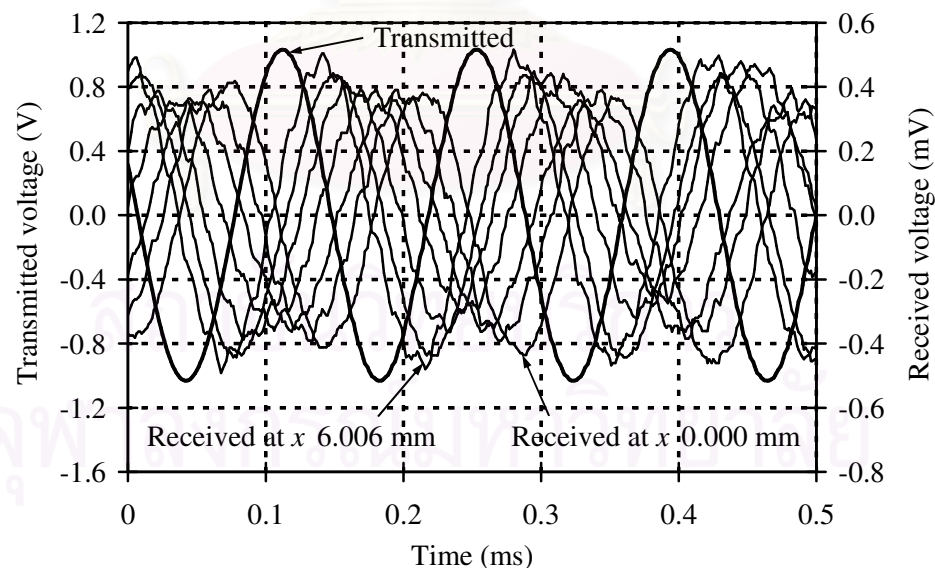


Figure 3.10 Recorded signals of transmitted and received at different positions for 7 kHz of frequency.

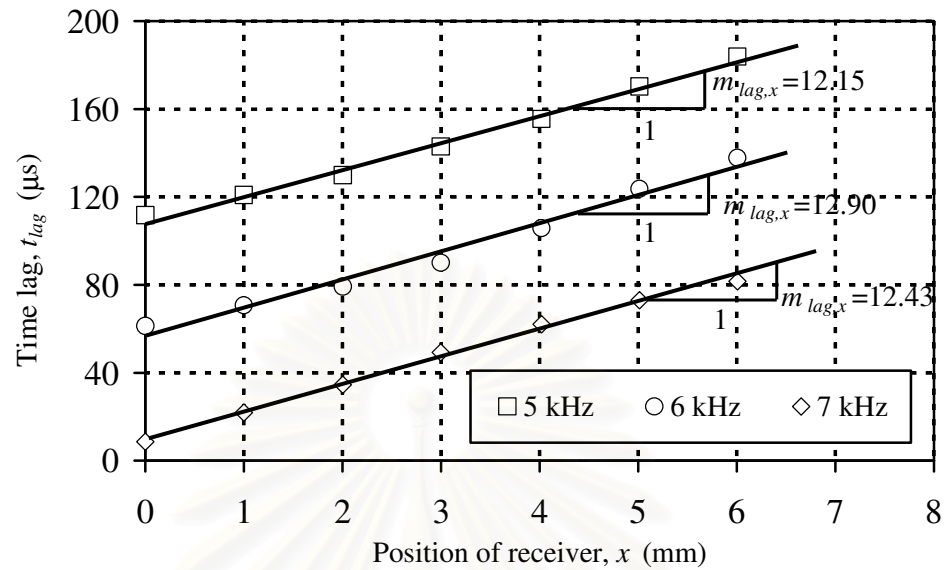


Figure 3.11 Variation of the time lag with positions of receiver determined by variable-path length method.

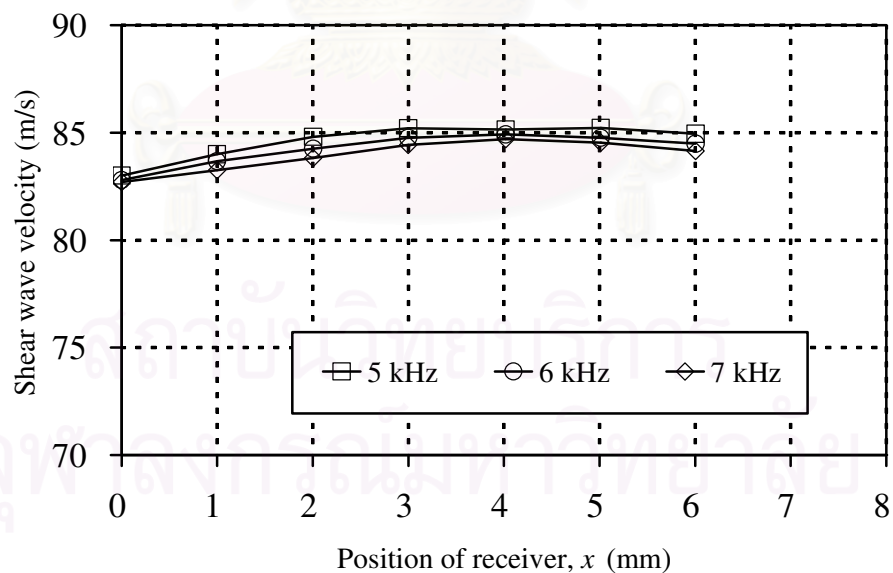


Figure 3.12 Variation of V_s with positions of receiver determined by time domain method.

3.4.5 Summary

The variable-path length method using continuous sinusoidal wave is presented. It is capable of measuring the v_{phase} of shear wave in a clay sample. The proposed method combined with conventional time domain method gives the explicit picture of the relationship between phase and group velocities. The uncertainty caused by the distance measurement can be avoided in the proposed method. The adapted continuous signal yields high signal recovery which is preferable for highly damped soil and in a noisy environment. Since the proposed method can determine v_{phase} at arbitrary frequency, this method should be able to be adopted for studying the frequency dependency of the V_s .

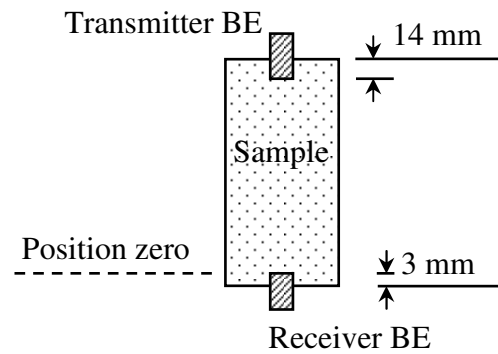
3.5 The Effects of the BE Installation on Shear Wave Velocity Measurement

3.5.1 Background

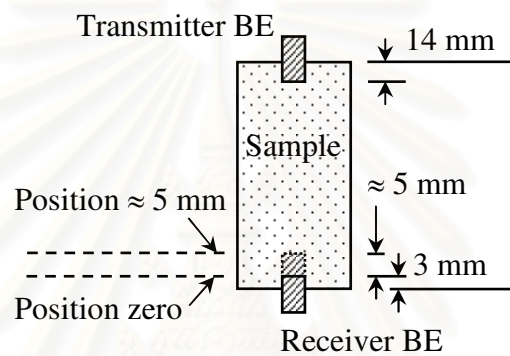
To perform the BEs test, the BE transducers are plugged into both ends of a clay sample as shown in Figure 3.13(a). It is doubtful that the installation of BEs may cause some degrees of disturbance to the clay sample. In this study, the effects of the BE installation on V_s measurement are investigated (Chan *et al.*, 2007). The effects are examined by comparing V_s obtained before and that after the receiver BE is penetrated into the soil sample.

3.5.2 Methodology

A series of experiment was carried out on 8 reconstituted Kasaoka clay samples. The test conditions for the samples are shown in Table 3.4. Triaxial apparatus shown in Figure 3.3 was used in this study. The vertical preconsolidation pressure, σ'_{pc} , for samples 1 to 6 was 70 kPa and that for samples 7 and 8 was 150 kPa. Prior to the BEs test, samples 1 to 8 were isotropically consolidated in triaxial apparatus with 200 kPa of back pressure. For samples 1 to 6, 300 kPa of cell pressure was applied. The cell pressures for samples 7 and 8 were 275 kPa and 250 kPa, respectively.



(a)



(b)

Figure 3.13 Installation of BEs (a) installation of transmitter and receiver BEs at both ends of the sample, (b) penetration of receiver BE into the sample to study the disturbance effects.

The width of the transmitter and receiver after coating was 11 mm. The free length of transmitter and receiver after coating and fixing were 14 mm and 12 mm, respectively. The initial embedded length of transmitter and receiver BEs into the sample were 14 mm and 3 mm, respectively.

At the position zero shown in Figure 3.13(b), a conventional BEs test using 5 kHz of single sine wave was conducted. The amplitude of the signal after amplification was ± 50 V. Then, the receiver BE was penetrated into the soil sample under a constant rate and stopped when it reached the next position. After that, the BEs test was conducted again and followed by penetration of the BE to the next position. The procedures were repeated until the final position of the receiver BE

reached approximately 5 mm. During the testing process, the drainage valve was kept open so that no excess pore water pressure could be generated.

The frequency of 5 kHz combined with the results of V_s determined in the test leads to the ratio L/λ which is greater than two so that the near-field effect can be reduced (Arroyo *et al.*, 2003; Sanchez-Salineró *et al.*, 1986). This will be presented later.

Table 3.4 Test conditions.

Test	σ'_c (kPa)	σ'_{pc} (kPa)	σ'_{mo} (kPa)	\overline{OCR}	D (mm)	H (mm)	Rate of penetration (mm/minute)	L (mm)
Sample 1	100	70	46.7	1	50	100	0.02	81.16
Sample 2	100	70	46.7	1	50	100	0.10	81.22
Sample 3	100	70	46.7	1	50	100	0.50	80.99
Sample 4	100	70	46.7	1	50	100	1.00	81.00
Sample 5	100	70	46.7	1	33	66	0.50	47.45
Sample 6	100	70	46.7	1	40	80	0.50	61.37
Sample 7	75	150	100	1.3	50	100	0.50	82.60
Sample 8	50	150	100	2	50	100	0.50	82.82

σ'_c is effective isotropic consolidation pressure in triaxial apparatus

σ'_{pc} is vertical preconsolidation pressure

σ'_{mo} is mean preconsolidation pressure $\left(\frac{\sigma'_{pc} + 2K_0\sigma'_{pc}}{3} \right)$, assume $K_0 = 0.5$

\overline{OCR} is mean overconsolidation ratio $\left(\frac{\sigma'_{mo}}{\sigma'_c} \right)$

D is diameter of sample before consolidation process

H is height of sample before consolidation process

L is initial tip-to-tip distance when the BEs test was performed

3.5.3 Study of the Disturbance

3.5.3.1 Penetration Test

The primary results from the test are the penetration positions of the rod and the travel time for each position. In this study, the travel distance is taken as the tip-to-tip distance and the initial tip-to-tip distances when the BEs test is performed are shown in Table 3.4. The new tip-to-tip distance for each position of receiver is calculated by deducting the initial tip-to-tip distance from the penetration position of the rod. For this study, the travel time BB' shown in Figure 3.15 is applied to determine shear wave velocities by using equation (2.5).

The disturbance caused by the BE installation is determined by the comparison of the V_s calculated for each position of the receiver BE and the results are plotted and shown in Figure 3.14. For sample 4, data in Figure 3.14(a) clearly show that the shear wave velocities of all positions are almost the same and the variation is only 0.9%. Figure 3.15 reveals the variation of the travel times, BB' , with penetration positions for sample 4. The travel time is getting smaller when the tip-to-tip distance is shorter.

By performing error study on the shear wave velocities occurring on sample 4 ($L = 81.00$ mm and 5.071 mm of penetration), if the travel time is not changed even the tip-to-tip distance is getting shorter, the maximum reduction of calculated V_s will be 6.7%. If disturbance caused by the BE installation occurs, the reduction of V_s should be 6.7% or more. Therefore, the installation of the BEs into the clay sample generates almost no disturbance because the variation of V_s for sample 4 is 0.9%.

The study also supports the research conducted by Viggiani and Atkinson (1995) and Dyvik and Madshus (1985) that the travel distance is determined based on the tip-to-tip distance between BE transducers.

The parametric study for penetration tests by varying the penetration rate, sample size and consolidation pressure is conducted. The results from the study also clarify that the installation of the BEs into the clay sample generates nearly no disturbance because the maximum variation of V_s from the results is less than 2.5%.

3.5.3.2 Parametric Study: Penetration Rate

Samples 1 through 4 are tested under the same condition except the rate of penetration is different for the receiver BE. Table 3.4 shows the penetration rate of each sample. The variation of shear wave velocities with penetration positions for samples 1, 2, 3

and 4 are 2.4%, 2.1%, 0.7% and 0.9%, respectively. It is seen from Figure 3.14(a) that the penetration rate does not affect the test results since the average shear wave velocities are 85.5, 88.1, 86.2 and 86.4 m/s for samples 1, 2, 3 and 4 each. According to the results shown in Figure 3.14(a), the penetration rate of sample 3 which is 0.50 mm/minute is employed for other tests.

3.5.3.3 Parametric Study: Sample Size

The testing conditions are the same for samples 5, 6 and 3, but the diameters and heights of samples are changed. The diameters for samples 5, 6 and 3 are 33, 40 and 50 mm, respectively; the height is two times the diameter of samples. In reference to Figure 3.14(b), the variation of V_s with penetration positions for each sample is about 1.1%, 1.9% and 0.7% for samples 5, 6 and 3. Figure 3.14(b) also shows that the sample size does not affect the test results since the average shear wave velocities for samples 5, 6 and 3 are 83.8, 86.0 and 86.2 m/s, respectively.

3.5.3.4 Parametric Study: Isotropic Consolidation Pressure

The vertical preconsolidation pressure, σ'_{pc} , for sample 3 is 70 kPa and that for samples 7 and 8 is 150 kPa. Prior to the BEs test, samples 3, 7 and 8 are isotropically consolidated with effective stresses of 100, 75 and 50 kPa, respectively. In reference to Figure 3.14(c), the average shear wave velocities decrease with the increase of mean overconsolidation ratio, \overline{OCR} , showing 86.2, 81.8 and 71.5 m/s for samples 3 ($\overline{OCR} = 1$), 7 ($\overline{OCR} = 1.3$) and 8 ($\overline{OCR} = 2$), respectively. The variations of V_s with penetration positions for samples 3, 7 and 8 are 0.7%, 1.9 % and 1.2 %, respectively.

3.5.4 Summary

The penetration tests performed by varying the rate of penetration, size of sample and isotropic consolidation pressure reveal that the installations of BEs into the clay sample generates almost no disturbance. Hence, BEs tests can be easily carried out for clay samples in the laboratory and in the field with nearly no effect of the BEs installation. The testing results also confirm the findings yielded from previous research that the wave propagates from the tip of transmitter to the tip of receiver BE.

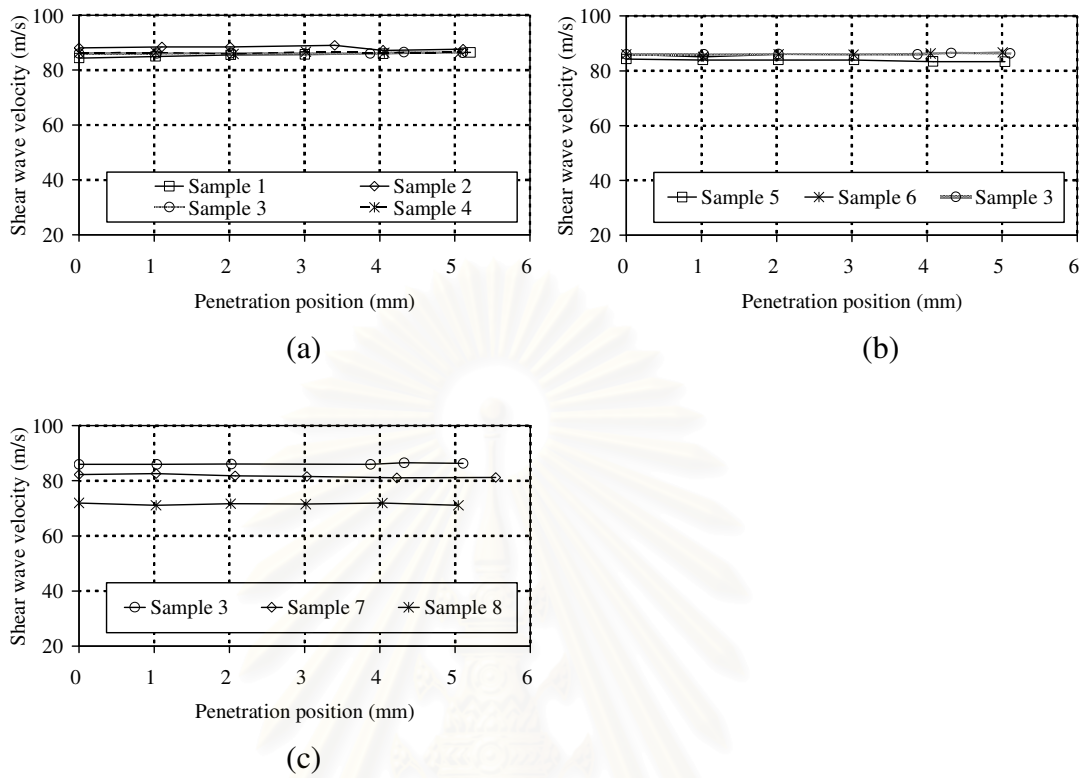
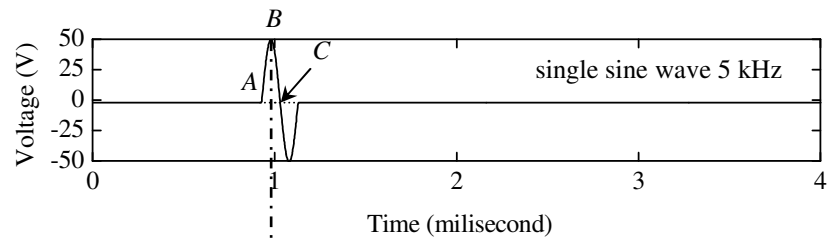
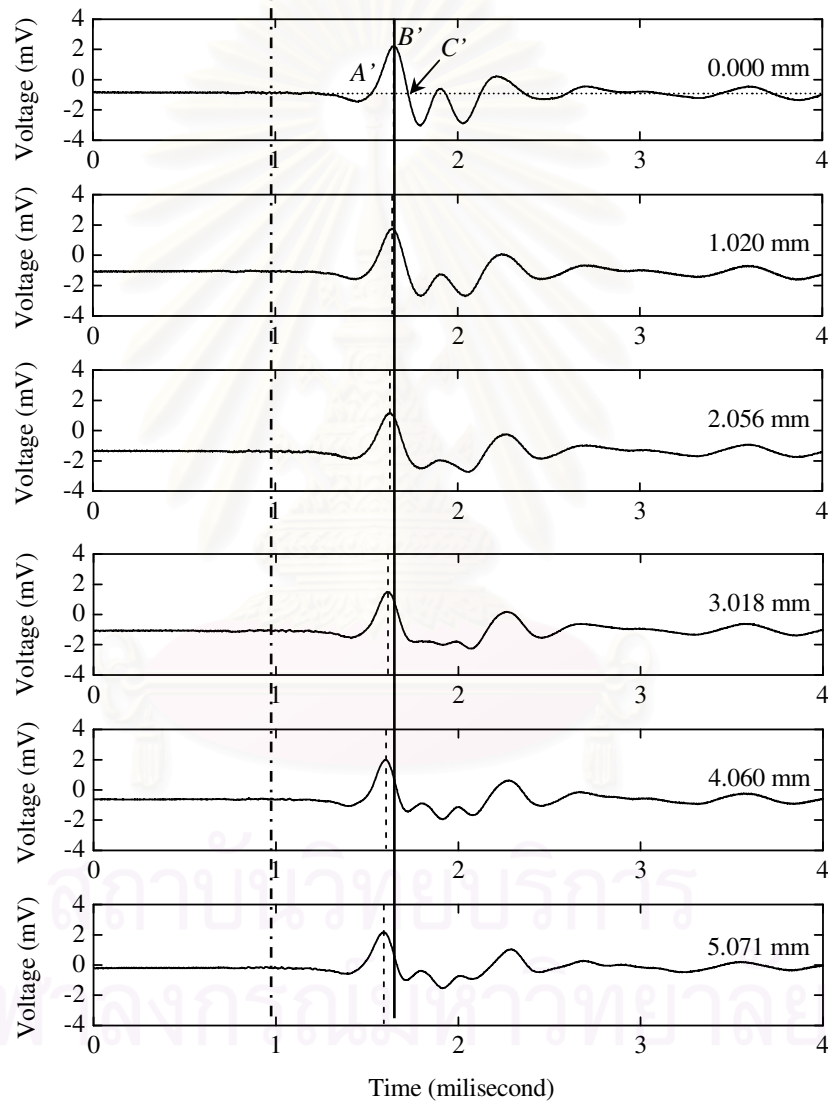


Figure 3.14 Variation of V_s with penetration positions (a) varying the penetration rate, (b) varying the sample size, (c) varying the consolidation pressure.



(a)



(b)

Figure 3.15 Transmitted and received signals for sample 4 (a) transmitted signal, (b) received signals at different positions.

3.6 The Magnitude of Shear Strain Generated by the BEs Test

3.6.1 Background

Generally, the shear strain induced by the BEs test is very small. Therefore, the G determined using BEs test is considered as the G_{max} . Dyvik and Madshus (1985) reported that the maximum shear strain generated by BE is approximately $10^{-3}\%$. Pennington *et al.* (2001) and Leong *et al.* (2005) researches show that the maximum shear strains generated by BE is in the order of $10^{-4}\%$.

The purpose of this study is to evaluate the magnitude of shear strain induced by BEs test (Chan and Boonyatee, 2006). With this regard, a direct measurement of the tip deflection of BEs is made. By calibrating the output signal of self-monitoring circuit (Schultheiss, 1982) with a laser displacement gauge, the deflection of BEs can be determined. Consequently, the particle velocity as well as the magnitude of shear strain can also be derived.

3.6.2 Concept of Shear Strain Calculation

When a vibrating wave travels through a soil body, the vibration energy makes the soil body moves as shown in Figure 3.16. The engineering shear strain, γ , can be calculated (White, 1965) by the following equation:

$$\gamma = \frac{\partial y}{\partial x} = \frac{V_{particle} \cdot dt}{V_s \cdot dt} = \frac{V_{particle}}{V_s} \approx \frac{2A}{\lambda/2} \quad (3.11)$$

where $V_{particle}$ is the particle velocity. It is obvious from equation (3.11) that if the values of $V_{particle}$ or $2A$ and V_s or $\lambda/2$ are known, then, the magnitude of the γ can be calculated. The V_s can be determined by various approaches such as the pulse method. A non-trivial aim of this study is finding an appropriate method to determine the value of $V_{particle}$.

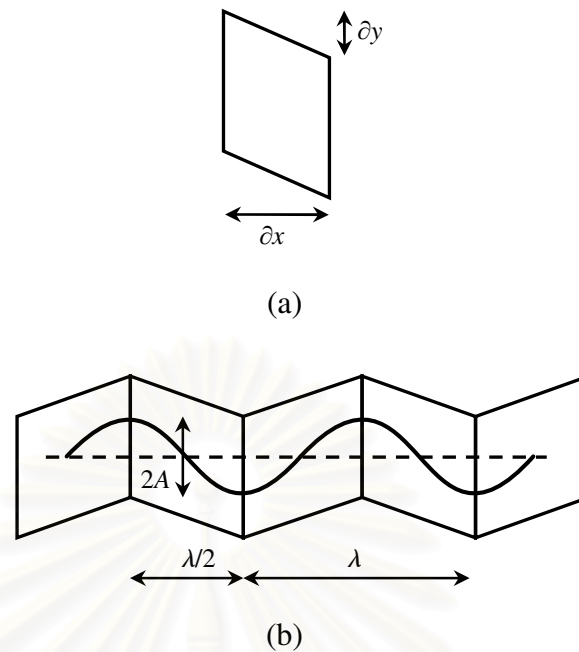


Figure 3.16 Movement of soil continuum forced by vibration energy (a) one element, (b) continuum elements.

3.6.3 Calibration of BEs Displacement

In order to utilise equation (3.11) for determining the γ , it is necessary that the tip displacement or $V_{particle}$ in the transverse direction be measured. Equation (3.1) shows that the relationship between the displacement and input voltage is linear for the parallel type BE. When BEs protrude into soil samples, the input voltage does not produce the same displacement calculated by equation (3.1) due to restraint from various factors such as the stiffness of the epoxy coating, the stiffness of the soil, the method of installation of BE to the base, etc. Therefore, instead of using equation (3.1) to calculate the displacement, a calibration process is performed by using self-monitoring signal of BE (Schultheiss, 1982) and a laser displacement gauge.

To calibrate the electrical voltage of the self-monitoring signal against the real movement of a BE, a laser displacement gauge is adopted as shown in Figure 3.17. The laser displacement gauge (KEYENCE, LC-2430) is a high accuracy, non-contact device which has a response frequency and resolution of 20 kHz and 0.02 μm , respectively. Since the electrical energy generated by the BEs is small and dissipates rapidly, the calibration must be done dynamically with a continuous voltage input to the BEs. Hence, a continuous sinusoidal signal is sent to the BEs with a constant

frequency and input voltage. Frequencies from 1 to 7 kHz are used to investigate the effect of frequency to the BE displacement. For each frequency, the input voltage applied is increased so that the linear relationship between BE displacement and self-monitoring signal can be obtained.

The data determined from the calibration process are self-monitoring voltage and displacement of BEs (from the laser displacement gauge) for the corresponding frequency and input voltage. These data are plotted and shown in Figure 3.18 to demonstrate the linear relationship. It can be noted that the gradient of the plots becomes smaller when the frequency is increased. However, for the receiver BE, the gradient for frequencies 3 and 4 kHz show a smaller value compared to frequencies 5, 6 and 7 kHz. The gradient of slope, m , determined from linear line fitting for each plot of frequency is shown in Table 3.5.

From the calibration process, the linear equation between BE displacement or transverse displacement, y , and self-monitoring voltage is

$$y = m \cdot (\text{self-monitoring voltage}) \quad (3.12)$$

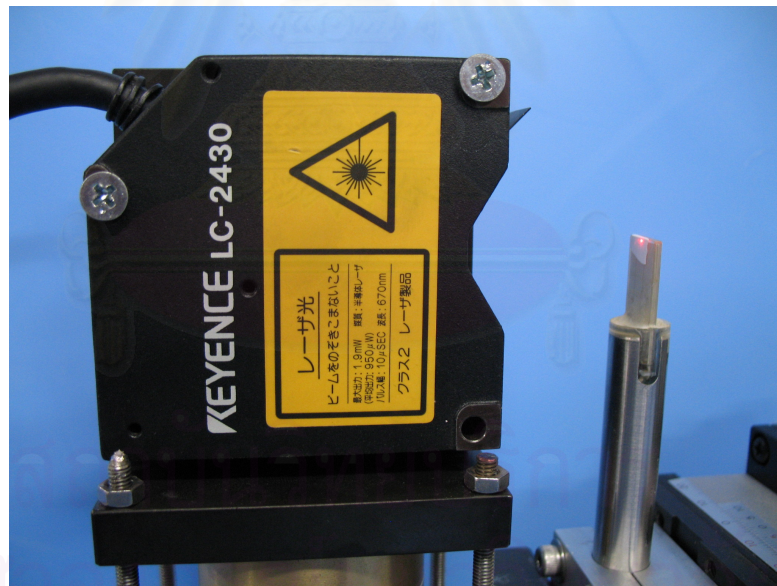
By measuring the self-monitoring signal and employing equation (3.12) by using the corresponding slope gradient, m , the transverse displacement near the BE in the soil sample can be calculated. Consequently, the particle velocity can be obtained from the differential of transverse displacement with time.

Table 3.5 The gradient of slope calculated from linear line fitting of BEs displacement calibration process.

Frequency (kHz)	Transmitter	Receiver
	Gradient of slope m_t (m/V)	Gradient of slope m_r (m/V)
1	3.867×10^{-5}	2.485×10^{-5}
2	3.841×10^{-5}	4.020×10^{-6}
3	2.200×10^{-5}	2.000×10^{-6}
4	1.073×10^{-5}	2.090×10^{-6}
5	7.450×10^{-6}	3.060×10^{-6}
6	4.190×10^{-6}	3.200×10^{-6}
7	2.300×10^{-6}	3.400×10^{-6}

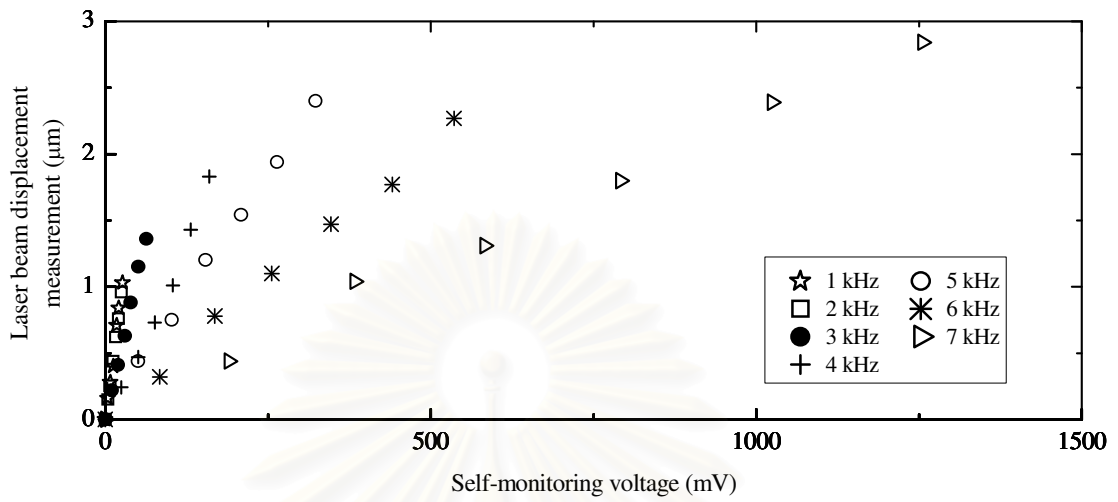


(a)

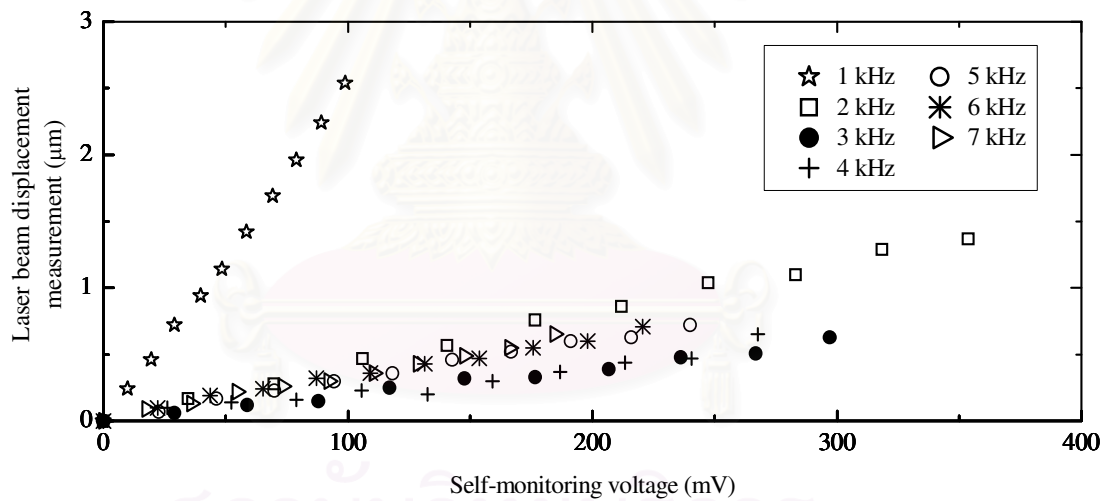


(b)

Figure 3.17 Measurement method to determine the displacement of BEs by using a laser displacement gauge (a) transmitter, (b) receiver.



(a)



(b)

Figure 3.18 Plot of laser beam displacement measurement versus BE self-monitoring voltage (a) transmitter, (b) receiver.

3.6.4 Methodology

A series of experiment was carried out on a reconstituted Kasaoka clay sample. The slurry of Kasaoka clay was preconsolidated under a vertical stress of 70 kPa. After that, the sample for BEs test was prepared to be tested in a triaxial apparatus shown in Figure 3.3. The diameter and height of the specimen were 50 and 100 mm, respectively. Prior to the BEs test, the specimen was isotropically consolidated in triaxial apparatus with 300 kPa of cell pressure and 200 kPa of back pressure.

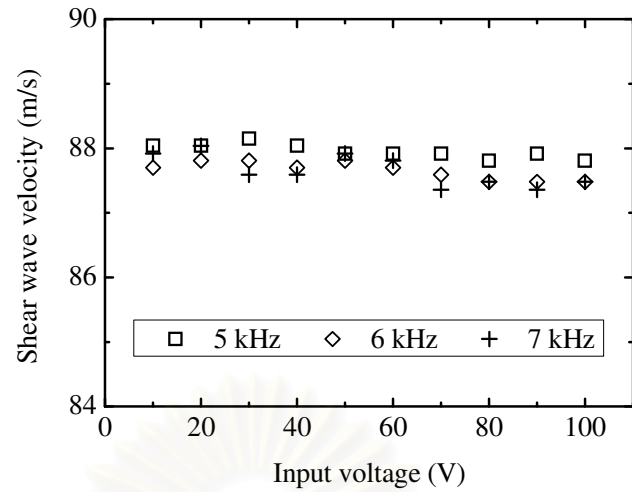
The widths of the transmitter and receiver after coating were 21 and 11 mm, respectively. The free lengths of transmitter and receiver after coating and fixing were 7.3 and 15 mm, respectively. The embedded lengths of transmitter and receiver BEs into the sample were 7.3 and 5 mm, respectively.

Single sine signal was utilised as the driving signal. To simulate various strains condition, frequencies of 5, 6 and 7 kHz were employed for single sine signals. For each frequency, the input voltage applied was increased from ± 10 V to ± 100 V. After the BEs tests completed, the specimen was isotropically consolidated again by increasing the cell pressure to be 500 kPa while keeping the back pressure to be 200 kPa. At the end of primary consolidation, the BEs tests performed earlier were repeated. The self-monitoring signals for the transmitter and receiver BEs were acquired by the NI 6120 card.

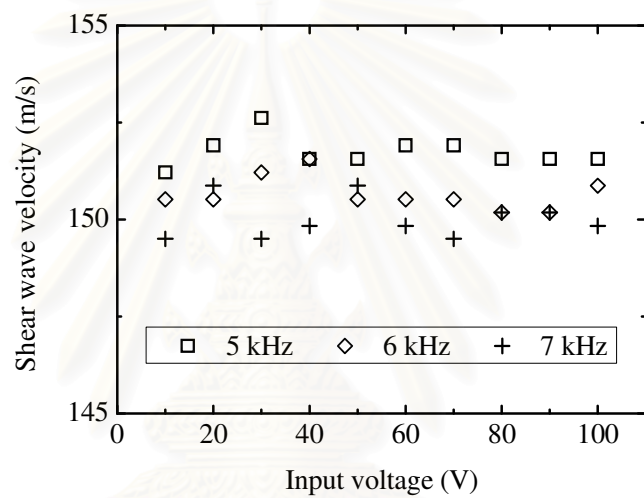
It is noted that the frequencies of 5, 6 and 7 kHz are used. The frequency combined with the results of V_s determined in the test leads to the ratio L/λ to be greater than two so that the near-field effect can be reduced (Arroyo *et al.* 2003; Sanchez-Salineró *et al.* 1986).

3.6.5 Calculation of Shear Wave Velocity

The V_s is computed by using equation (2.5). The cross-correlation method proposed by Viggiani and Atkinson (1995) is used to determine the travel time. The tip-to-tip distance for 100 and 300 kPa of isotropic consolidation pressure are 85.94 and 82.41 mm. The shear wave velocities calculated are plotted and shown in Figure 3.19. This figure reveals that the V_s of each frequency is almost constant even when the input voltage is increased. The maximum variation of V_s for 100 and 300 kPa of isotropic consolidation pressure is not more than 1%. The average V_s for 100 and 300 kPa of isotropic consolidation pressure are 87.76 and 150.80 m/s, respectively.



(a)



(b)

Figure 3.19 Variation of V_s versus input voltage (a) 100 kPa of isotropic consolidation pressure, (b) 300 kPa of isotropic consolidation pressure.

3.6.6 Calculation of Particle Velocity

The primary data from the BEs test are the transmitted and received self-monitoring signals. These signals can be used to calculate the $V_{particle}$ near BEs. The derivation of $V_{particle}$ for transmitted self-monitoring signal for ± 50 V input voltage and 5 kHz of frequency at 100 kPa of isotropic consolidation pressure is shown in Figure 3.20. The signals from BEs test are plotted in the graph of voltage versus time and the data are converted to transverse displacement by using equation (3.12) with the corresponding slope gradient, m_t . Then, the $V_{particle}$ can be determined by differentiating the displacement curve with time. Point A in the graph of $V_{particle}$ versus time is the

maximum particle velocity, $V_{max,particle}$, which is used for the γ calculation. The $V_{particle}$ near the transmitter and receiver for all the testing conditions is computed.

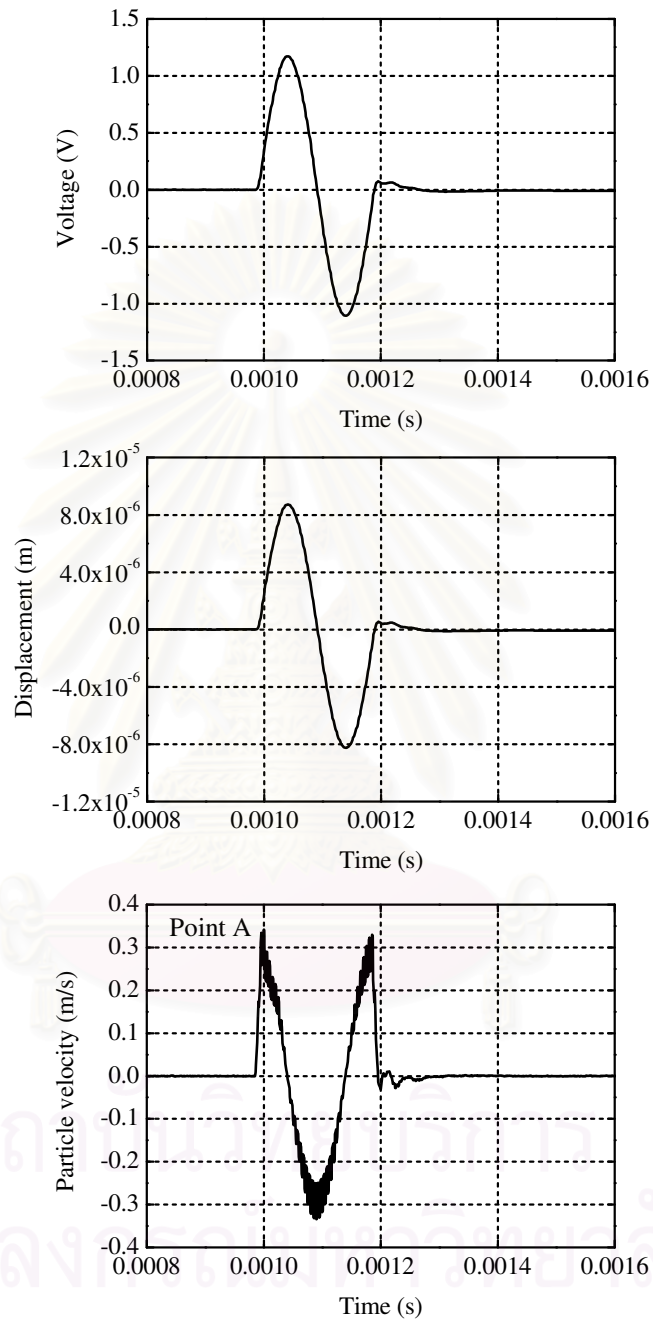


Figure 3.20 Derivation of $V_{particle}$ from transmitted self-monitoring signal for ± 50 V input voltage and 5 kHz of frequency at 100 kPa of isotropic consolidation pressure.

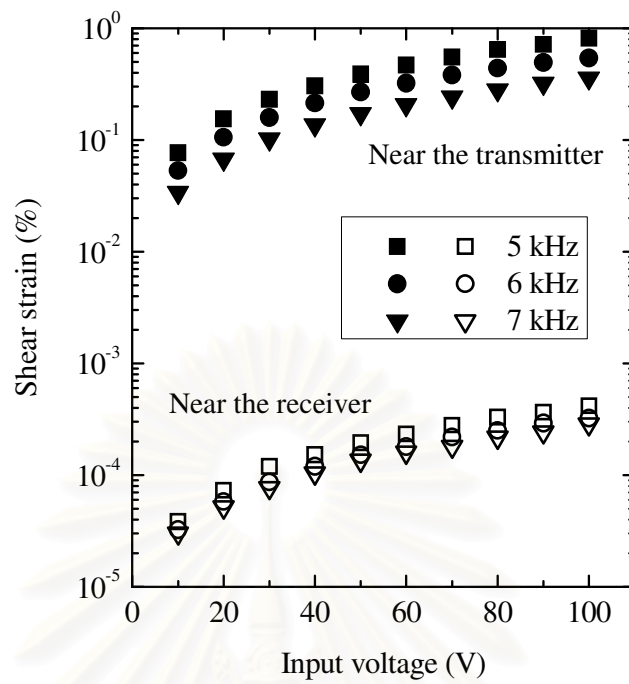
3.6.7 Calculation of Shear Strain

The γ is determined by using equation (3.11) which is the ratio between the $V_{max,particle}$ and V_s . The shear strains determined are plotted and shown in Figure 3.21. The results show that the γ increases when the input voltage is increased. The increase of γ is about 1 cycle of log scale for ± 90 V of increment of input voltage. It is noted that the ratios between γ near the transmitter and receiver are almost constant for all the input voltages with the corresponding frequency and isotropic consolidation pressure.

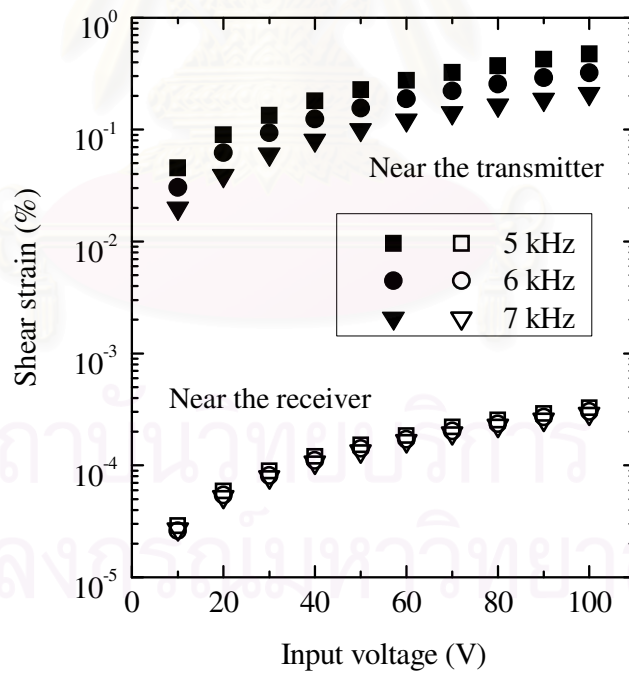
When the isotropic consolidation pressure is increased from 100 to 300 kPa, the stiffness of the soil increases and as a result the V_s also increases. However, it is found that the $V_{particle}$ is also increased in the same proportion. Therefore, the γ calculation is not affected by the isotropic consolidation pressure as shown in Figure 3.21.

The maximum shear strains near the transmitter and receiver are $10^{-1}\%$ and $10^{-4}\%$, respectively. The shear strains level near the transmitter ($10^{-1}\%$) is classified in the intermediate strains region (Atkinson and Salfors, 1991). This means that the stiffness or V_s is decreasing when the γ or input voltage increases. However, Figure 3.19 shows that the V_s does not decrease when the input voltage increases. This means the γ computed near the transmitter BE cannot be considered as the shear strains level generated by the BEs test.

Reference is made to Figure 3.19. The shear wave velocities determined are relatively constant although the γ increases about 1 cycle of log scale when the input voltage increases. Therefore, the 'average' γ in BEs test should still be in the very small strains region. Although the exact value cannot be identified and bracketed between $10^{-1}\%$ and $10^{-4}\%$, the authors believe that the induced γ may decrease significantly within a few distance away from the transmitter BE. Therefore, the magnitude of γ in BEs test shall be represented by the value near the receiver ($10^{-4}\%$) which means the stiffness or V_s is relatively large and constant. Pennington *et al.* (2001) state that the tip deflection for mini BEs is approximately $0.3 \mu\text{m}$ and this value is used for estimating maximum shear strains which is in the order of $10^{-4}\%$. Leong *et al.* (2005) indirectly determine the tip deflection of BE using the piezoelectric constant and report that the maximum shear strain value is in the order of $10^{-4}\%$. The finding from this study based on the direct measurement of tip deflection of BE is similar to the finding reported by Pennington *et al.* (2001) and Leong *et al.* (2005).



(a)



(b)

Figure 3.21 Variation of γ versus input voltage (a) 100 kPa of isotropic consolidation pressure, (b) 300 kPa of isotropic consolidation pressure.

3.6.8 Summary

In this section, a deterministic approach for evaluating the magnitude of γ in the BEs tests is presented. A laser displacement gauge and self-monitoring circuit are used in the calibration process to circumvent the effect of epoxy coating and soil stiffness.

Conclusions made from this study are:

1. The magnitude of induced γ is not affected by the isotropic consolidation pressure.
2. The maximum γ near the transmitter and receiver are $10^{-1}\%$ and $10^{-4}\%$, respectively.
3. The V_s is relatively constant even when the magnitude of induced γ increases.
4. The ratios between shear strains near the transmitter and receiver are almost constant for all the input voltages with the corresponding frequency and isotropic consolidation pressure.
5. The magnitude of γ for BEs tests shall be represented by the maximum γ near the receiver BE which is $10^{-4}\%$.

CHAPTER IV

SHEAR WAVE VELOCITY DETERMINATION BASED ON TIME DOMAIN METHOD

4.1 Shear Wave Velocity Determination Based on Swept Signal

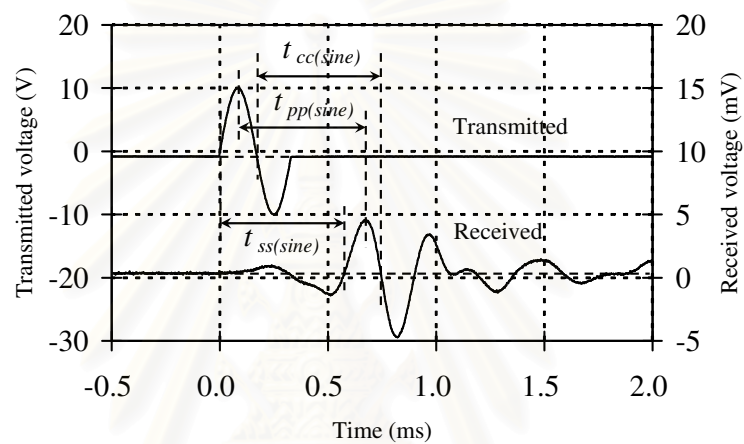
4.1.1 Background

In general, the signals used for calculating the travel time are single sine wave or step wave. Although both signals are used, the determination of the exact point of the arrival signal is still in need of engineering judgement. To address this uncertainty, the typical transmitted and received signals for single sine and step waves are shown in Figure 4.1. In this figure, it is still not clear which travel time should be used in order to obtain the most appropriate V_s .

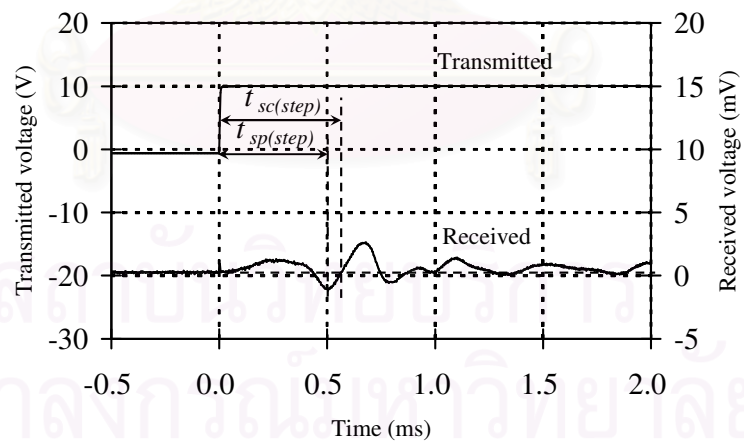
Before the single sine wave is introduced, the step wave has been generally used as the signal. From Figure 4.1(b) when the step wave is used, it is doubtful whether the travel time is $t_{sp(step)}$ or $t_{sc(step)}$. According to Viggiani and Atkinson (1995), for simple analyses the travel time $t_{sp(step)}$ can be applied to calculate V_s and may cause the overestimation of the G of up to about 14%. Dyvik and Madshus (1985) used the travel time $t_{sp(step)}$ to determine the V_s . A research study conducted by Arroyo *et al.* (2003) yielded findings namely step wave travelled in the normalised distance $L/\lambda = 2.5$, and the travel time $t_{sp(step)}$ point gave almost 30% of the maximum peak. Based on their criterion, to successfully identify the first arrival time, peaks below 10% of the maximum peak were ignored. For the step wave, they mentioned that the normalised distance of $L/\lambda = 9$ was needed to achieve the criterion. Findings of a study performed by Blewett *et al.* (1999) confirmed that $t_{sp(step)}$ might not correspond to the absolute time of flight. Lohani *et al.* (1999) and Kawaguchi *et al.* (2001) suggested that the travel time could be taken as $t_{sc(step)}$.

Viggiani and Atkinson (1995) proposed the use of single sine wave to overcome the uncertainty occurring in using the step signal. In their study, they suggested that cross-power spectrum and cross-correlation methods could be used to determine the accurate travel time. Typical transmitted and received signals for the single sine wave are shown in Figure 4.1(a). Brignoli *et al.* (1996) used the travel time $t_{ss(sine)}$ to

compute the V_s . The travel time between characteristic peaks of transmitted and received signals, $t_{pp(sine)}$ was studied by Viggiani and Atkinson (1995) and Arulnathan *et al.* (1998). Lohani *et al.* (1999) proposed that the time $t_{cc(sine)}$ gave less errors compared to $t_{pp(sine)}$ when it was used for calculating V_s . Distortion caused by near-field effects still occurred when using the single sine wave. Therefore, Jovicic *et al.* (1996) introduced distorted single sine wave. Arroyo *et al.* (2003) reported that when single sine and distorted single sine waves travelled in the normalised distance $L/\lambda = 2.5$, the initial bumps were 10% and 5% of the maximum peak, respectively.



(a)



(b)

Figure 4.1 Typical transmitted and received signals for (a) single sine wave, (b) step wave.

In recent years, many techniques have been suggested to determine the travel time. Blewett *et al.* (1999) proposed the phase-sensitive detection technique. Greening and Nash (2004) suggested the π -point phase comparison method which was the frequency domain technique. Arulnathan *et al.* (1998) and Lee and Santamarina (2005) presented the multiple reflection signals technique in which the reflection signals were detected using the same bender element.

In this research study, the swept wave which is adopted from the radar technology (Smith, 1999) is proposed as an alternative signal (Boonyatee and Chan, 2006). It is used in determining the travel time for calculating the V_s . The cross-correlation technique is employed in the proposed signal to gain a clear maximum peak. To validate the application of cross-correlation technique to the swept wave, a study is carried out comparing with the single sine wave and step wave. The purpose of this study is to demonstrate that the swept wave can be used to determine the travel time.

4.1.2 Swept Signal Theory

The swept signal is made by linearly increasing the frequency of contiguous waves in a wave train. There are three parameters needed to derive the signal. They are initial frequency, f_o , bandwidth, Δf , and target time, t_{target} . The swept signal can be generated using the following equations:

$$y = A \sin(\omega t) \quad (4.1)$$

where,
$$\omega = 2\pi \left(f_o + \frac{t}{t_{target}} \Delta f \right)$$

The typical transmitted and received signals when using the swept wave are shown in Figure 4.2. By applying cross-correlation technique, the weak and lengthy swept waveform can be transformed into a clear maximum peak as shown in Figure 4.3.

Figure 4.3 shows the cross-correlation between transmitted and received signals for the swept wave ($f_o = 500$ Hz, $\Delta f = 1.5$ kHz and $t_{target} = 10$ ms) and single sine wave with 2 kHz of frequency ($f = 2$ kHz). The travel time is located at the peak of the cross-correlation signals, an error may occur when reading the peak of the single sine

cross-correlation signal because the peak of the correlated signal seems uniform. However, the error can be reduced if the width of the correlated signal is compressed to form a clear maximum peak using the swept signal.

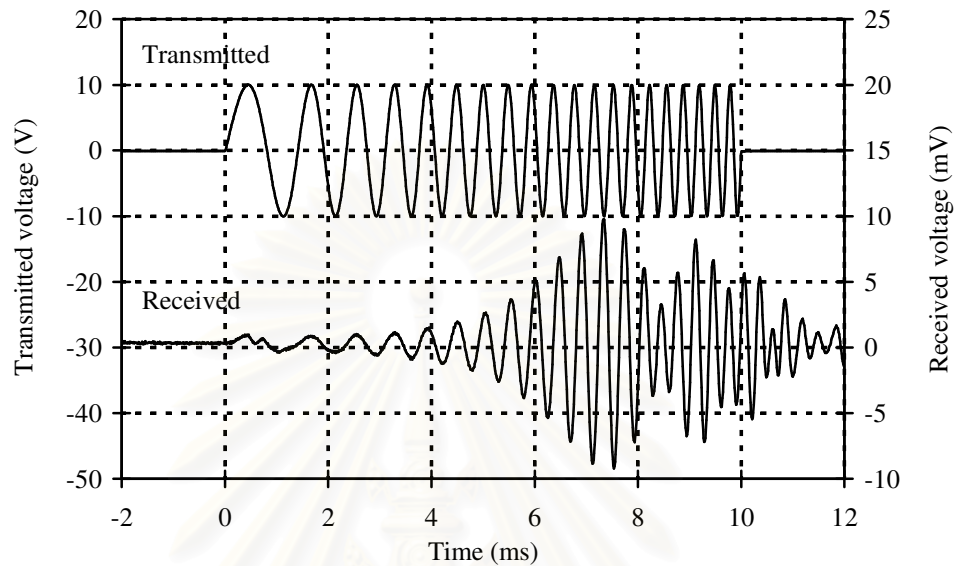


Figure 4.2 Typical transmitted and received signals for a swept wave.

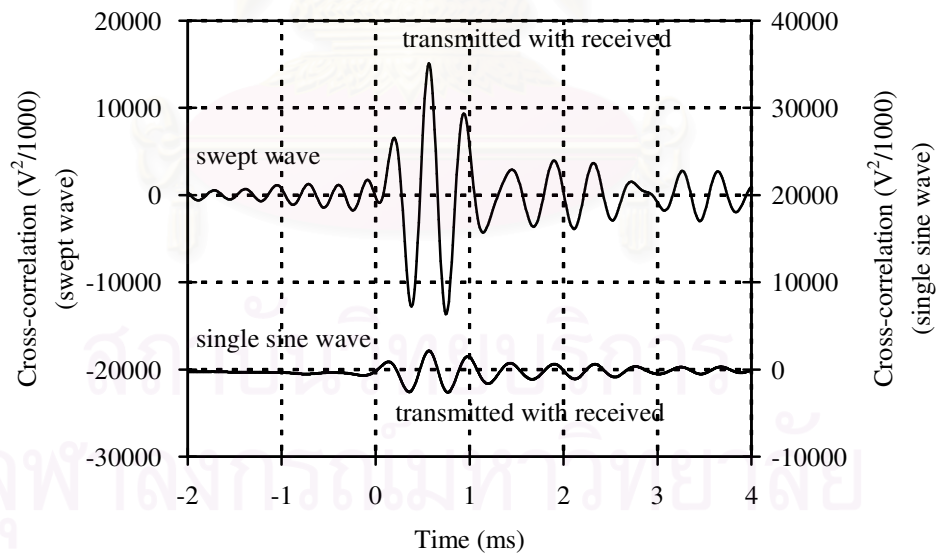


Figure 4.3 Cross-correlation between transmitted and received signals for a swept wave ($f_0 = 500$ Hz, $\Delta f = 1.5$ kHz and $t_{target} = 10$ ms) and single sine wave ($f = 2$ kHz).

4.1.3 Methodology

A series of experiment was carried out on three samples as shown in Table 4.1. Sample 1 was tested in a modified consolidometer. Both a transmitter and receiver were embedded 5 mm in the sample. The schematic view of BEs test arrangement for the consolidometer is the same as shown in Figure 3.3 except that the triaxial apparatus is replaced with the consolidometer. Prior to the test, the sample was consolidated under a vertical pressure of 56 kPa. Samples 2 and 3 were tested by using the triaxial apparatus as shown in Figure 3.3. The transmitter and receiver of the BEs were embedded 14 mm and 3 mm in the sample, respectively. Prior to the test, the samples were isotropically consolidated with 300 kPa of cell pressure and 200 kPa of back pressure. The diameter of the modified consolidometer and triaxial test samples were 48 mm and 50 mm, respectively.

Table 4.1 Description of tested soils.

Test	Soil type	Depth of borehole (m)	σ'_{pc} (kPa)	Diameter of sample ¹ (mm)	Height of sample ¹ (mm)	Tip-to-tip distance ² (mm)
Sample 1	Bangkok clay	5	-	48	45	32.63
Sample 2	Reconstituted Kasaoka clay	-	70	50	75	56.40
Sample 3	Reconstituted Kasaoka clay	-	70	50	100	81.26

σ'_{pc} - vertical preconsolidation pressure

¹before consolidation process

²after consolidation process

Three types of signals were used as the transmitted signal. The first signal generated was the swept wave and followed by the single sine and step waves. Configuration test was carried out for the swept and single sine waves. For the swept wave, a different initial frequency, f_0 , was used for the test where the value was from 500 Hz to 2 kHz. For each initial frequency, the Δf of the signal was increased from 1.5 to 10 kHz with 10 ms of the target time. When generating the single sine wave,

the frequency was increased in steps over a range of 1.5 to 10 kHz. The input voltage for the step wave is 10 V. The input voltage for swept and single sine waves is ± 10 V.

4.1.4 Analyses and Discussion

Equation (2.5) is used for calculating the V_s . The tip-to-tip distances of the samples during testing are shown in Table 4.1. The travel times $t_{pp(sine)}$, $t_{cc(sine)}$, $t_{sp(step)}$ and $t_{sc(step)}$ proposed by previous researchers are used in the validation study (Figure 4.1).

Cross-correlation technique is used to determine the travel time for the swept signal. Figure 4.4 shows the typical cross-correlation signals for the transmitted and received signals from the swept wave. The correlation signal on the left hand side is obtained by correlating the transmitted signal with itself and correlation signal on the right is achieved by correlating the transmitted with the received signals. The travel time is measured between the two peaks of the cross-correlation signals as shown in Figure 4.4. The travel time, $t_{(swept)}$, is used for calculating the V_s for all the configurations and the results are presented in Figure 4.5.

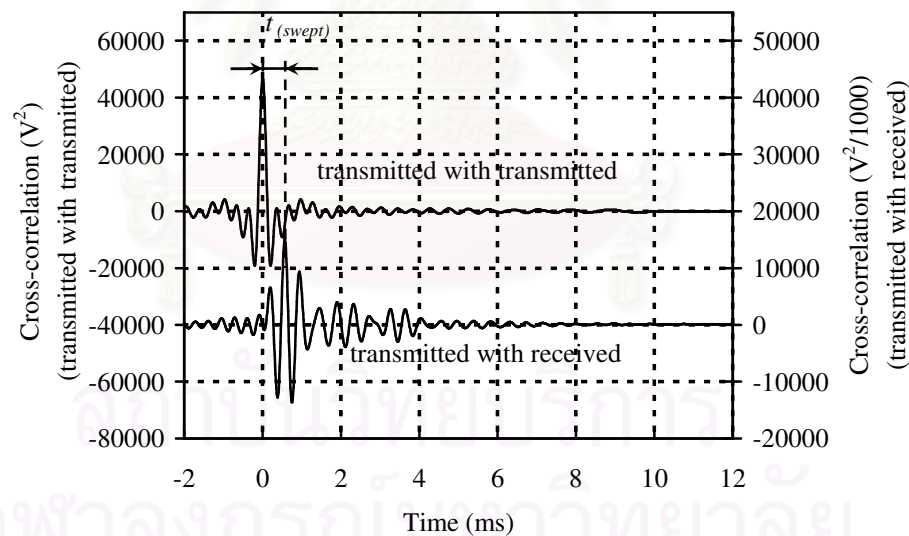


Figure 4.4 Typical cross-correlation signals from the transmitted and received swept wave shown in Figure 4.2.

According to Figure 4.5, the shear wave velocities calculated approach a constant, V_s , for each sample. The V_s variations of samples 1, 2 and 3 are about 7.7%, 3.4% and 2.3% respectively. The initial frequency and bandwidth of the swept wave are not the main criteria to create a graph that shows convergence. From the present

results, small f_o , and Δf can be used to determine the V_s with the error not exceeding 8% because using higher f_o and Δf requires the higher resolution of a signal generator and sampler. The convergence V_s for samples 1, 2 and 3 are 54.66, 77.13 and 85.31 m/s, respectively. These velocities are employed for the validation study.

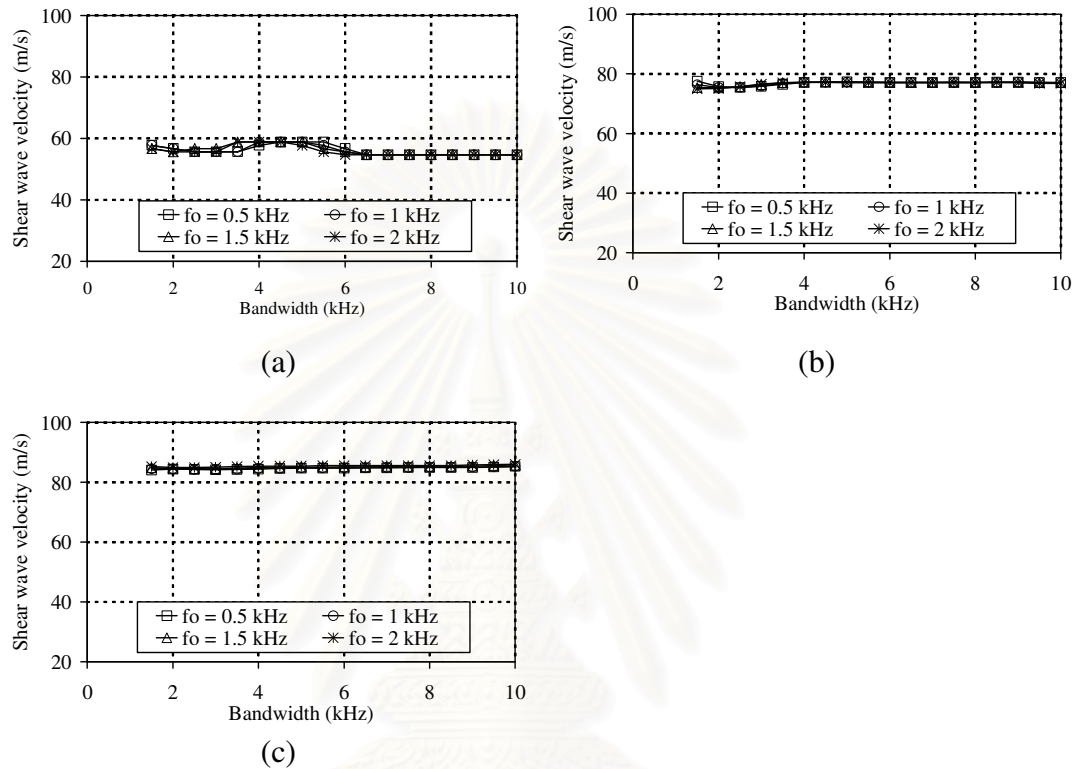


Figure 4.5 Variation of shear wave velocity with bandwidth for the swept wave at different initial frequency (a) sample 1, (b) sample 2, (c) sample 3.

To validate the results of swept wave by comparing to those of the single sine wave, the travel times $t_{pp(sine)}$ and $t_{cc(sine)}$ are used in determining the V_s . The shear wave velocities calculated are plotted and shown in Figure 4.6. The horizontal line represents the convergence V_s determined from Figure 4.5. The shear wave velocities calculated by using $t_{pp(sine)}$ and $t_{cc(sine)}$ are close to the horizontal line with average errors of 1.0%, 0.2% and -0.3% for samples 1, 2 and 3, respectively.

For the step wave, the travel times $t_{sp(step)}$ and $t_{sc(step)}$ are used in the validation analyses. The V_s calculated using $t_{sp(step)}$ overestimates the V_s calculated by the swept wave about 19.1%, 11.6% and 9.9% for samples 1, 2 and 3, respectively. However,

the errors of V_s determined by using $t_{sc(step)}$ compared to those by using the swept wave are as small as 5.6%, 2.3% and -1.2% for samples 1, 2 and 3, respectively.

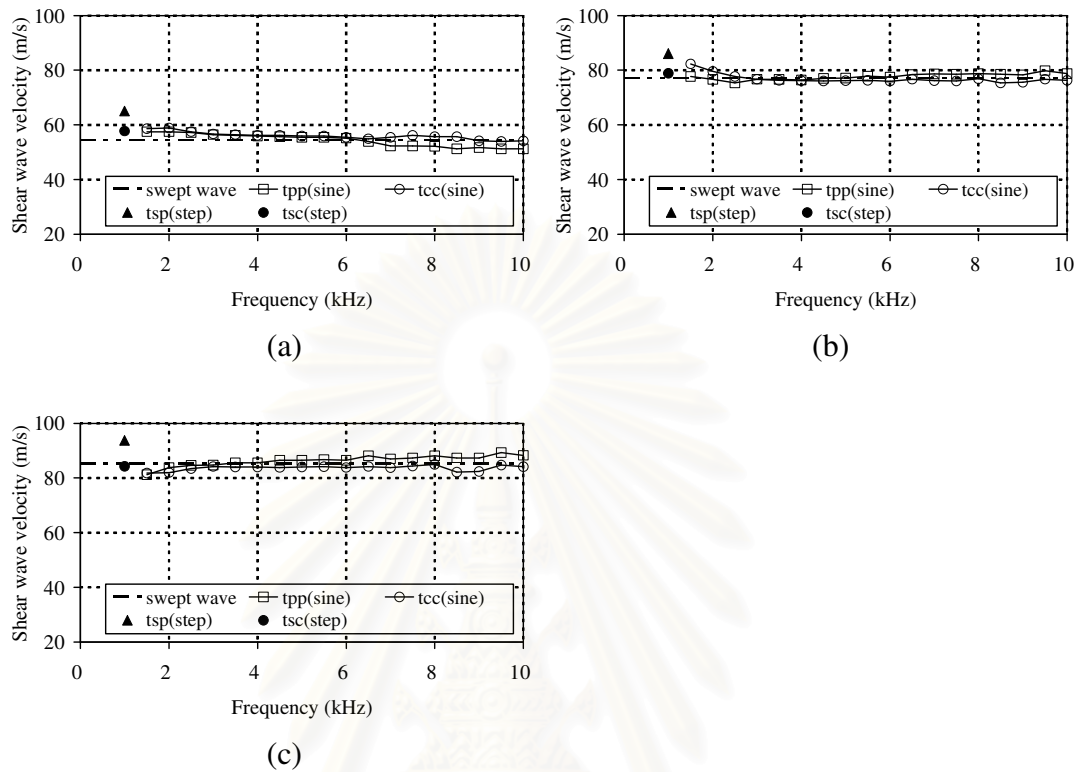


Figure 4.6 Variation of shear wave velocity with frequency for the single sine wave and step wave calculated based on different travel time (a) sample 1, (b) sample 2, (c) sample 3.

4.1.5 Summary

From the validation study, it is found that the V_s determined by using $t_{(swept)}$ is close to the travel time reported by previous researchers. Therefore, the primary finding of this research study demonstrates that the swept wave can be used as an alternative signal for the measurement of V_s with a laboratory modified consolidometer and triaxial test. In a noisy environment, the cross-correlation technique can transform the weak and long stimulating swept wave into a clear maximum peak for easy determination of the travel time.

4.2 Regeneration of Received Signal Based on the BEs Test by Using the Swept Signal

4.2.1 Background

Santamarina and Fam (1997) and Blewett *et al.* (2000) mentioned the linearity of testing apparatus. Santamarina and Fam (1997) pointed out that frequency response of the system could be identified by impulse, white noise or frequency sweep excitation. This means that received wave for any transmitted signal can be obtained by the convolution of impulse response with transmitted signal in time domain or product of frequency response and transmitted signal in frequency domain. An experimental technique to identify frequency response using the swept signal, calculation of received wave for various frequency and comparison with observed waveform are described in this study. The advantage of using the swept signal in addition to use the conventional signals is suggested.

4.2.2 System of the BEs Test

BEs testing system can be interpreted as a linear system of which transmitted and received wave are input and output, respectively. Blewett *et al.* (2000) and Lee and Santamarina (2005) described that BEs testing system is composed of linear subsystems each of which should independently be determined by characteristics of transmitter and receiver BEs and soil specimen. Santamarina and Fam (1997) mentioned that output of the system is represented by a damped, single-degree-of-freedom system subjected to forced vibration. Blewett *et al.* (2000) also suggested that the system is comprised of transmitter and receiver BEs of which response follows harmonic oscillation and a soil sample of which response is in a manner of Biot medium. Hence, the output of the system should be a function governed by the input and dynamic property of the system. Assuming linearity of the system, the output of the system for arbitrary input is represented convolution integral given by equation (4.2).

$$y(t) = \int_0^t x(s) z(t-s) ds \quad (4.2)$$

where, s is a parameter, $y(t)$ and $x(t)$ are output and input, respectively and $z(t)$ is impulse response of the system, which is equivalent to output for an impulse input. In frequency domain, equation (4.2) which is represented in time domain can be represented in more simple expression given by equation (4.3).

$$Y(f) = X(f).Z(f) \quad (4.3)$$

where, $Y(f)$ and $X(f)$ are Fourier transform of $y(t)$ and $x(t)$, respectively and $Z(f)$ is frequency response function, which is equivalent to Fourier transform of impulse response $z(t)$. In equations (4.2) and (4.3), $z(t)$ or $Z(f)$ comprises dynamic property of the testing system and should be affected by dimensions of transmitter and receiver benders and condition of specimen such as type of soil sample, dimensions, boundary condition, consolidation stress, and so on. Therefore, when $z(t)$ or $Z(f)$ is known, the output of the system can be calculated analytically by, in particular, a simple equation in frequency domain.

4.2.3 Identification of Frequency Response Function

As mentioned by Santamarina and Fam (1997), there are some procedures to identify frequency response function or impulse response of linear system. The swept signal is one of the practical input signals to identify the frequency response function or impulse response. Since the meaning of impulse response is the output of the system for unit impulse input, to use unit impulse as transmitter pulse may be considered the simplest way. However, this method generally does not provide enough accuracy because of technical problems. The swept signal, often called “chirp signal”, is a signal of which frequency is stretched along time axis. This signal is equivalent to impulse in terms of the amplitude of each frequency component. This signal has an advantage in signal to noise ratio over other signals such as an impulse or white noise.

In this study, two types of swept signals are used. First, Time-stretched pulse (TSP) is adopted. TSP suggested by Aoshima (1981) is described by the following equation:

$$X(k_f) = \begin{cases} \exp\left(i \frac{m_f \pi k_f^2}{N^2}\right) & 0 \leq k_f \leq \frac{N}{2} \\ X^*(N - k_f) & \frac{N}{2} + 1 \leq k_f \leq N \end{cases} \quad (4.4)$$

where k_f is discrete frequency, $X(k_f)$ is Fourier transform of TSP, i is complex number, m_f and N are integer numbers and asterisk represents complex conjugate. m_f relates to degree of frequency sweep: the larger value provides more stretched pulse in time domain. Secondly, a linearly swept sine pulse (LSSP) is adopted. LSSP is given by

$$y = A \sin(\omega t) \quad (4.1)$$

$$\text{where, } \omega = 2\pi \left(f_o + \frac{t}{t_{target}} \Delta f \right)$$

TSP where $m_f = 150$ and $N = 2048$ and LSSP where $f_0 = 0.5$ kHz, $\Delta f = 10$ kHz and $t_{target} = 10$ ms are compared in both time and frequency domain in Figure 4.7. Time histories of waveforms are shown in the left side of the figure in time domain and amplitude spectrum normalised by the maximum value A_{max} and phase spectrum are shown in the right side in frequency domain. Although these two signals are essentially the same in frequency-swept terms, it is found that there are differences in waveforms or amplitude and phase of each frequency component. In LSSP, frequency is linearly shifted in proportion to time, whereas phase is shifted in proportion to square of frequency in TSP.

An inverse filter of swept signals is needed for reconstruction of frequency response. From its nature, the inverse filter, which is given by complex conjugate of the signal, restores the swept signal into an impulse. It follows this routine when a received signal is put through the inverse filter, the received signal corresponding to the impulse is restored. Since applying the inverse filter to signals can be represented by a complex product in frequency domain, frequency response function is given by the following equation:

$$Z(f) = X^*(f) \cdot Y(f) \quad (4.5)$$

where $X(f)$ is Fourier transform of swept signal and $Y(f)$ is corresponding received signal in this equation. Note that equation (4.5) resulted in cross-spectrum of $X(f)$ and $Y(f)$.

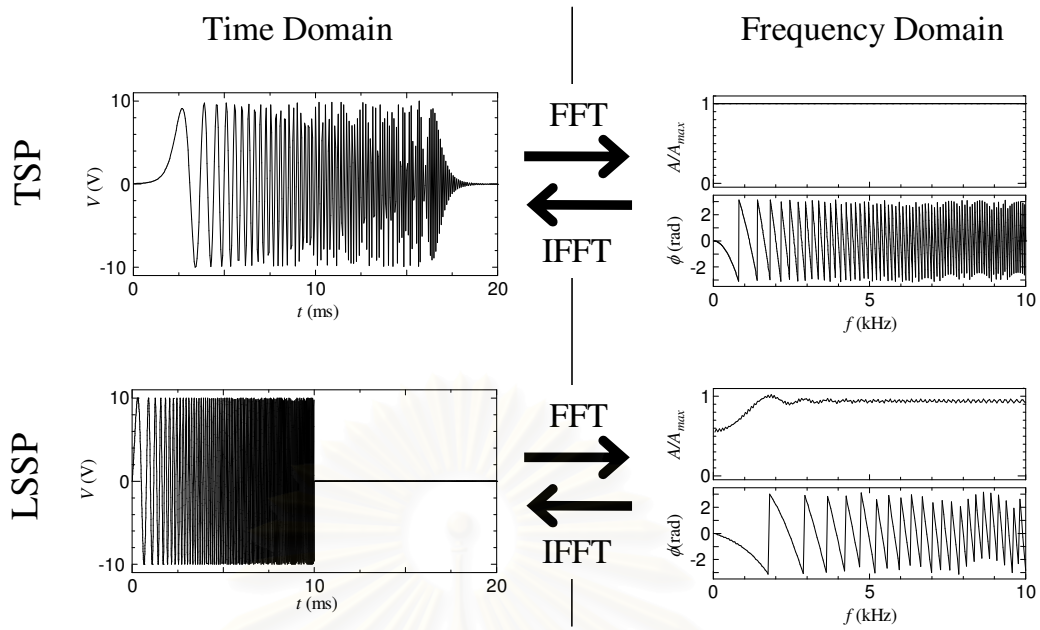


Figure 4.7 TSP and LSSP in time and frequency domain (TSP: $m_f = 150$, $N = 2048$; LSSP: $f_o = 0.5$ kHz, $\Delta f = 10$ kHz and $t_{target} = 10$ ms).

4.2.4 Methodology and Soil Properties

Three types of reconstituted samples which were NSF clay, Kasaoka clay and Akita peat were used in the tests (see Table 3.1). In order to confirm that the technique proposed in this study does not depend on the testing system, two types of testing apparatus: an consolidometer and a triaxial apparatus are prepared. These apparatuses are altogether different in lateral boundary conditions of specimen: rigid boundary can be assumed in consolidometer, while flexible boundary in triaxial apparatus. Furthermore, two different dimensions of specimens and BEs are examined on the triaxial apparatus. A series of incremental loading consolidation tests are performed on these samples. In the tests using a triaxial cell, specimens are isotropically consolidated in the triaxial cell. Note that the height of consolidometer is modified to be available for specimen of 75 mm in height so that enough height could be ensured when highly compressible peat sample is consolidated. For the triaxial test, the slurry of the reconstituted sample is preconsolidated in a preconsolidation cell. However, for the consolidometer test, the slurry is consolidated in the apparatus. Testing apparatuses, samples and test conditions are summarised in Table 4.2.

At the end of primary consolidation of each prescribed incremental stress, BEs tests were performed using two kinds of transmitted signals: swept signal and single

sine wave of which frequency varies from 0.5 to 10 kHz in incremental steps. Two types of swept signals are used. They are TSP and LSSP. The input voltage is ± 10 V. The schematic view of BEs test arrangement for triaxial apparatus and consolidometer is shown in Figure 3.3. For the consolidometer test, the triaxial apparatus in Figure 3.3 is replaced with the consolidometer.

Table 4.2 Testing apparatuses, samples and test conditions.

Testing apparatus	Sample	Consolidation pressure (kPa)	Swept signal	Initial height of sample (mm)	Initial diameter of sample (mm)	Dimensions of transmitter BE (mm)	Dimensions of receiver BE (mm)
Triaxial apparatus	Kasaoka clay	100	LSSP	100, 75, 50	50	14.0x10x0.7	3.0x10x0.7
	Akita peat	80, 100, 200, 300	TSP	150	70	11.5x10x0.5	11.1x10x0.5
Consolidometer	NSF clay	20, 50, 100	TSP	75	60	7.4x10x0.5	7.5x10x0.5
	Akita peat	20, 40, 60, 80	TSP	75	60	7.4x10x0.5	7.5x10x0.5

4.2.5 Input/output Characteristics of the Testing System

Since the technique proposed in this study is based on the linear system theory, it is important to confirm the linearity of testing system. As shown later (Figure 4.12), since system response is up to 7 kHz for all tests, frequency range less than 10 kHz is considered in this study. Swept signals were designed to cover the range. The range is determined by parameters N , m_f , f_0 , Δf and t_{target} in equations (4.4) and (4.1). These parameters should be determined in each case according to the range of system response so that precise frequency response function can be identified. For example, if harder sample such as sand is tested, frequency range would shift to higher side.

Signals actually driving transmitter element are checked in Figure 4.8, showing amplitude spectra of transmitted swept signals observed by self-monitoring circuit. An output signal of self-monitoring circuit can represent the displacement of the BE itself (Nishio and Hotta, 2000). These spectra are slightly different from those in Figure 4.7, which are based on equations (4.4) and (4.1), and are not actual transmitted signals. Although the amplitude of actual driving signal gradually decreases with frequency, in particular, in TSP, it is found that they are kept more than 80% of its maximum value at frequency of 7 kHz and even 60% at 10 kHz.

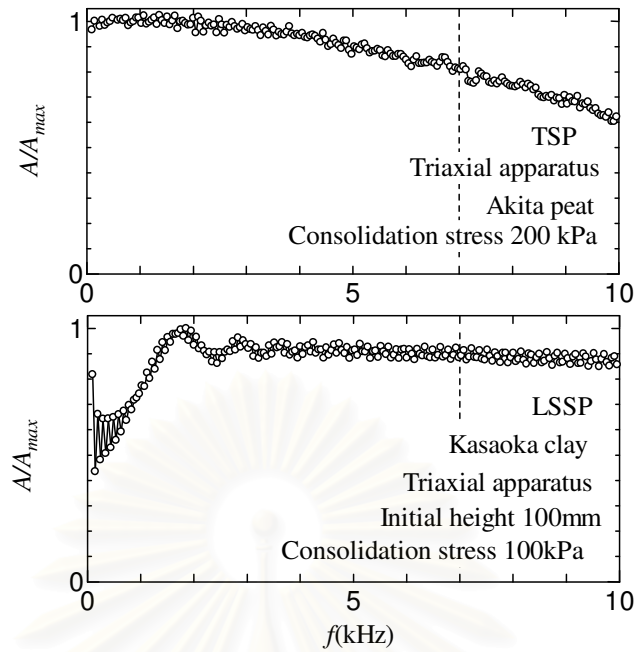


Figure 4.8 Amplitude spectra of TSP and LSSP given by self-monitoring signals.

Coherence function R^2 is used to represent the degree of linearity, described in the following equation:

$$R^2 = \frac{\overline{|P_{xy}|^2}}{P_{xx} \cdot P_{yy}} \quad (4.6)$$

where P_{xy} is cross spectrum of the received signal with transmitted signal, and P_{xx} and P_{yy} are mean amplitude of spectrum for transmitted and received signals, respectively. Figure 4.9 shows coherence function of received wave for LSSP. Since four times of signals are averaged in Figure 4.9, coherence function in this figure represents the effect of random noise, which is a factor affecting the accuracy of calculation. It can be seen that the value of coherence function is nearly one in given frequency bandwidth. It follows that a random noise less affected to the system.

The coherence function of received signal for various transmitted wave, on the other hand, is shown in Figure 4.10. Transmitted waves are LSSP and single sine waves of which frequency are 0.5, 1.0, 2.0, 3.0, 4.0 and 5.0 kHz. This figure is considered to represent the linearity of system in given frequency range. Coherence is approximately 0.8 or higher between 0.5 and 7 kHz and indicates that the testing

system is considered to show sufficiently linear behaviour in this frequency range. Similar results are also shown for TSP.

4.2.6 Frequency Response and Impulse Response Obtained from the Swept Signal

Typical transmitted and received waveforms for TSP and LSSP under triaxial consolidation are shown in Figure 4.11. Entire waveform of both transmitted and received waves must be sampled to restore frequency response. Signal duration of transmitted can be varied by the parameters m_f and t_{target} in equations (4.4) and (4.1). The duration become long when these parameters are large. These parameters consequently affect the amplitude of frequency response because longer duration signal provides more energy. Therefore, when larger output is needed, longer signal should be used. However, the signal of which length is longer than that of received wave decreases resolution of time scale for impulse response due to limitation of sampling number of data acquisition card. The decrease in resolution affects accuracy of travel time determination. It follows that high resolution in time scale and high output are conflicting requirements. Hence parameters m_f and t_{target} should be determined by balancing resolution of output and time scale necessary for calculated wave.

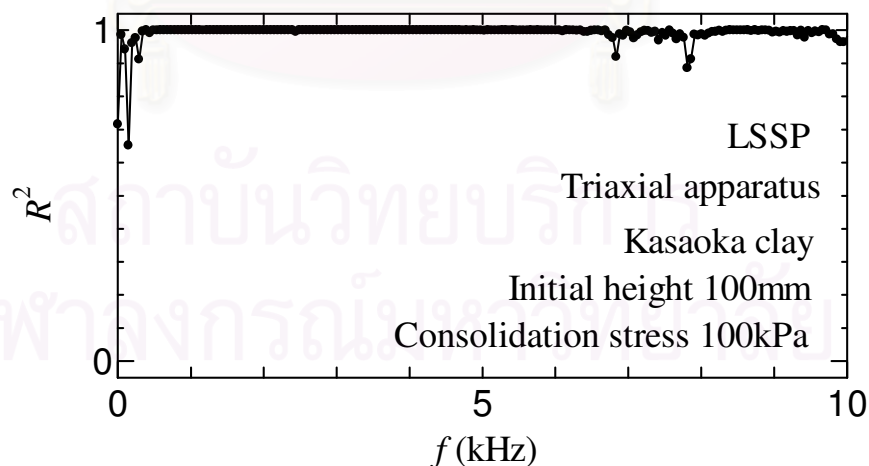


Figure 4.9 Coherence for four times swept signal inputs.

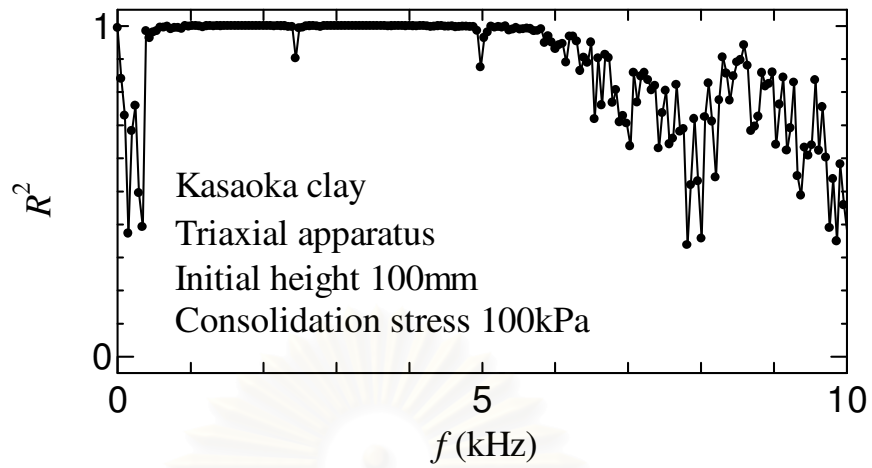


Figure 4.10 Coherence for various signal inputs.

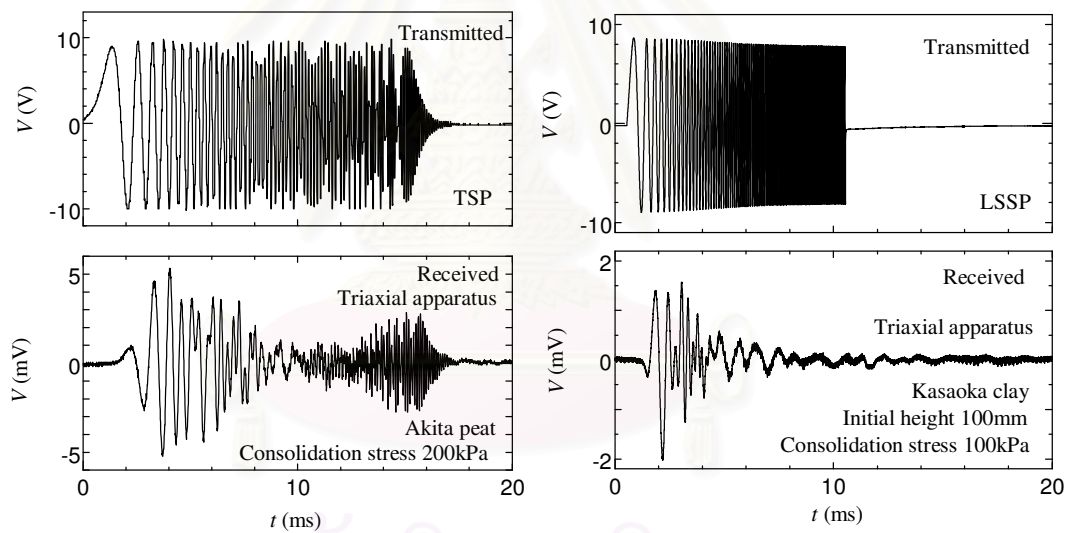
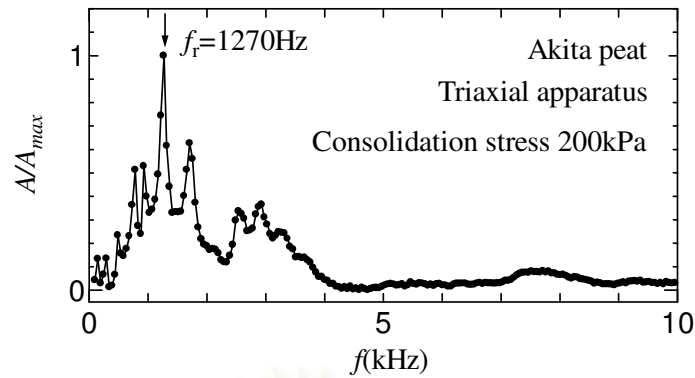
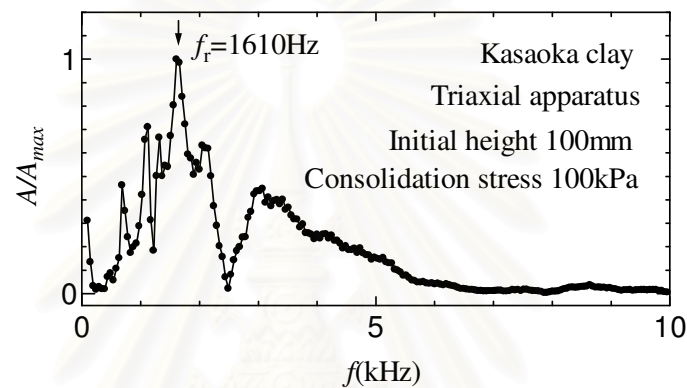


Figure 4.11 Typical transmitted and received signals for TSP and LSSP.



(a)



(b)

Figure 4.12 Typical frequency responses restored by (a) TSP, (b) LSSP.

Figure 4.12 shows frequency response obtained from received wave shown in Figure 4.11. It is found that the range of frequency response in which amplitude exists is less than 7 kHz. There are differences in the shape of spectrum between these figures. The shape of spectrum is considered to be affected by the difference of testing system involving the boundary condition or dimensions of specimen, soil sample, consolidation stress and dimensions of BEs. Resonant frequency, denoted as f_r in Figure 4.12, can be an index which represents the characteristics of the spectrum shape. Figure 4.13 shows change in resonant frequency with consolidation stress for each sample shown in Table 4.2. Results from the triaxial apparatus are located below those from the consolidometer. This indicates that the boundary condition greatly affects resonant frequency. Resonant frequencies are also affected by consolidation stress and the type of soil samples. It can also be seen from the results by Kasaoka clay that resonant frequency is little affected by tip-to-tip distance L . Since resonant frequency is mainly affected by soil density and stiffness (Blewett *et al.*, 2000; Lee

and Santamarina, 2005), this difference or change in resonant frequency can reasonably be explained by these soil characteristics: Resonant frequency increases with consolidation stress because both soil density and stiffness increase with consolidation stress. Resonant frequency for Akita peat also locates below the data for clay samples due to its low density and stiffness, if the boundary conditions are the same.

As they are a pair of Fourier transform (equations (4.2) and (4.3)), the impulse response can be given by calculating inverse FFT of frequency response. Since the physical meaning of impulse response is a received wave when an ideal unit impulse is given to a linear system. The impulse response should be, in principle, similar to the received wave when an impulse-type signal such as step signal is used. Figure 4.14(a) shows an impulse response for Akita peat calculated from the frequency response function shown in Figure 4.12 (a) and a unit transmitter pulse. Figure 4.14(b) shows a step transmitter signal and measured received signal. Indeed, it seems that waveform of impulse response is similar to received waveform shown in Figure 4.14(b). This agreement indicates that the impulse response can be used to estimate the travel time of shear wave as it is (Ogino *et al.*, 2006).

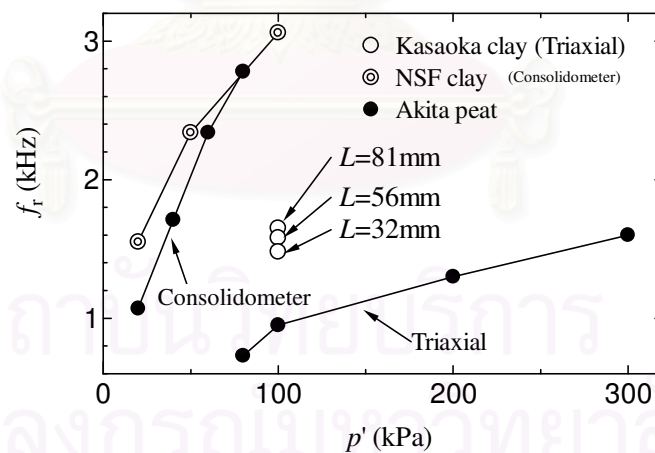


Figure 4.13 Relationship of resonant frequency versus consolidation pressure.

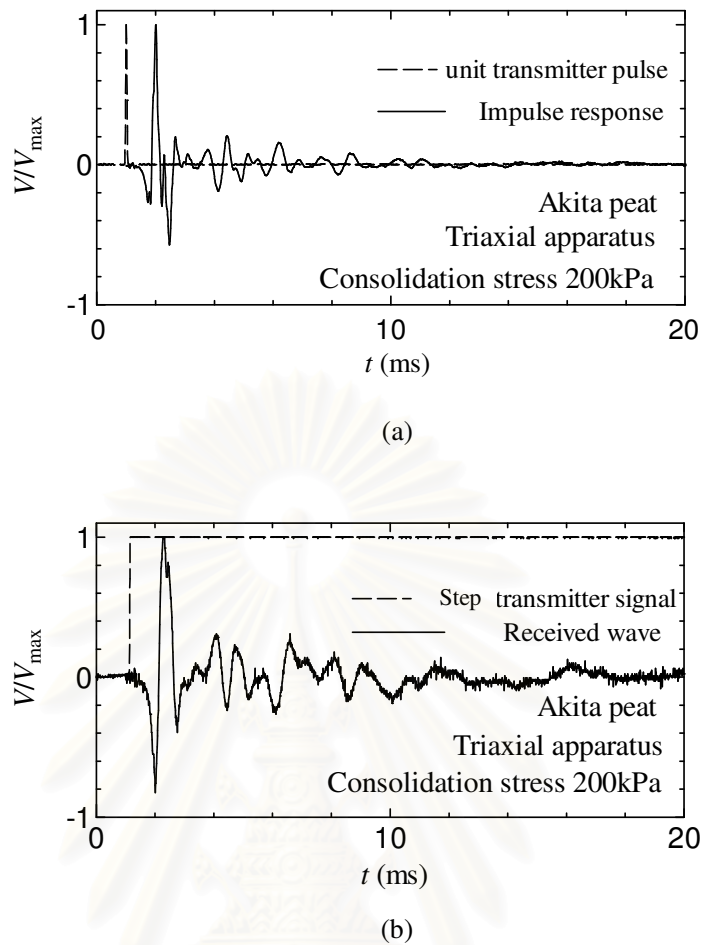


Figure 4.14 Comparison between (a) impulse response, (b) received signal for step wave input.

4.2.7 Comparison Between Regenerated and Observed Received Signals

Seven cases of calculated and observed received waveforms for single sine transmitter signals are compared in Figure 4.15. Frequencies of single sine transmitter signals are 2, 3, 4, 5, 6, 8, 10 kHz. Calculated waves are given by equation (4.3) in the frequency domain. In these cases, $X(f)$ should be FFT of each single sine transmitter signal and $Z(f)$ should be the frequency response function given by the cross-spectrum of swept signal and corresponding received signal shown in the right side of Figure 4.11. Hence, calculated received waves are given by inverse FFT of equation (4.3). It can be seen that there is little difference between calculation and observation through transmitting frequency between 2 and 10 kHz. The amplitude of calculated wave corresponds with that of observed wave in each case. Decreasing of amplitude by increasing frequency is also expressed. Moreover, the distortion resulted from near-

field effect is described in calculated waveforms: clear troughs are found in the beginning of both observed and calculated waveforms when transmitting frequency is less than 5 kHz. It follows the fact that this technique can restore any received waves for an arbitrary transmitter signal. This agreement is also shown in some characteristic points commonly used as travel time determination. Calculated and observed waveforms are again compared in Figure 4.16. Figure 4.16(a) is the results obtained from the triaxial apparatus tested on the Akita peat sample and Figure 4.16(b) is from the consolidometer on NSF clay. Time axis is enlarged so that the differences of these points are obviously clear.

Some characteristic points on calculated waveforms are also denoted as point A (first deflection), point B (first bump of reverse), point C (zero-crossing point) and point D (first peak) in Figure 4.16. Although a slight difference is found at point C for NSF clay (Figure 4.16(b)), there is little difference in arrival times determined at each of these characteristic points between calculation and observation. This means that this technique can provide V_s which is equivalent to that obtained from observed wave in time domain technique regardless of where the arrival point of shear wave is. Consequently, V_s can be verified for any transmitting waveforms even after the BEs test is completed. This may be adopted, for example, when reasonable V_s is not obtained from an ordinary BEs test because of uncertainty of travel time due to an influence of near-field effect. Furthermore, it should be noted that testing system and swept signal used for identification of frequency response are different among in Figure 4.15 and Figure 4.16: soil samples, testing apparatuses, consolidation stress, dimensions of BEs and type of swept signals are altogether different among results in these figures. It follows that this technique can be applied irrespective of sample, testing apparatus and type of swept signal.

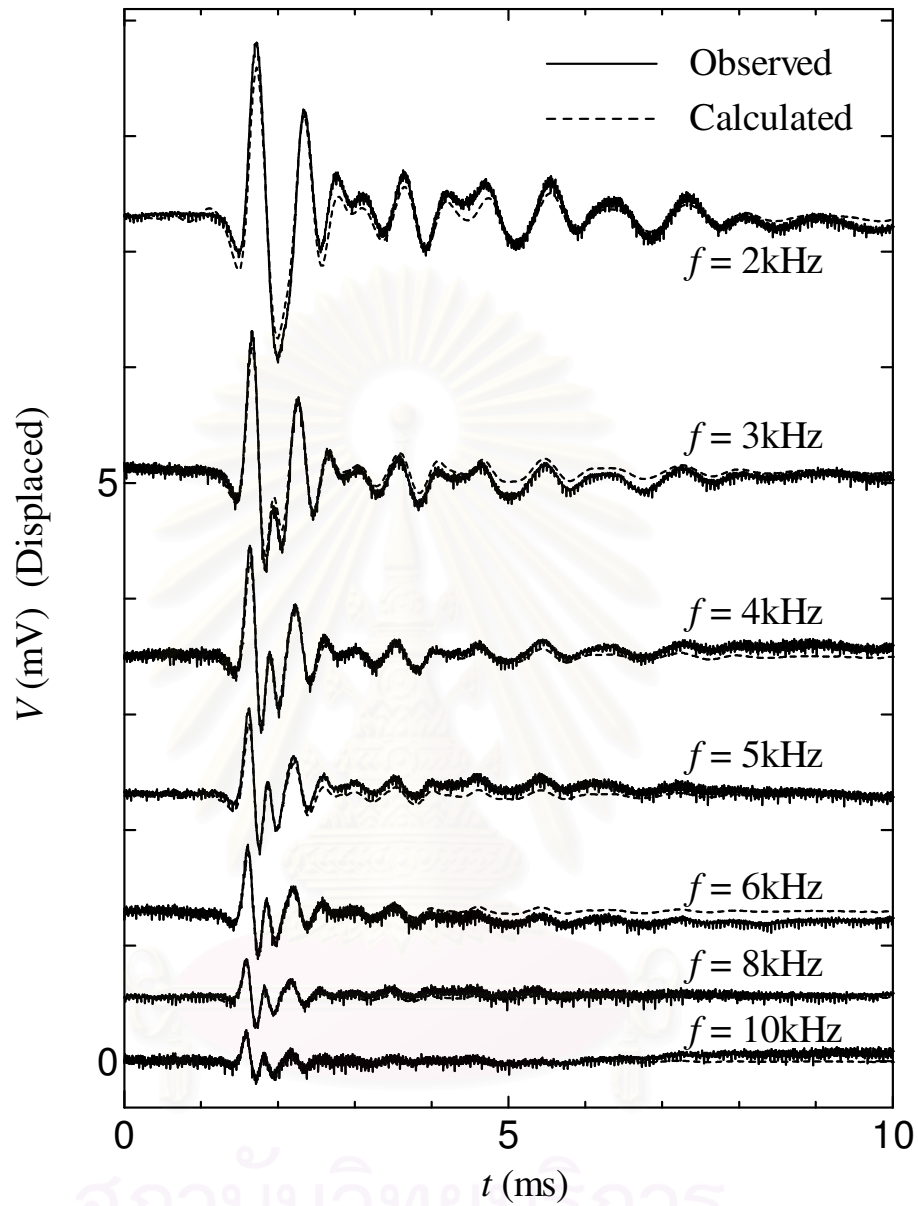


Figure 4.15 Comparison between observed and calculated received waves for various frequencies of single sine wave inputs (Kasaoka clay, triaxial apparatus, consolidation stress: 100kPa, initial height: 100mm).

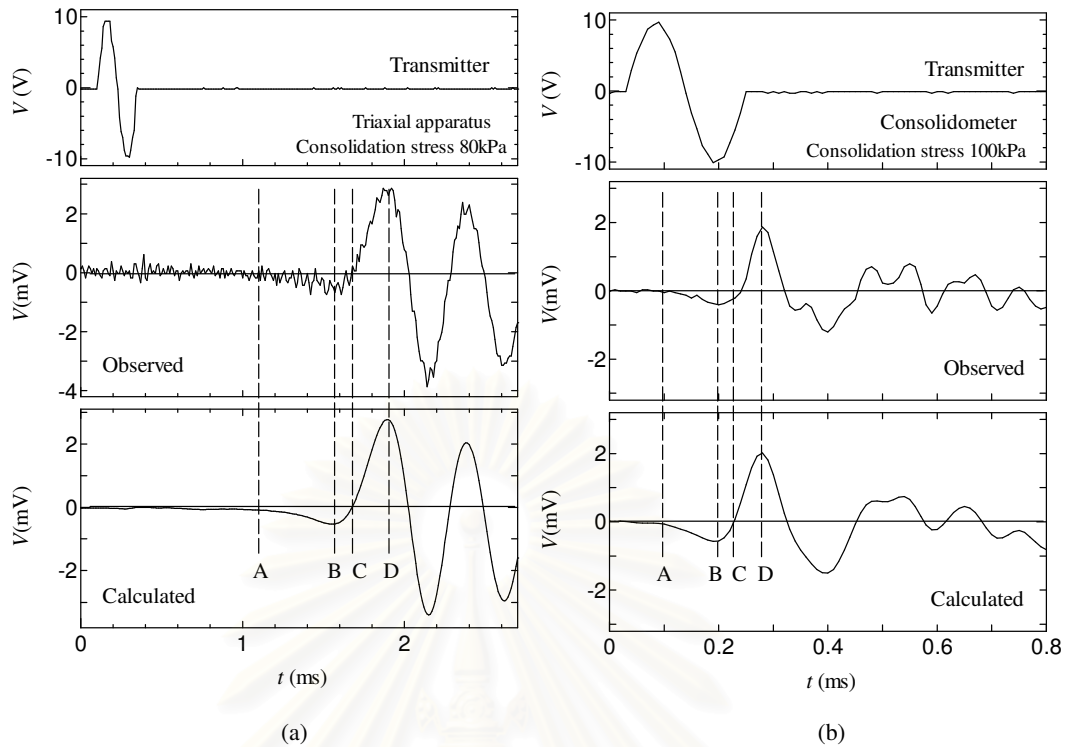


Figure 4.16 Comparison of arrival times at characteristic points (a) Akita peat, (b) NSF clay.

There is an advantage in signal to noise ratio for calculated wave. Disturbance due to random noise coming from outside of the testing system can be seen in the observed received waves shown in Figure 4.15 and Figure 4.16(a), while smooth lines are shown in the calculated waves. This contrast becomes more significant when the frequency of transmitted signal increases because the amplitude of observed wave becomes smaller while the amplitude of noise remains. As mentioned above, since the amplitude of swept signal has high energy because of its long duration, this high energy provides improvements in signals to noise ratio of received wave for the swept signal and eventually calculated wave. In fact, there is little disturbance due to random noise in the received wave shown in Figure 4.11 or restored impulse response shown in Figure 4.14. This is the reason why calculated wave does not contain random noise. This can be advantageous when sufficient amplitude of received wave cannot be ensured, for example, because of long distance between transmitter and receiver elements or high-frequency of transmitting signal.

4.2.8 Shear Wave Velocity Obtained from Calculated Wave

By using equation (2.5), shear wave velocities obtained from observed and calculated waveforms are compared and shown in Figure 4.17. For the sake of convenience, travel time of shear wave is determined by the distance between the start of transmitted and zero-crossing point of received wave (point C in Figure 4.16). Most of data plots are on the one-to-one relation and spread within the range from +10% to -10%. The difference is less than 8 %. This result confirms that calculated wave can obtain reasonable V_s as close as observed wave regardless of soil samples and testing apparatuses (Ogino *et al.*, 2008).

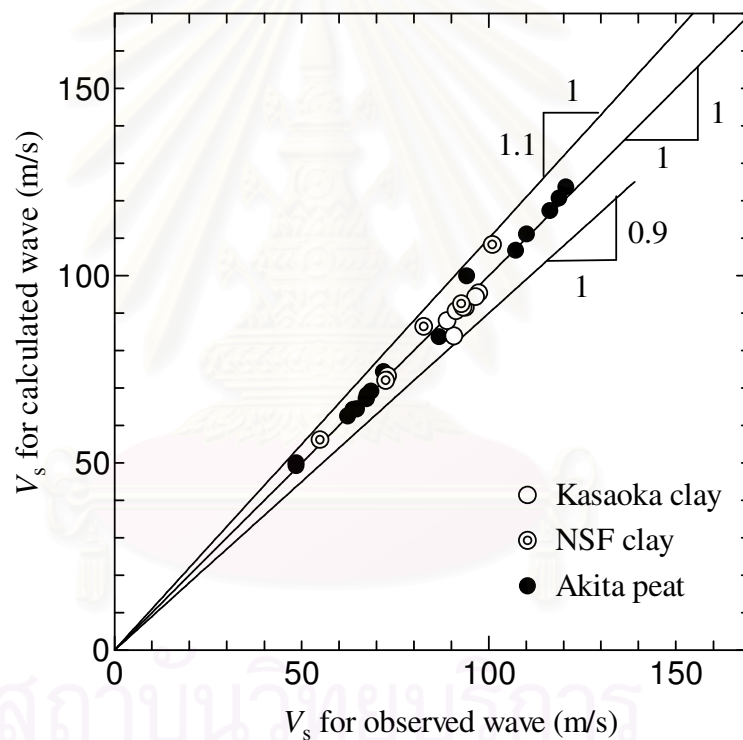


Figure 4.17 Comparison of shear wave velocities between observed and calculated waves.

4.2.9 Summary

A technique for identifying frequency response of BEs testing system based on linear system theory is demonstrated. Frequency responses for several different testing systems involving conditions of specimens and dimensions of BEs are experimentally identified using the swept signal and applied to compute the received waveforms for arbitrary transmitted wave. Calculated waveforms are compared with experimental data. The main observations from this study are as follows:

1. Received waveforms of the BEs test can be regenerated by frequency response of the testing system obtained by swept signals. Two types of swept signals (TSP and LSSP) designed by different formula are tested. Calculated received waveforms are in good agreement with the observed ones irrespective of the types of swept signals or frequencies.
2. This method for received wave regeneration can be applied irrespective of a testing system. Test results which examine the influence of the testing system using different samples, different testing apparatus and different dimensions of specimen and BEs do not affect the applicability of this technique.
3. The shape of frequency response changes depending on testing system. In particular, change in resonant frequency is reasonably explained by change of soil stiffness and density.
4. Shear wave velocities obtained from calculated and observed received waves show good agreement in any testing system. Difference of shear wave velocities is less than 8%.

CHAPTER V

STRAIN DEPENDENCY OF SHEAR MODULUS

5.1 Background

The non-linearity of stress-strain relationship is not new to geotechnical engineers. There are many nonlinear models proposed and used for a design of structures such as the works of Seed and Idriss (1970) and Mair (1993). It is essential to determine the stiffness at very small strains ($<10^{-4}\%$) to intermediate strains ($<10^{-1}\%$) region since the stress-strain relationships are non-linear. Figure 5.1 shows a typical modulus-strain curve for soil. The curve can be divided into three regions which are the very small strains region, intermediate strains region and large strains region. For very small strains region, the stiffness is almost constant and relatively large. In the intermediate strains region, the soil shows degradation of modulus when the induced strain increases. The large strains region is the zone that the soil is sheared until it is about to fail, the modulus of soil decreases significantly and converges to a small value.

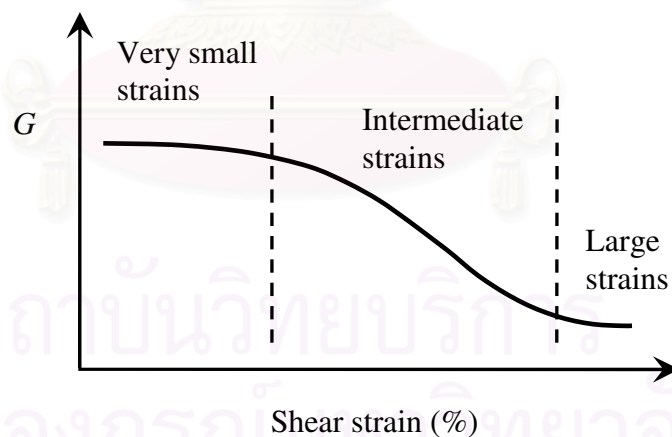


Figure 5.1 Shear modulus degradation curve for soil (after Atkinson and Salfors, 1991).

The modulus in a very small strains region can be measured by using dynamics method. However, with current technology, a local displacement gauge can be used to determine the soil modulus in very small strains region. The BEs test, resonant column test and cyclic triaxial test are among the dynamics method used. In the field,

a seismic cone penetration test, cross-hole and down-hole test can be employed to determine the G_{max} . To calculate the modulus in the intermediate strains region, local displacement gauge may be the most appropriate method although dynamics and conventional testing methods can be used. For large strains region, the local displacement gauge and conventional soil testing can be employed because the sample is sheared to failure. By using conventional soil testing to calculate G , the G is estimated based on E and ν . The relationship between these parameters is explained in later section.

In this study, a testing methodology is proposed. The methodology allows the BEs test to be performed after the triaxial sample is sheared. This method also allows G to be calculated based on the BEs test, G_{bender} , at higher shear strain level to be carried out. The G_{bender} degradation curve can be obtained by the proposed methodology.

5.2 Testing Equipment and Soil Properties

Triaxial apparatus shown in Figure 3.3 was employed for the testing. K_0 -condition for consolidated-undrained triaxial compression test with pore water pressure measurement was carried out in this study. A series of BEs tests was performed on reconstituted and undisturbed samples shown in Table 5.1 while the samples were sheared. The preparation method for reconstituted sample was mentioned in Section 3.3. Three types of reconstituted samples were used in this study which was Kasaoka clay, Fujinomori clay and NSF clay and the properties of these clay samples were shown in Table 3.1. Two undisturbed samples which were Mihara clay and Bangkok clay were used in this study. Mihara clay was collected from the depth of 11 to 12 m at Mihara, Hokkaido. For Bangkok clay, the samples were collected at five different depths which were at the depths of 6–7 m, 8–9 m, 10–11 m, 12–13 m and 14–15 m. Bangkok clay samples were collected by using a thin wall sampler from a site in Soi Sukhumvit 24. Bangkok clay samples were extracted from the thin wall sampler and sealed with wax at Chulalongkorn University before transported to Hokkaido University for testing. Reference is made to Table 5.1; the names of samples listed on the table were in accord with the site and depth where they were collected, for example, the sample's name was Bangkok 8. It was a clay sample collected at the depth of 8–9 m in Bangkok.

Table 5.1 Description of soil samples and testing conditions.

Sample	Depth of borehole (m)	Present insitu overburden pressure, σ'_i ¹ (kPa)	OCR*	Target Axial pressure, σ'_a		Total density of sample before shearing test, ρ (kg/m ³)
				Consolidation test under K_0 -condition (kPa)	Swelling test under K_0 -condition (kPa)	
Kasaoka 1	-	70.0	1	100.0	-	1833
Kasaoka 2	-	70.0	1	100.0	-	1829
Kasaoka 3 [#]	-	70.0	1	100.0	-	1827
Fujinomori	-	70.0	1	100.0	-	1723
NSF	-	150.0	1	170.0	-	1804
Mihara	11 - 12	57.1	1	57.1	-	1671
Bangkok 6	6 - 7	55.4	1.3	72.0	55.4	1772
Bangkok 8	8 - 9	68.6	1.3	89.1	68.6	1268
Bangkok 10	10 - 11	79.6	1.3	103.4	79.6	1607
Bangkok 12	12 - 13	92.3	1.3	120.0	92.3	1657
Bangkok 14(1)	14 - 15	104.3	1.3	135.6	104.3	1752
Bangkok 14(2)	14 - 15	104.3	1.3	135.6	104.3	1754
Bangkok 14(3) [#]	14 - 15	104.3	1.3	135.6	104.3	1739

[#] The BEs test was performed once before the sample was sheared. After that, the sample was sheared continuously under monotonic loading with 0.05 %/minute of strain rate until the maximum axial strain reaches 15%.

¹ Reconstituted Kasaoka clay, Fujinomori clay and NSF clay were preconsolidated under vertical pressure of 70, 70 and 150 kPa, respectively.

OCR – overconsolidation ratio

* OCR for undisturbed Bangkok clay was assumed to be 1.3 (Shibuya, 2001; Tamrakar, 2001; Shibuya and Tamrakar, 2003)

5.3 Determination of Soil Parameters from Triaxial Testing

5.3.1 The Undrained Poisson's Ratio

The triaxial test, by using cylinder sample, is a common test to determine the Young's and shear modulus of soil sample. The triaxial test can be classified into two main tests which are drained and undrained tests. In the drained test, the drainage valve is kept open so that the excess pore water pressure can flow out while the sample is sheared under monotonic loading. For the undrained test, the shearing is done with the drainage valve closed and this means that the volume of the sample is unchanged when shearing. Hence, the Poisson's ratio, ν , for the drained and undrained tests are different. It is known that the drained Poisson's ratio, ν' , is smaller than the undrained Poisson's ratio, ν_u , which is 0.5. The value 0.5 is derived from the elastic stress-strain relationship shown below. Reference is made to Figure 5.2; the stress-strain relationships in the directions of x , y and z axes (Timoshenko, 1970) are given in equations (5.1) to (5.3).

$$\Delta\varepsilon_x = \frac{\Delta\sigma'_x}{E_x} - \nu_{xy} \frac{\Delta\sigma'_y}{E_y} - \nu_{xz} \frac{\Delta\sigma'_z}{E_z} \quad (5.1)$$

$$\Delta\varepsilon_y = \frac{\Delta\sigma'_y}{E_y} - \nu_{yz} \frac{\Delta\sigma'_z}{E_z} - \nu_{yx} \frac{\Delta\sigma'_x}{E_x} \quad (5.2)$$

$$\Delta\varepsilon_z = \frac{\Delta\sigma'_z}{E_z} - \nu_{zx} \frac{\Delta\sigma'_x}{E_x} - \nu_{zy} \frac{\Delta\sigma'_y}{E_y} \quad (5.3)$$

$$\text{where, } E_x = E_y = E_z \quad (\text{isotropic behaviour}) \quad (5.4)$$

For an undrained test condition, $\Delta\varepsilon_x + \Delta\varepsilon_y + \Delta\varepsilon_z = 0$ and assuming the soil behaves isotropy, the undrained Poisson's ratio is ν_u , by adding together equations (5.1), (5.2) and (5.3), the new equation is

$$(1 - 2\nu_u)\Delta\sigma'_x + (1 - 2\nu_u)\Delta\sigma'_z + (1 - 2\nu_u)\Delta\sigma'_y = 0 \quad (5.5)$$

In the triaxial test, $\Delta\sigma'_x = \Delta\sigma'_z$ and equation (5.5) becomes

$$(1 - 2\nu_u)(2\Delta\sigma'_x) + (1 - 2\nu_u)\Delta\sigma'_y = 0 \quad (5.6)$$

For the undrained triaxial test, it is known that the value of $\Delta\sigma'_x$ and $\Delta\sigma'_y$ in equation (5.6) may not become zero. Hence, for equation (5.6) to become zero, it is necessary that

$$1 - 2\nu_u = 0 \quad (5.7)$$

or in other words, the undrained Poisson's ratio, $\nu_u = 0.5$.

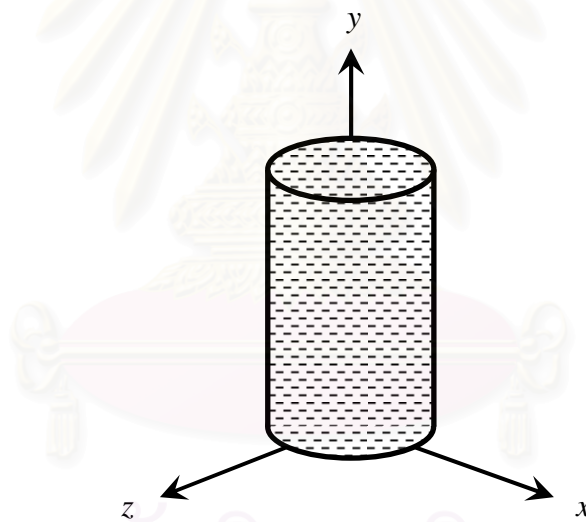


Figure 5.2 Cylinder sample in orthogonal space.

5.3.2 Determination of G

Figure 5.3 illustrates the typical stress-strain relationship of geomaterial. Young's modulus, E , can be defined by using the relationship between deviatoric stress, q , and axial strain, ε_a . The secant Young's modulus, E_{secant} , and tangent Young's modulus, $E_{tangent}$, are defined as follows:

$$E_{secant} = (q - q_0) / \varepsilon_a \quad (5.8)$$

$$E_{tangent} = dq / d\varepsilon_a \quad (5.9)$$

where q_0 is initial deviatoric stress. Identically, the G can be obtained from the relationship between shear stress, τ , and shear strain, γ . Secant and tangent shear moduli are

$$G_{secant} = \tau / \gamma \quad (5.10)$$

$$G_{tangent} = d\tau / d\gamma \quad (5.11)$$

Bulk and shear moduli can be related to Young's modulus and Poisson's ratio. Equations of bulk and shear moduli in the drained condition are given as

$$K' = \frac{E'}{3(1 - 2\nu')} \quad (5.12)$$

$$G' = \frac{E'}{2(1 + \nu')} \quad (5.13)$$

where, K' is effective bulk modulus, G' and E' are drained shear and Young's moduli, respectively. It is known that the G is not influenced by the excess pore water pressure. For the undrained triaxial test of fully saturated sample, the relationship between shear and Young's moduli is given by

$$G' = G_u = \frac{E_u}{2(1 + \nu_u)} = \frac{E_u}{3} \quad (5.14)$$

where G_u and E_u are undrained shear and Young's moduli, respectively, and $\nu_u = 0.5$.

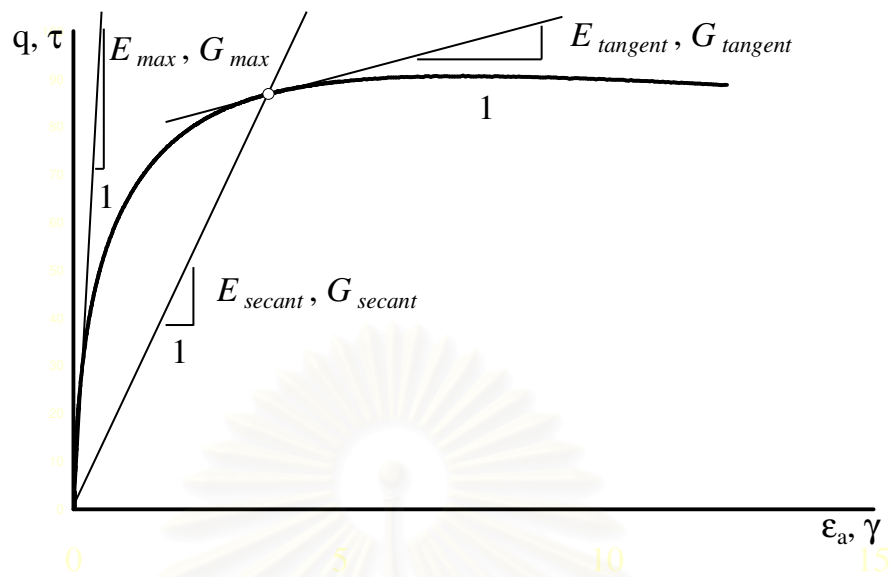


Figure 5.3 Definition of Young's and shear moduli

5.3.3 Determination of γ

As we know, for triaxial test, the shear strain, γ , and volumetric strain, ε_v , are related to axial strain, ε_a , and radius strain, ε_r . The relationship is shown in equations (5.15) and (5.16).

$$\Delta\gamma = \frac{2}{3}(\Delta\varepsilon_a - \Delta\varepsilon_r) \quad (5.15)$$

$$\Delta\varepsilon_v = \Delta\varepsilon_a + 2\Delta\varepsilon_r \quad (5.16)$$

For the undrained test, $\Delta\varepsilon_v = 0$. Therefore, by substituting this condition into equation (5.16) and by substituting equations (5.16) into (5.15), the γ is related to the ε_a as shown in equation (5.17).

$$\Delta\gamma = \Delta\varepsilon_a \quad (5.17)$$

5.4 Methodology

The K_0 -condition for a consolidated-undrained triaxial compression test with pore water pressure measurement was performed. The triaxial sample was sheared in steps and the BEs test was performed when the shearing process stopped. For Kasaoka 3 and Bangkok 14(3), the BEs test was carried out once before shearing test and after that the sample was sheared continuously to failure.

At the beginning the sample was trimmed to 50 and 100 mm in diameter and height, respectively. The initial water content and initial mass of the trimmed sample were measured so that initial density could be calculated. The sample was saturated so that Skempton B -parameter was more than 0.97. To determine the density of sample after consolidation process, the water content of the consolidated sample is measured after the test. Total density of sample after consolidation test or before shearing test is shown in Table 5.1.

For reconstituted samples, the samples were consolidated under the K_0 -condition with the target axial pressure, σ'_a , which was higher than the vertical preconsolidation pressure, σ'_{pc} , for each sample. The Mihara clay sample was consolidated under the K_0 -condition to the in situ overburden pressure which was 57.1 kPa. The reason why the overburden pressure for the Mihara clay sample was low even though it was collected at the depth of 11-12 m was because this clay layer was overlaid by 2-3 m thick of peat layer. Overconsolidation ratio, OCR , for the Bangkok clay samples were assumed to be 1.3 (Shibuya, 2001; Tamrakar, 2001; Shibuya and Tamrakar, 2003). Hence, for the Bangkok clay samples, the samples were consolidated under K_0 -condition to target axial pressure 1.3 times the in-situ overburden pressure and then the sample was swelled to the in-situ overburden pressure before it was sheared (consolidation and swelling curves are presented in Appendix C).

Figure 5.4 shows the flow chart of the testing methodology. At the end of the primary consolidation or swelling test, the drainage valve was closed. After that, the BEs test was performed by using time domain method to determine V_s . The driving signal used in the BEs test was swept signal (equation (4.1)). The initial frequency, f_0 , bandwidth, Δf , and target time, t_{target} , were 2 kHz, 5 kHz and 10 ms, respectively. The input voltage for the swept signal was ± 30 V. The widths of the transmitter and

receiver after coating were 21 and 11 mm, respectively. The embedded lengths of transmitter and receiver BEs into the sample were 7.3 and 5 mm, respectively.

After that, the sample was sheared under monotonic loading (stress-strain curves are presented in Appendix D). The axial strain rates used were 0.002, 0.02 and 0.05 %/minute based on the level of ε_a . The condition for selecting the strain rate is shown in Figure 5.4 and Table 5.2. For ε_a less than 0.01%, the strain rate of 0.002 %/minute was applied. If the ε_a was in between 0.01% and 0.1%, the strain rate of 0.02 %/minute was employed. The axial strain rate of 0.05 %/minute which was recommended by Japanese Geotechnical Standards (JGS-0523-2000) for clayey soil was used for ε_a more than 0.1%. One of the reasons why a different strain rate was used in the shearing test was because the author would like to get more data in the very small and intermediate strains region. By referring to Table 5.2, when the target axial strain of 0.1 % reached, the monotonic loading process was stopped. The strain rate was changed to 0.05 %/minute and the next target axial strain was set to be 0.15 %. After that, the monotonic loading process was started again. For each time the monotonic loading process stopped, the BEs test was performed which took less than one minute. Hence, the total number of the BEs tests for each sample was 27. The monotonic loading process was stopped when the maximum axial strain reached 15% (recommended by JGS-0523-2000).

The ε_a for each step of shearing was calculated based on the measured data and it was not based on the program setting shown in Table 5.2. For the undrained triaxial test, the γ was equal to the ε_a as explained in Section 5.3.3. The G_{bender} was calculated by using equation (2.6) where the V_s was calculated by using equation (2.5). The travel distance was measured as the tip-to-tip distance between BEs transducers (Viggiani and Atkinson, 1995). The travel time was determined based on cross-correlation method (Boonyatee and Chan, 2006). The soil density used in equation (2.6) is shown in Table 5.1. The G for the conventional test was calculated based on equation (5.14). The G_{secant} and $G_{tangent}$ depending on the E_{secant} and $E_{tangent}$, respectively, were used in equation (5.14). The secant and tangent Young's moduli are shown in equations (5.8) and (5.9), respectively.

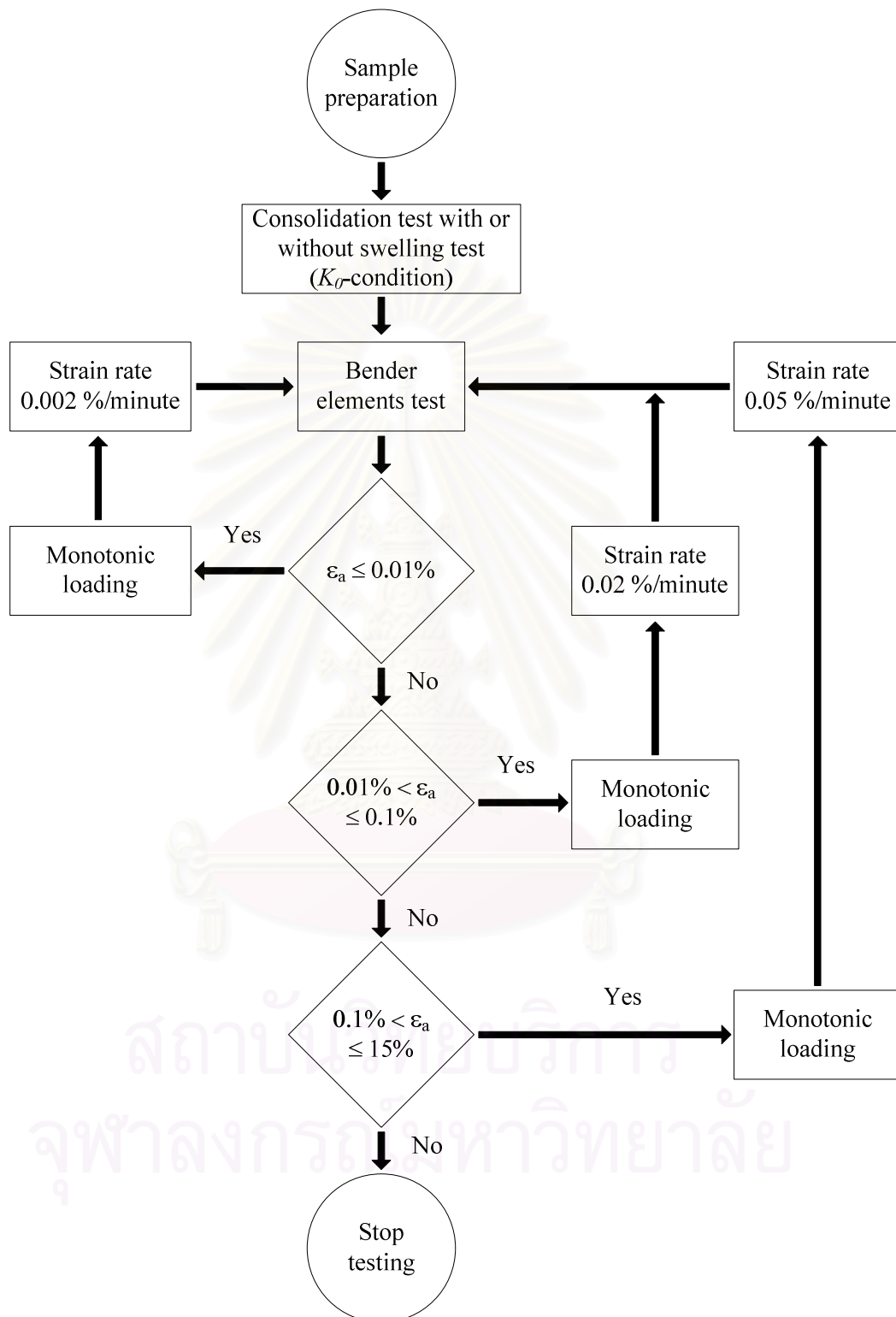


Figure 5.4 Flowchart of the axial monotonic loading test with the BEs test.

Table 5.2 Condition of the axial monotonic loading test with the BEs test.

BEs test	Axial monotonic loading strain rate (% / minute)	Target axial strain (%)
1 (After consolidation / swelling test)	-	-
2	0.002	0.002
3	0.002	0.005
4	0.002	0.01
5	0.02	0.02
6	0.02	0.04
7	0.02	0.06
8	0.02	0.08
9	0.02	0.1
10	0.05	0.15
11	0.05	0.2
12	0.05	0.3
13	0.05	0.4
14	0.05	0.5
15	0.05	0.7
16	0.05	1
17	0.05	1.5
18	0.05	2
19	0.05	3
20	0.05	4
21	0.05	5
22	0.05	6
23	0.05	7
24	0.05	8
25	0.05	10
26	0.05	12.5
27	0.05	15

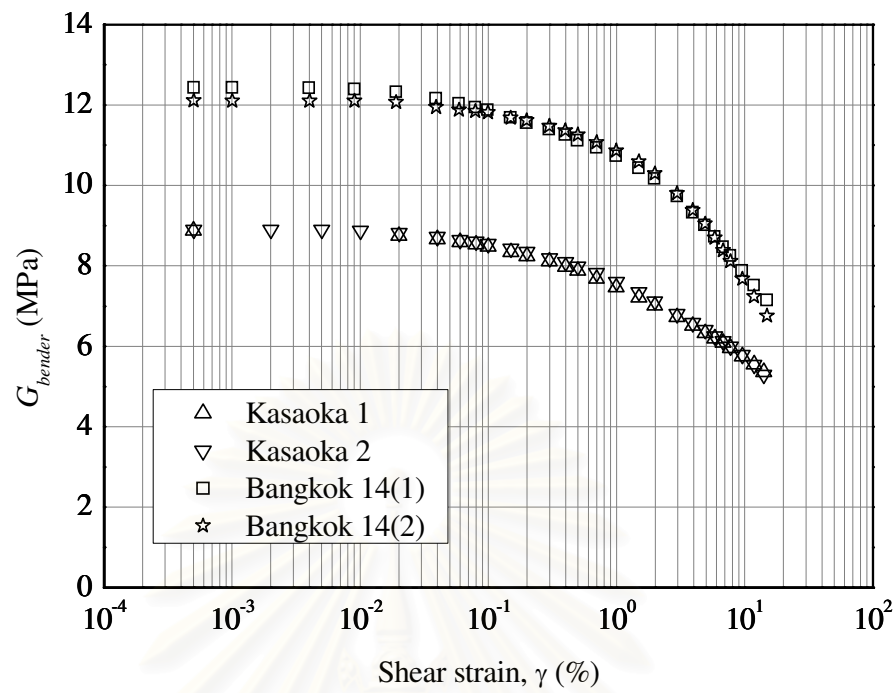
จุฬาลงกรณ์มหาวิทยาลัย

5.4.1 Consistency of Proposed Methodology

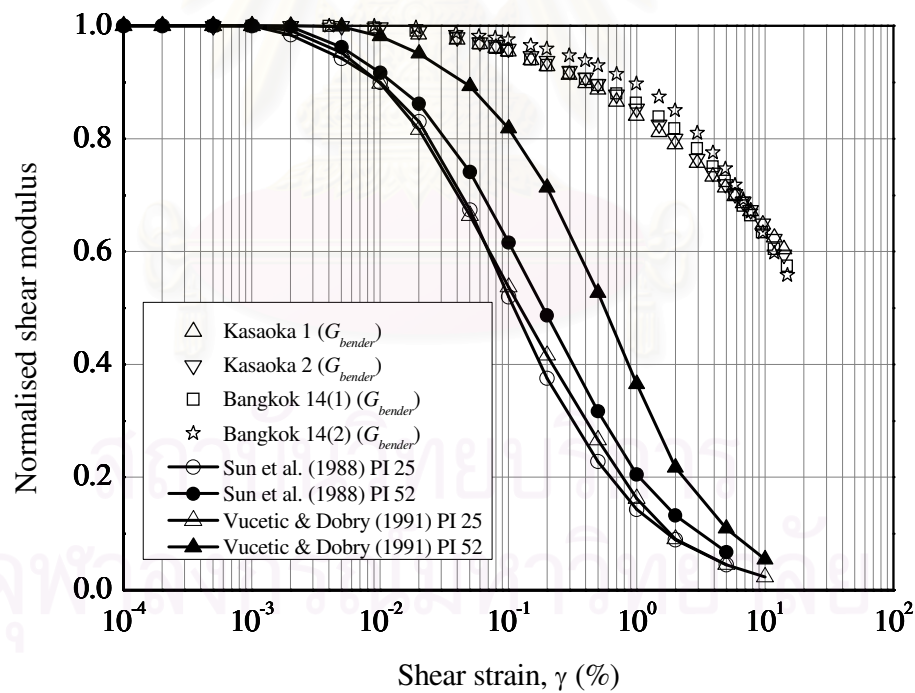
Kasaoka 1, Kasaoka 2, Bangkok 14(1) and Bangkok 14(2) are used to investigate the consistency of the testing methodology. The result of G_{bender} is plotted and shown in Figure 5.5. It is noted that the result for Kasaoka clay samples duplicated each other well. The reason for this is that the Kasaoka sample is reconstituted sample where the uniformity of the sample is more controllable than the undisturbed soil. The normalised G degradation curves of the four samples are shown in Figure 5.5(b). This figure also shows the degradation curves proposed by Sun *et al.* (1988) and Vucetic and Dobry (1991) with 25 and 52 plasticity indices. From the results presented in Figure 5.5, it can be concluded that the proposed methodology has a good consistency in the G_{bender} determination.

5.4.2 The Effects of the Proposed Methodology on the Critical Stress Path

By performing the testing methodology, the sample is sheared in 26 steps with three different strain rates. The BEs tests are performed after each shearing process stopped. The testing conditions proposed may affect the stress path of the soil sample. Hence, to study the effects of the testing methodology on the critical stress path, two types of samples are used which is Kasaoka clay and Bangkok clay. For each type of clay, three samples are consolidated under the same testing condition. Two samples are sheared by using the proposed methodology and the other one is sheared under standard test condition, i.e., the sample is sheared continuously with 0.05 %/minute of strain rate until the maximum ε_a reaches 15%. Kasaoka 1, 2, 3 and Bangkok 14(1), 14(2) and 14(3) are the samples used in the study where Kasaoka 3 and Bangkok 14(3) are sheared under standard condition. From Figure 5.6, the stress path results are well matching with each other especially for a reconstituted sample. There is a bit difference in the starting point even though the same type of soil samples is tested under the same condition. This difference may be due to the factor such as sample disturbance during sampling and trimming. However, this difference is considered insignificant and can be ignored. For samples tested using proposed methodology, the plot shows lines extending out from the stress path. These lines represent the relaxation of the samples when the monotonic loading process stopped to allow the BEs test to be carried out. Refer to Figure 5.6, M is critical stress ratio.

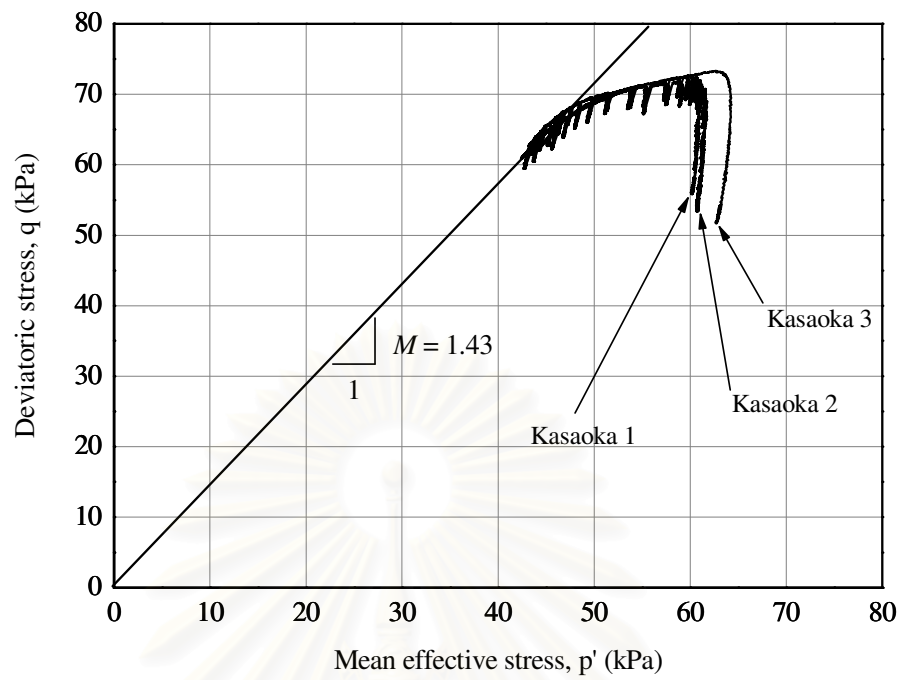


(a)

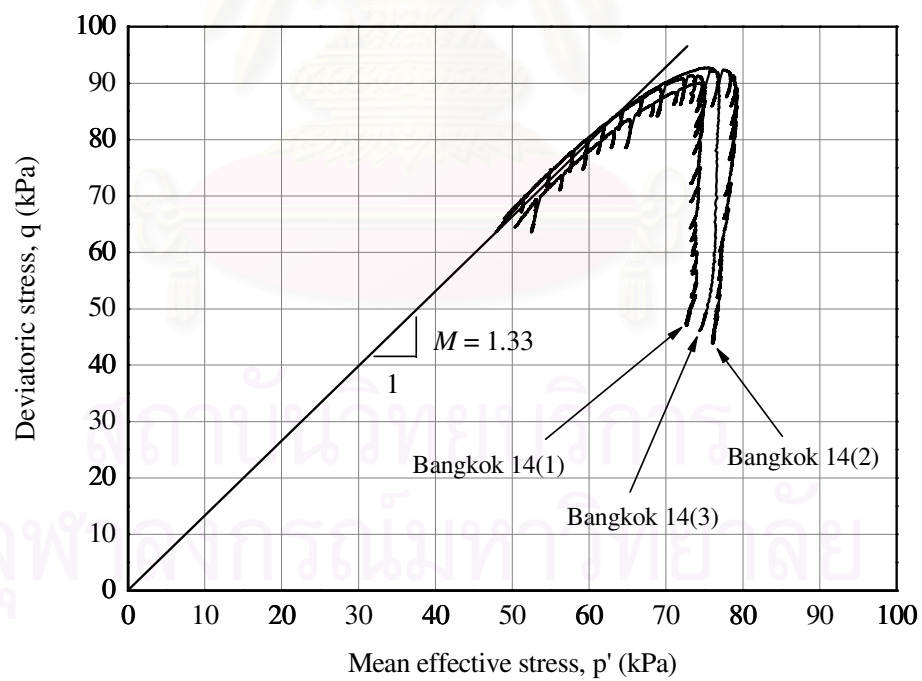


(b)

Figure 5.5 (a) Plot of G_{bender} versus γ , (b) normalised G degradation curve.



(a)



(b)

Figure 5.6 Plot of $p' - q$ (a) reconstituted samples, (b) undisturbed samples.

5.5 G_{bender} Degradation Curve

The shear moduli are calculated based on the BEs test by using the proposed method. They are presented in Figures 5.7, 5.8 and 5.9. Figures 5.7 and 5.8 present the results of reconstituted and undisturbed samples, respectively. Figure 5.9 illustrates the results of all the samples. By referring to Figure 5.7, it can be noticed that G_{bender} for Fujinomori clay is higher than Kasaoka clay although both samples are consolidated under the same target axial pressure. This difference is due to the fact that Fujinomori clay contains silt material which is stiffer than Kasaoka clay. It is obvious that G_{bender} for NSF clay is higher than Fujinomori and Kasaoka clays because the target axial pressure for NSF clay, 170kPa, is highest.

For Figure 5.8, G_{bender} for Bangkok 6 which is collected at the depth of 6-7 m is higher than Bangkok clay collected at deeper depth such as Bangkok 12 and Bangkok 14(1). The reason is that from the test preparation of Bangkok 6, it is notice that the sample contains a lot of silt material which may make the sample stiffer.

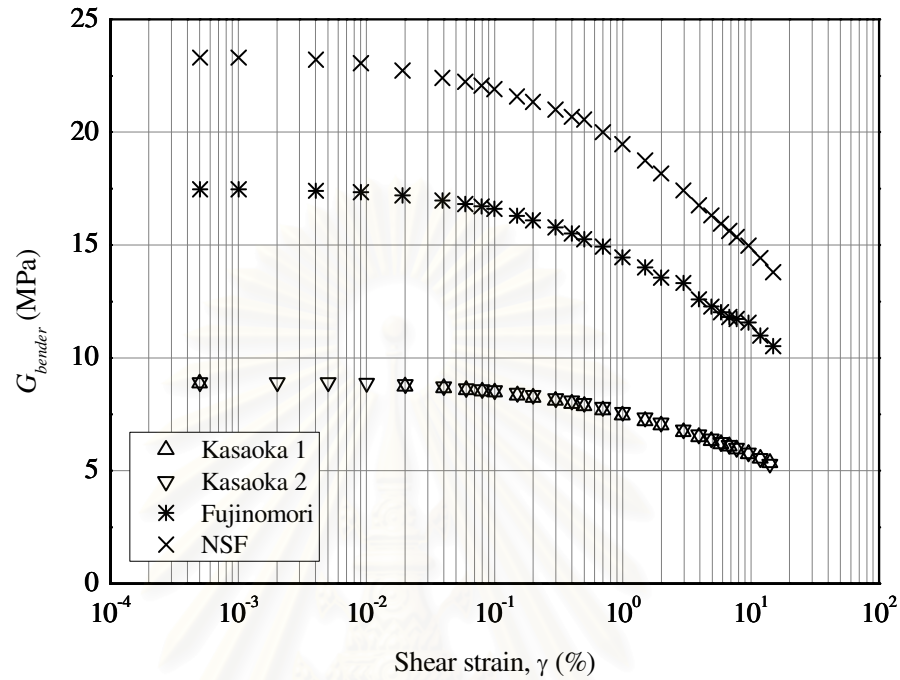
Normalised G degradation curve proposed by Sun *et al.* (1988) and Vucetic and Dobry (1991) with plasticity index of 52 is plotted and shown in Figure 5.9(b). Vucetic and Dobry (1991) reported that the normalised G degradation curve for clay is controlled by the plasticity index. However, normalised G_{bender} degradation curves shown in Figure 5.9(b) are almost identical even with the plasticity indices ranging from 25 to 52. Therefore, it can be concluded that normalised G_{bender} degradation curve is not influenced by the plasticity index. Besides, the shape of normalised G_{bender} degradation curve is different from that of normalised G degradation curve proposed by the researchers. For normalised G_{bender} , the curves degrade slowly and do not decrease near zero even when the induced shear strain becomes large.

Reference to Figure 5.9(b), the G_{bender} is a function of γ . The G_{bender} results in Figure 5.9(b) are plotted again in Figure 5.10. By curve fitting the results in Figure 5.10, the relationship between G_{bender} and γ can be determined. This relationship is shown as follows:

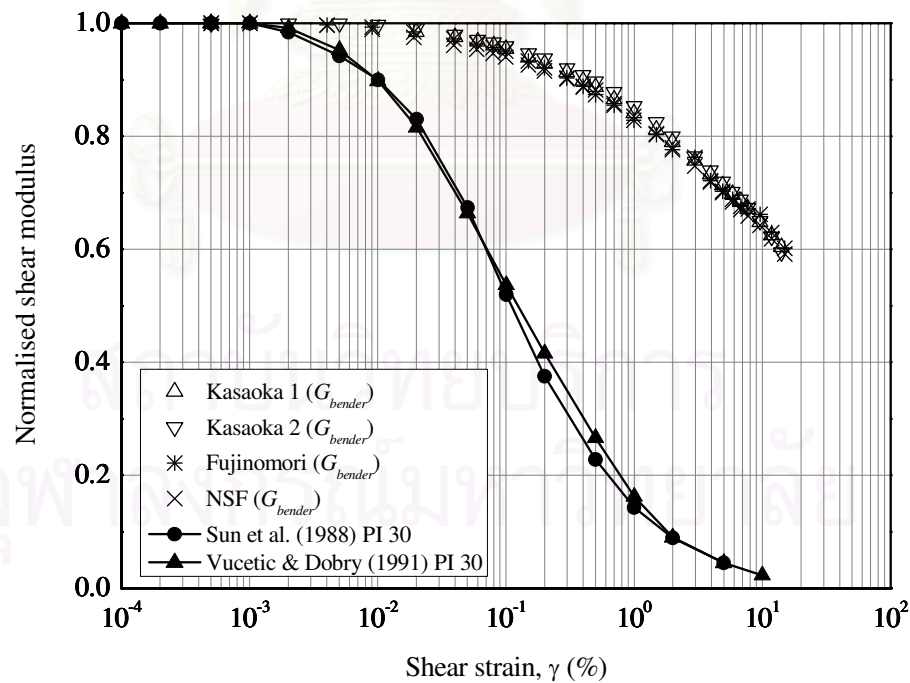
$$G_{bender} = [1.015 - 0.155 \gamma^{0.41}] G_{max,bender} \quad (5.18)$$

where, $G_{max,bender}$ is the maximum value of G_{bender} . By using equation (5.18), the G_{bender} degradation curve can be calculated once the $G_{max,bender}$ is determined.

G_{bender} curves shown in Figure 5.9(a) are normalised with p' and plotted in Figure 5.11. The curves shown in Figure 5.11 degrade when the γ increases. The curves of (G_{bender} / p') normalised with $(G_{bender} / p')_{max}$ are presented in Figure 5.12.

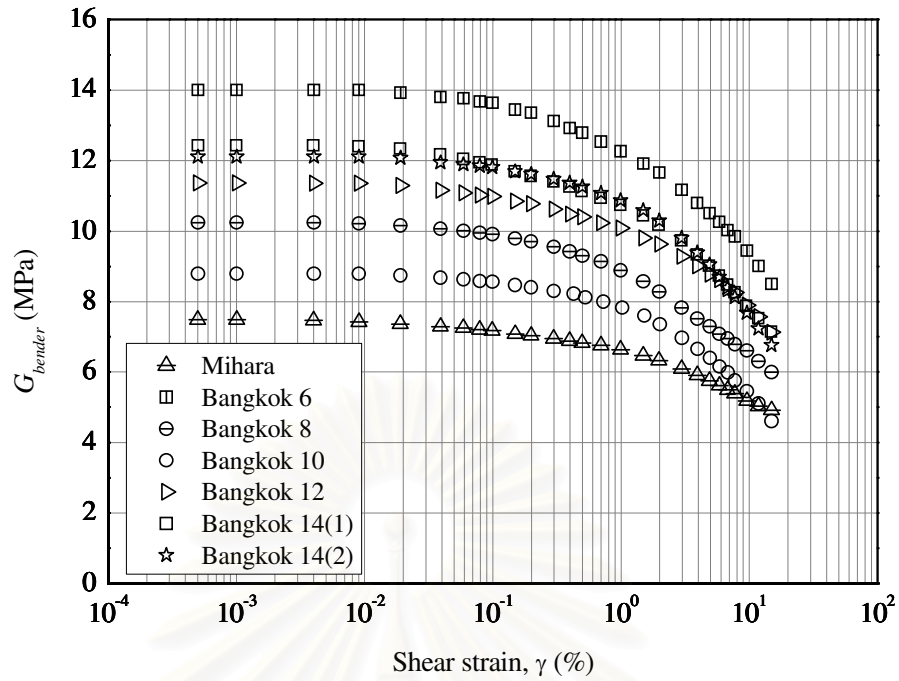


(a)

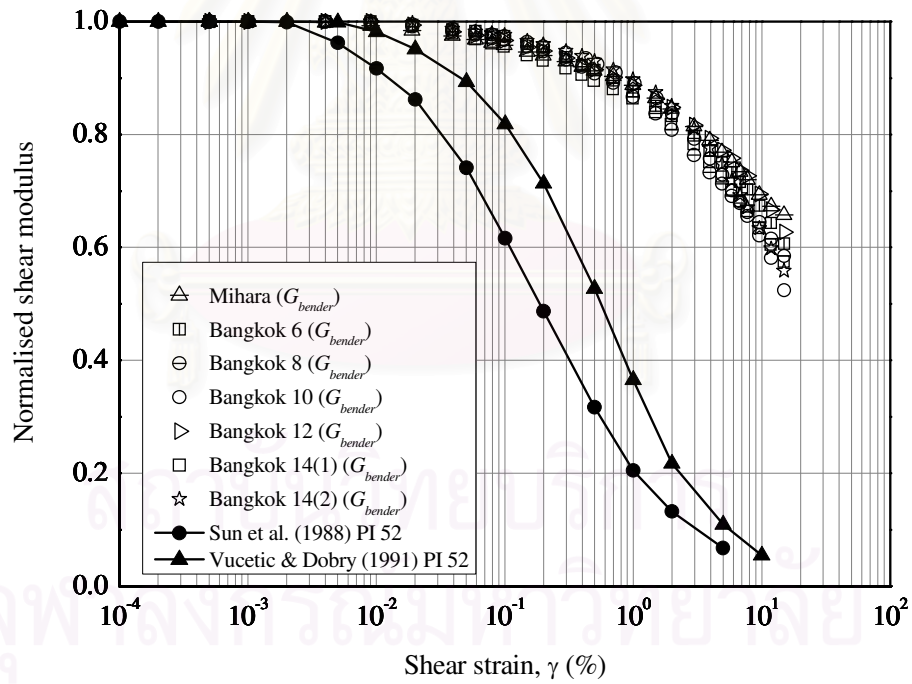


(b)

Figure 5.7 Test results for reconstituted samples (a) G_{bender} versus γ curve, (b) normalised G degradation curve.

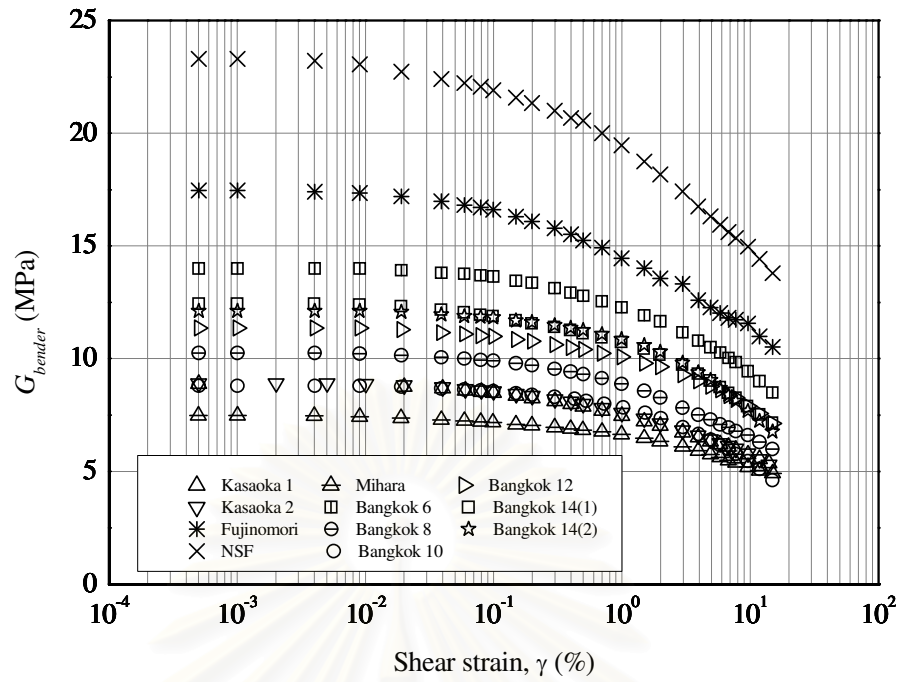


(a)

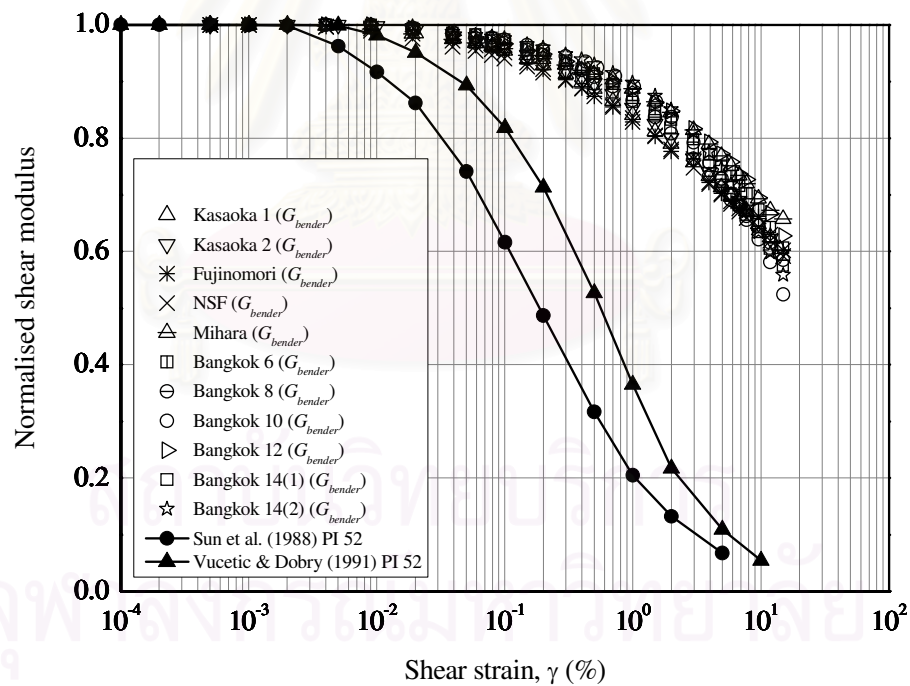


(b)

Figure 5.8 Test results for undisturbed samples (a) G_{bender} versus γ curve, (b) normalised G degradation curve.



(a)



(b)

Figure 5.9 Test results for samples in Figures 5.7 and 5.8 (a) G_{bender} versus γ curve, (b) normalised G degradation curve.

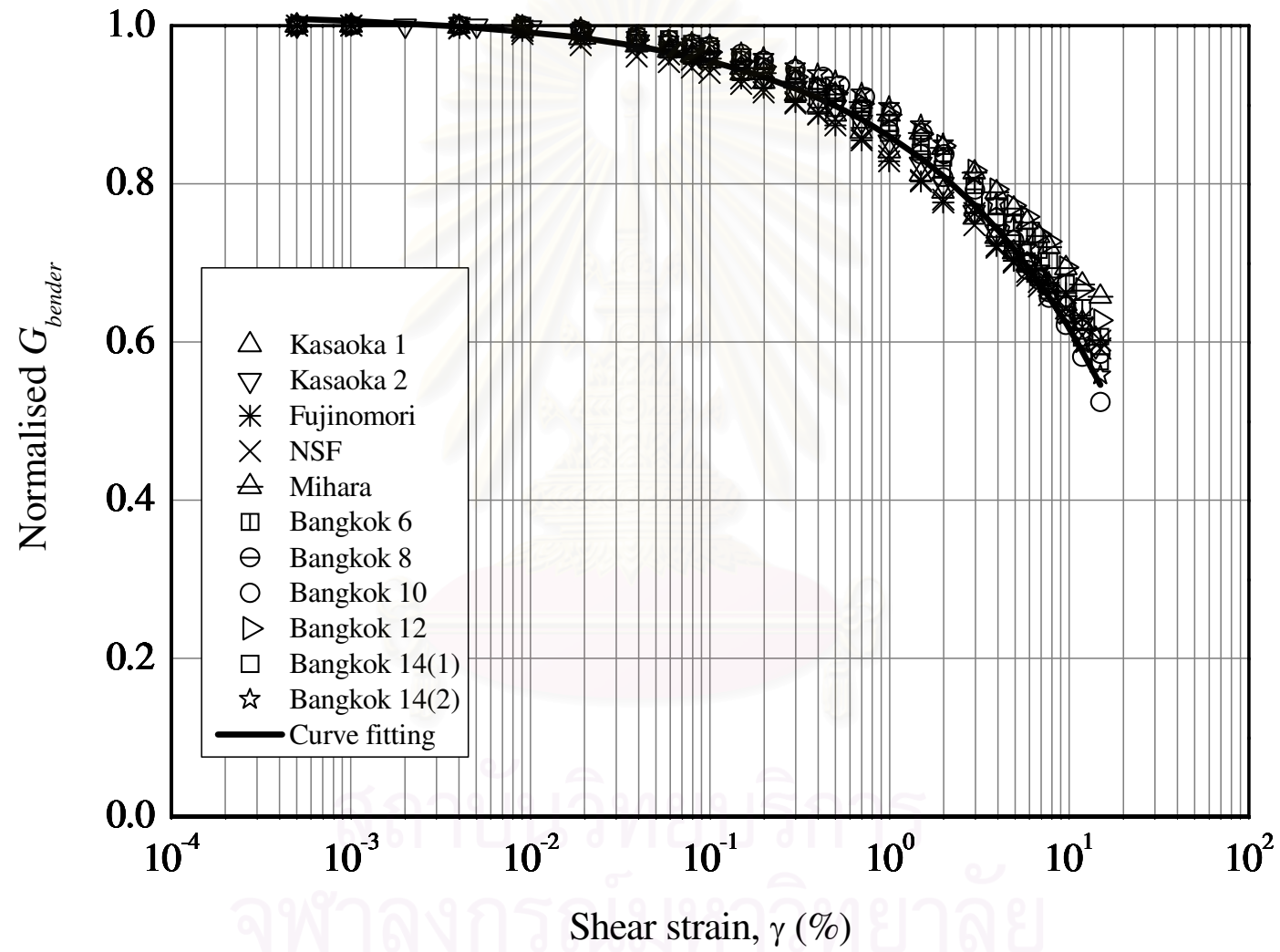


Figure 5.10 Curve fitting and the plot of normalised G_{bender} versus γ .

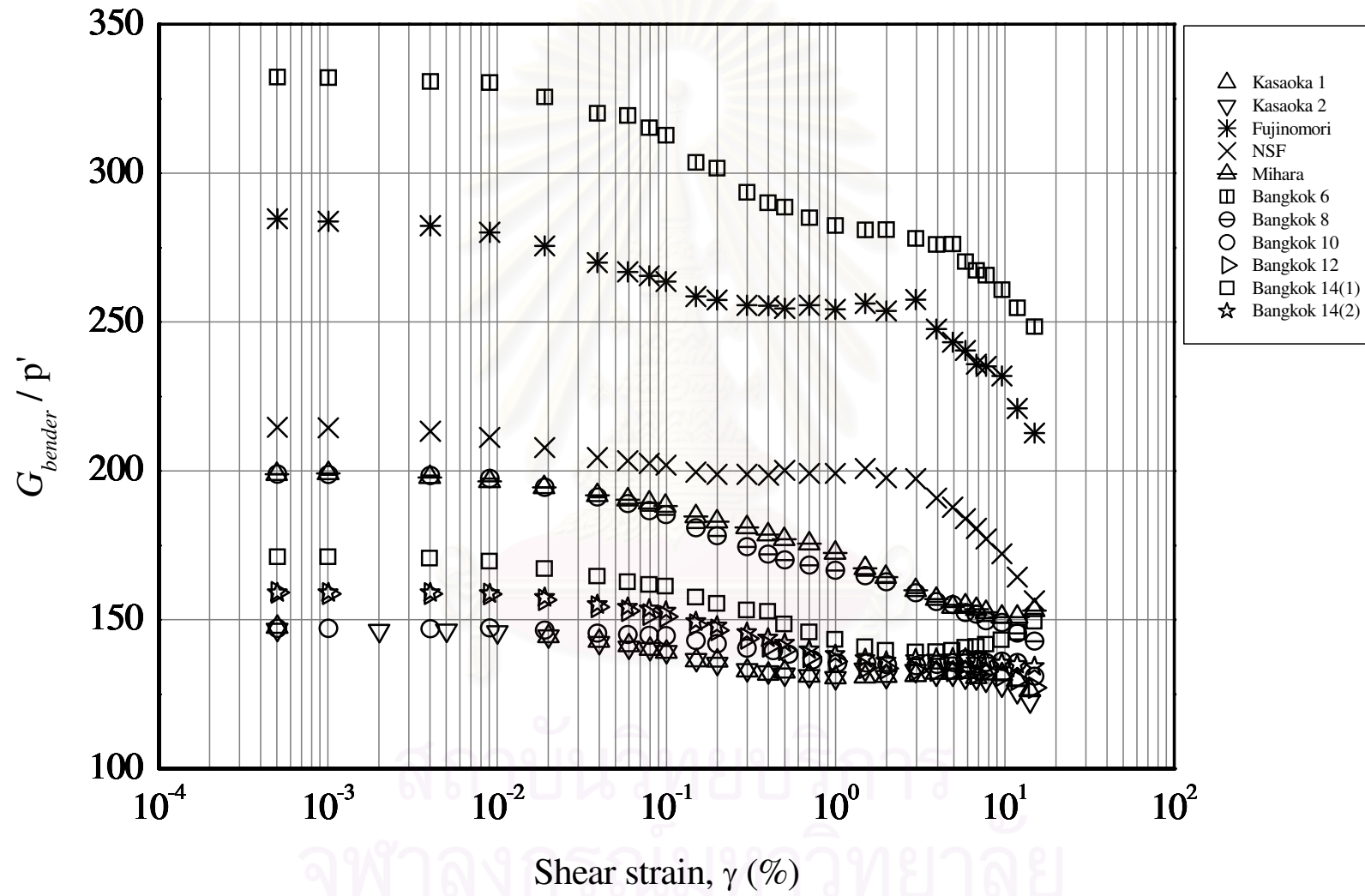


Figure 5.11 Curves for G_{bender} normalised with p' versus γ .

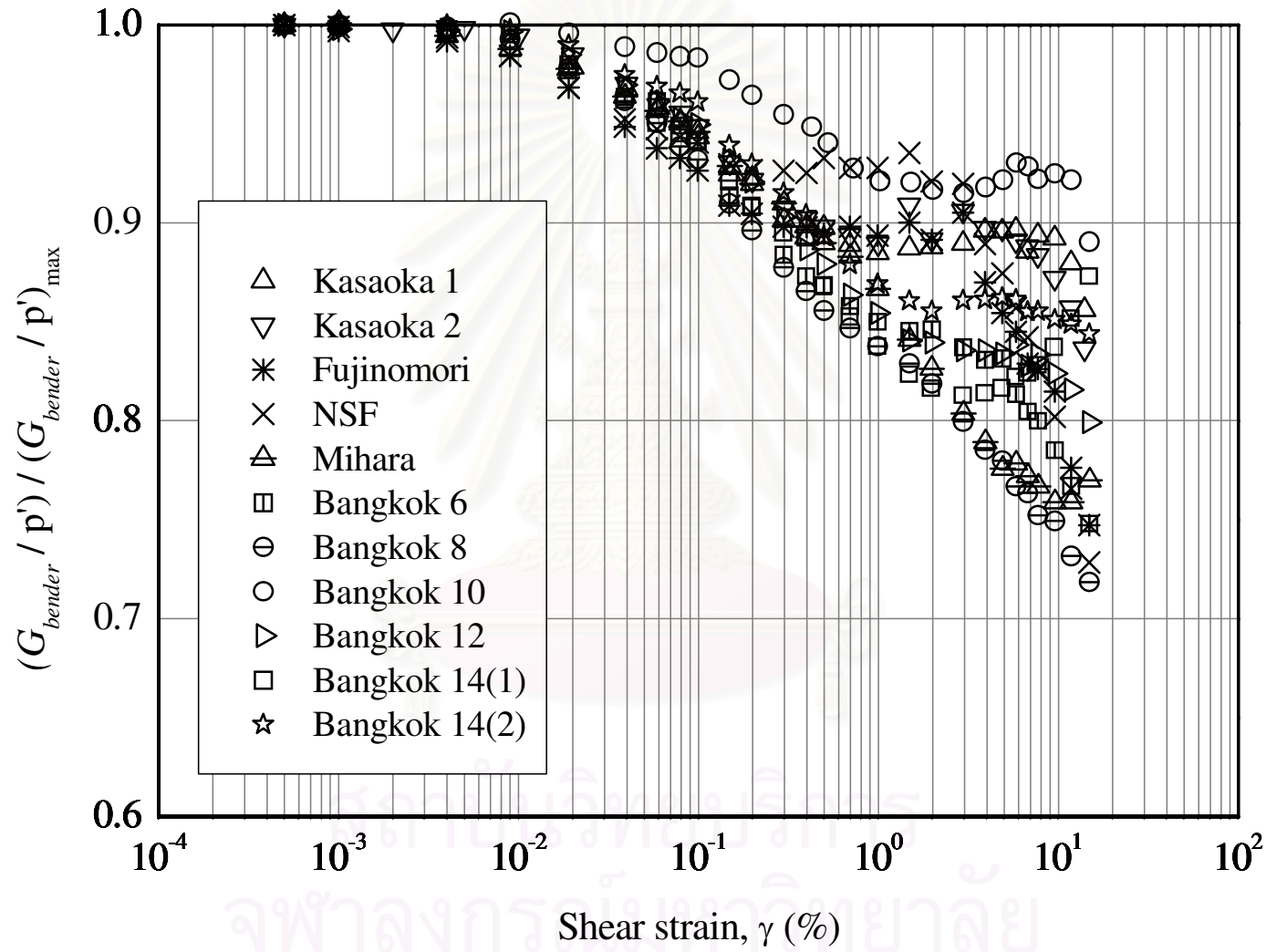


Figure 5.12 Curves for (G_{bender} / p') normalised with $(G_{bender} / p')_{\max}$ versus γ .

5.6 G Degradation Curve

Figure 5.13 shows the G degradation curves based on G_{bender} , G_{secant} and $G_{tangent}$ calculations. Normalised G degradation curves for samples in Figure 5.13 are shown in Figure 5.14. G_{secant} and $G_{tangent}$ are computed from a conventional compression triaxial test. The maximum values of G_{bender} , G_{secant} and $G_{tangent}$ for reconstituted samples are almost the same especially for Kasaoka 1 and NSF clays. However, for undisturbed samples, the maximum values of G_{secant} and $G_{tangent}$ are less than that of G_{bender} . The difference may be caused by the sample disturbance during sampling. They include sample extraction from a sampler, trimming process in the laboratory, anisotropic in stiffness (Shibuya, 2001) and the bedding error due to the axial displacement measurement for a triaxial sample. The bedding error due to the axial displacement measurement for a triaxial sample is considered insignificant for a soft sample but it becomes more significant in a stiff sample (Tatsuoka and Shibuya, 1991).

By referring to the G results presented in Figure 5.13, the maximum value of G_{bender} is higher than those of G_{secant} and $G_{tangent}$ because the method to determine maximum value of G_{bender} is free from disturbance effects. Shibuya and Tamrakar (2003) reported that G determined from the BEs test was close to G calculated from a seismic cone penetration test at the field. Therefore, maximum value of G_{bender} can be referred as G at very small strains and is suitable to be adopted in finite element analysis.

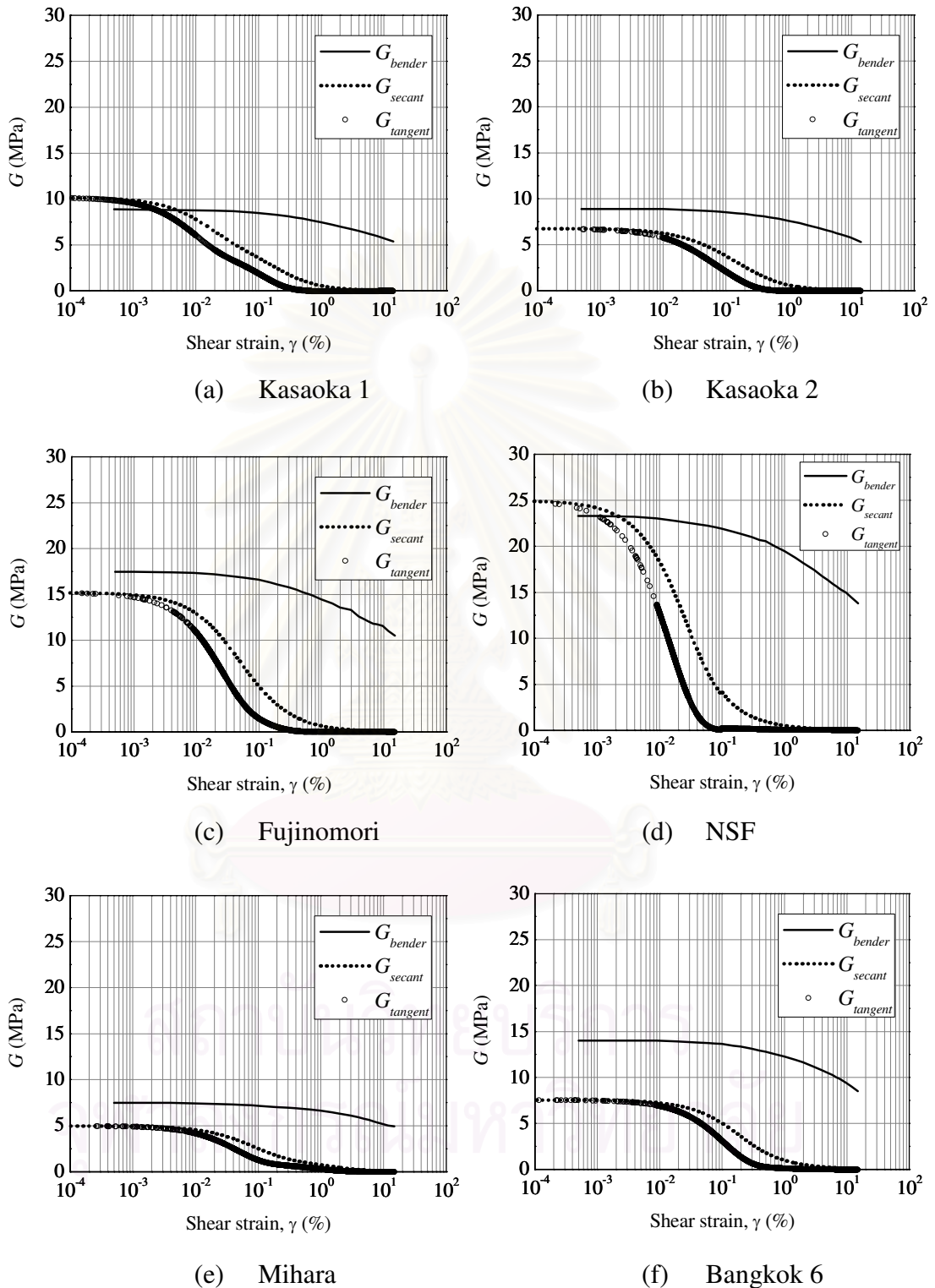


Figure 5.13 G degradation curves based on the calculation of G_{bender} , G_{secant} and $G_{tangent}$ (continue).

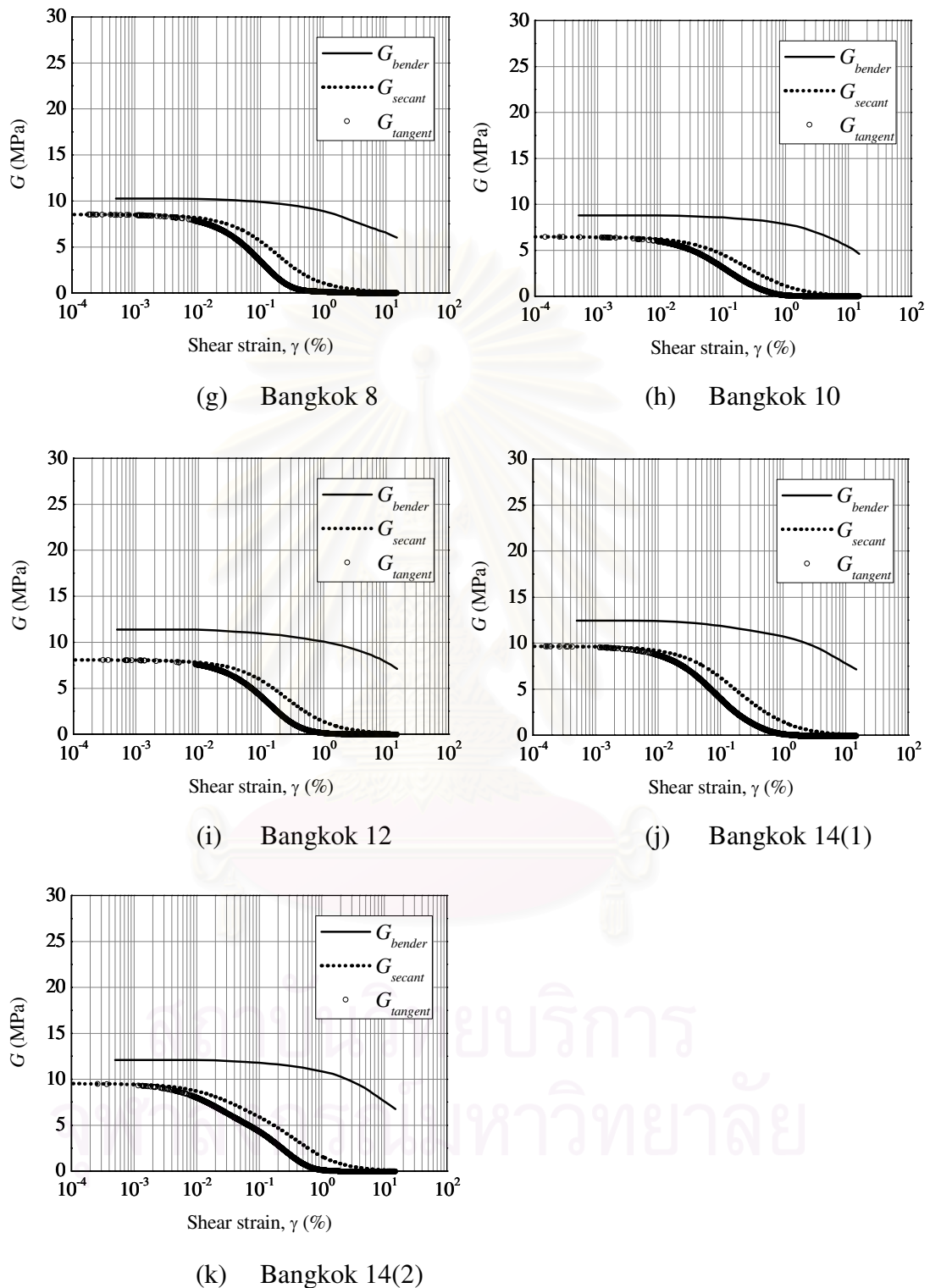


Figure 5.13 G degradation curves based on the calculation of G_{bender} , G_{secant} and $G_{tangent}$.

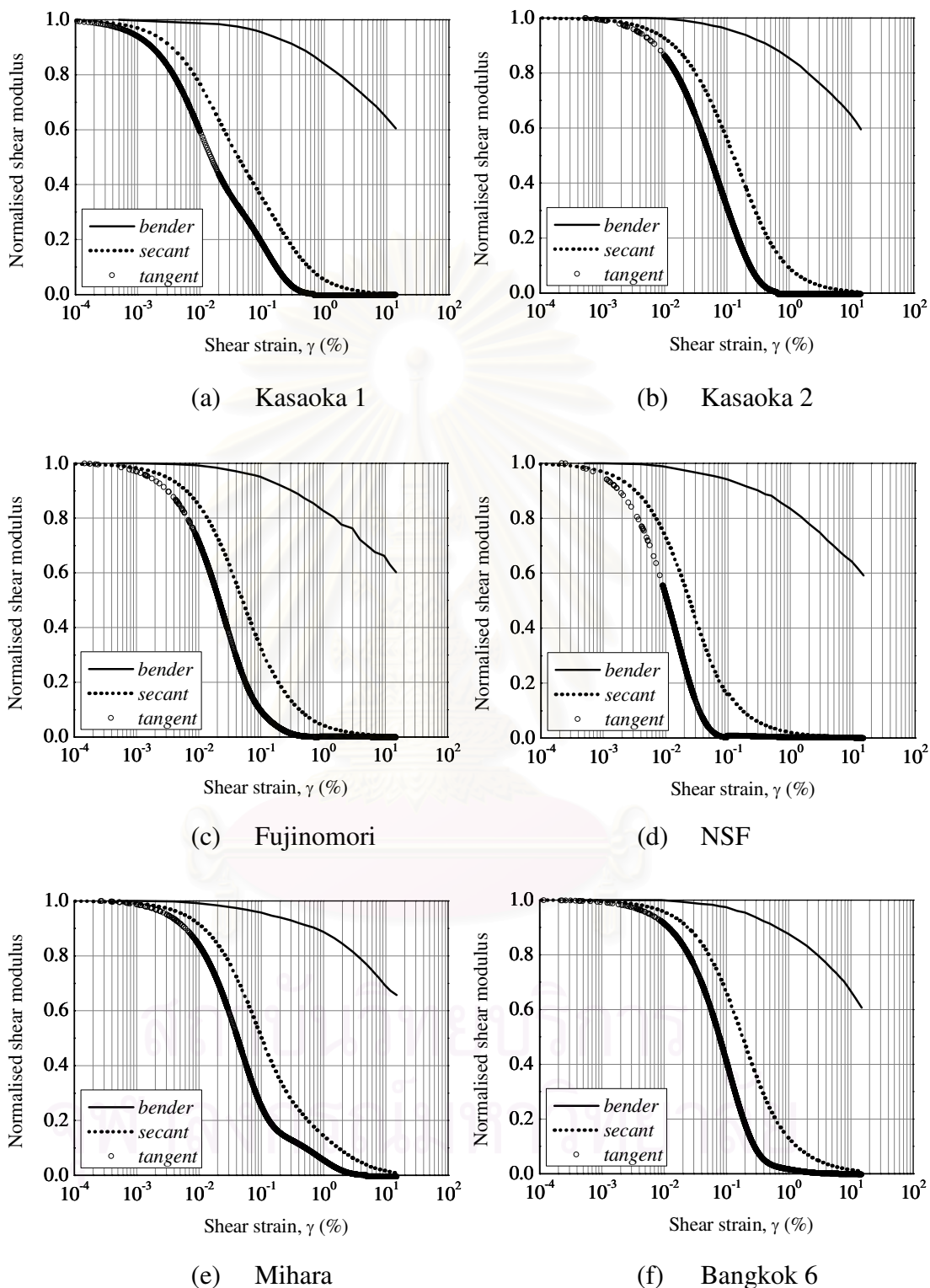


Figure 5.14 Normalised G degradation curves for samples in Figure 5.13 (*continue*).

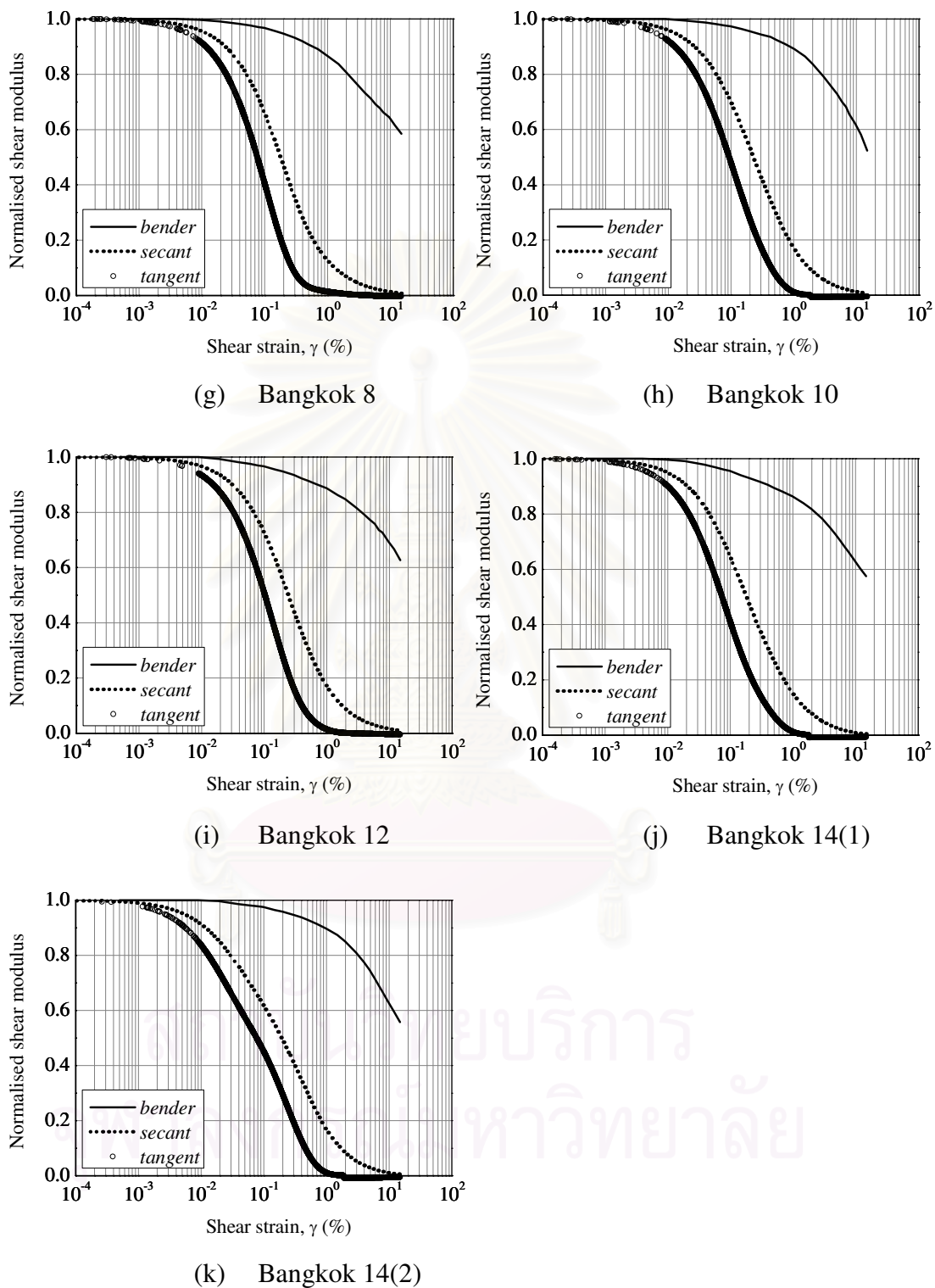


Figure 5.14 Normalised G degradation curves for samples in Figure 5.13.

5.7 Relationship between G Determined from the BEs Test, G_{bender} , and G Determined from Conventional Triaxial Test

By referring to Figure 5.9(b), the shape of the normalised G degradation curve for G_{bender} is almost the same. The author proposes that there is a relationship among $G_{max,bender}$, G_{secant} , $G_{tangent}$ and G_{bender} as shown in Figure 5.15. In Figure 5.15, $G_{max,bender}$ represents the maximum value of G_{bender} , or G_{bender} in very small strains region. The $G_{max,bender}$ can be determined before the shearing process when the sample is still in the elastic zone (Shibuya, 2001). When the sample is sheared, the behaviour of the sample changed from elastic to elasto-plastic. Therefore, the G_{bender} determined after shearing reflects elasto-plastic soil behaviour (Kawaguchi, 2007).

In short, G_{bender} before shearing is equal to $G_{max,bender}$. However after shearing, G_{bender} is less than $G_{max,bender}$. From Figure 5.15, the relationship among G_{bender} , $G_{max,bender}$, G_{secant} and $G_{tangent}$ are as follows:

$$G_{bender} = (1 - \alpha)G_{max,bender} + \alpha G_{secant} \quad (5.19)$$

$$G_{bender} = (1 - \theta)G_{max,bender} + \theta G_{tangent} \quad (5.20)$$

where α and θ are a function of shear strains. From equations (5.19) and (5.20), when α and θ are equal to zero, G_{bender} is equal to $G_{max,bender}$ and this happens before a shearing test. Equations (5.19) and (5.20) are strain dependency because G_{bender} , G_{secant} and $G_{tangent}$ depend on the induced γ . The values of α and θ can be obtained by using the following equations:

$$\alpha = \frac{G_{bender} - G_{max,bender}}{G_{secant} - G_{max,bender}} \quad (5.21)$$

$$\theta = \frac{G_{bender} - G_{max,bender}}{G_{tangent} - G_{max,bender}} \quad (5.22)$$

To determine the strain functions of α and θ , the α and θ values calculated from equations (5.21) and (5.22), respectively, are plotted against γ as shown in Figure 5.16 and Figure 5.17, respectively. Figure 5.16 and Figure 5.17 illustrate that

the scatter of the results is small and the curve fitting can be obtained to give the strain functions of α and θ as follows:

$$\alpha = 0.16 \gamma^{0.35} \quad (5.23)$$

$$\theta = 0.14 \gamma^{0.41} \quad (5.24)$$

where shear strain, γ , is in percent. By substituting, equation (5.23) into equation (5.19) and equation (5.24) into equation (5.20), the new equations for equations (5.19) and (5.20) are

$$G_{bender} = \left[1 - (0.16 \gamma^{0.35}) \right] G_{max,bender} + (0.16 \gamma^{0.35}) G_{secant} \quad (5.25)$$

$$G_{bender} = \left[1 - (0.14 \gamma^{0.41}) \right] G_{max,bender} + (0.14 \gamma^{0.41}) G_{tangent} \quad (5.26)$$

By using equation (5.25) or (5.26), G_{bender} at a particular γ can be computed. The testing methodology proposed to determine a G_{bender} degradation curve can be cut short by only performing the BEs test at the stage before shearing (to calculate $G_{max,bender}$) and then, continuously shearing the sample under monotonic loading with 0.05 %/minute of strain rate until 15% of maximum axial strain. For example, to calculate G_{bender} at γ equal to 1%, the parameter needed is $G_{max,bender}$ from the BEs test and G_{secant} or $G_{tangent}$ at γ equal to 1% determined from a conventional compression triaxial test.

Kasaoka 3 and Bangkok 14(3) are tested under continuous monotonic loading with the BEs test performed once at the stage before the shearing test. The secant and tangent shear modulus determined from a conventional triaxial test for Kasaoka 3 and Bangkok 14(3) are shown in Figure 5.18. The G_{bender} degradation curves for these two samples can be calculated based on equation (5.25) or (5.26) and the results are plotted together with Kasaoka 1, 2, Bangkok 14(1) and 14(2). The G_{bender} degradation curves calculated based on G_{secant} and $G_{tangent}$ are shown in Figure 5.19 and Figure 5.20, respectively. According to Figures 5.19 and 5.20, the calculated G_{bender} for Kasaoka 3 and Bangkok 14(3) fit well with the results of Kasaoka 1, 2, Bangkok 14(1) and 14(2). The shape of the G degradation curves are almost the same. This

concludes that equation (5.25) or (5.26) can be used to estimate the G_{bender} degradation curve.

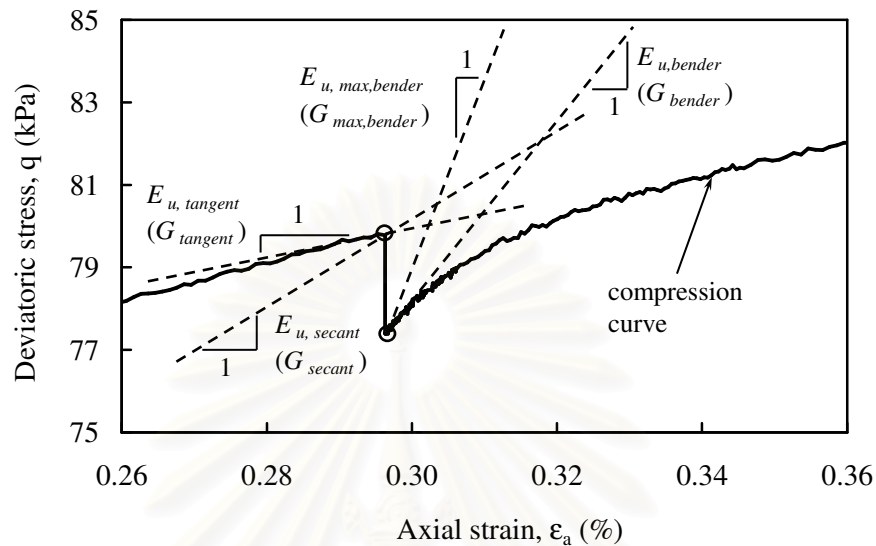


Figure 5.15 Diagram showing the relationship among $G_{max, bender}$, G_{bender} , G_{secant} and $G_{tangent}$.

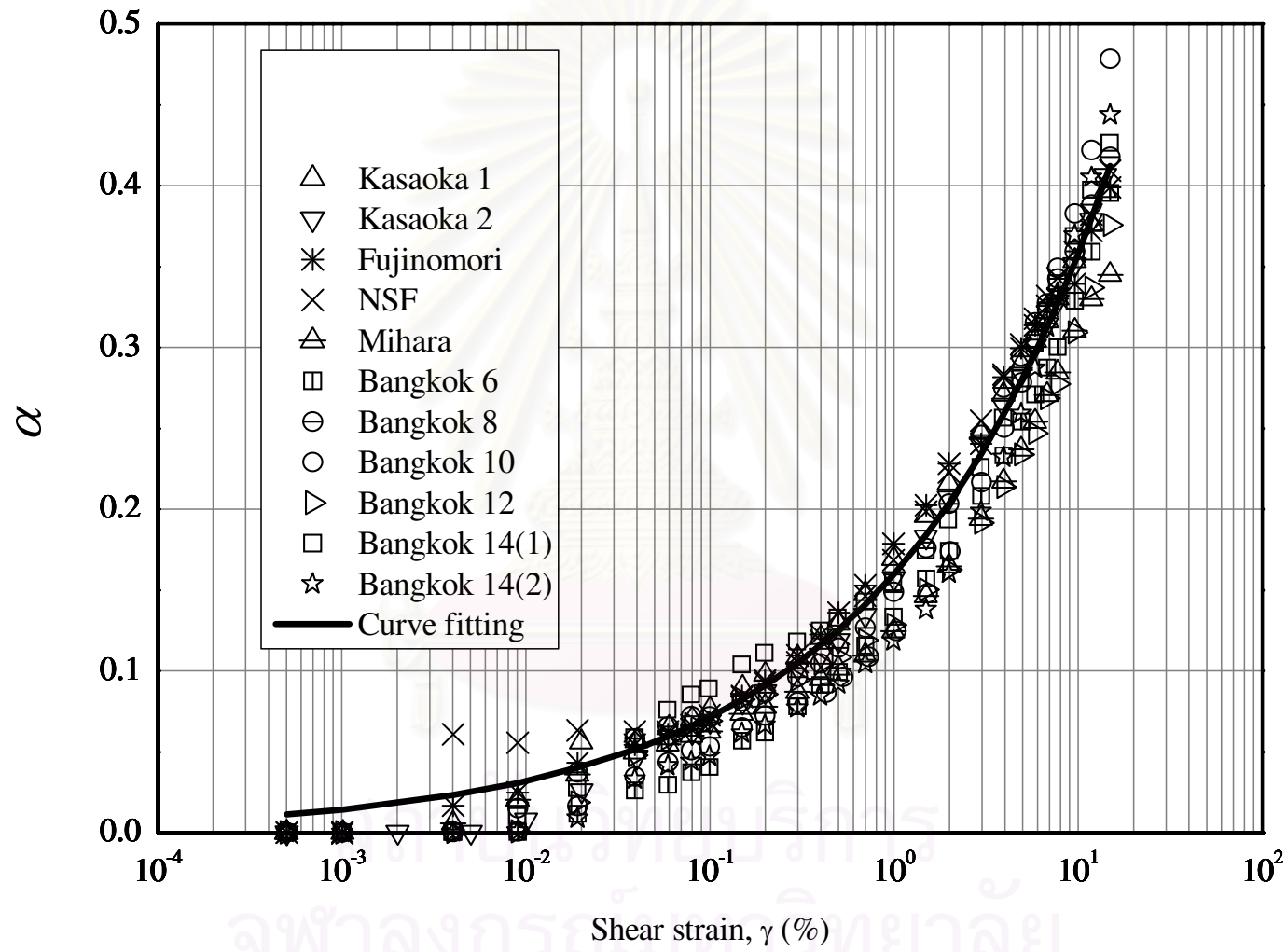


Figure 5.16 Curve fitting and the plot of α versus γ .

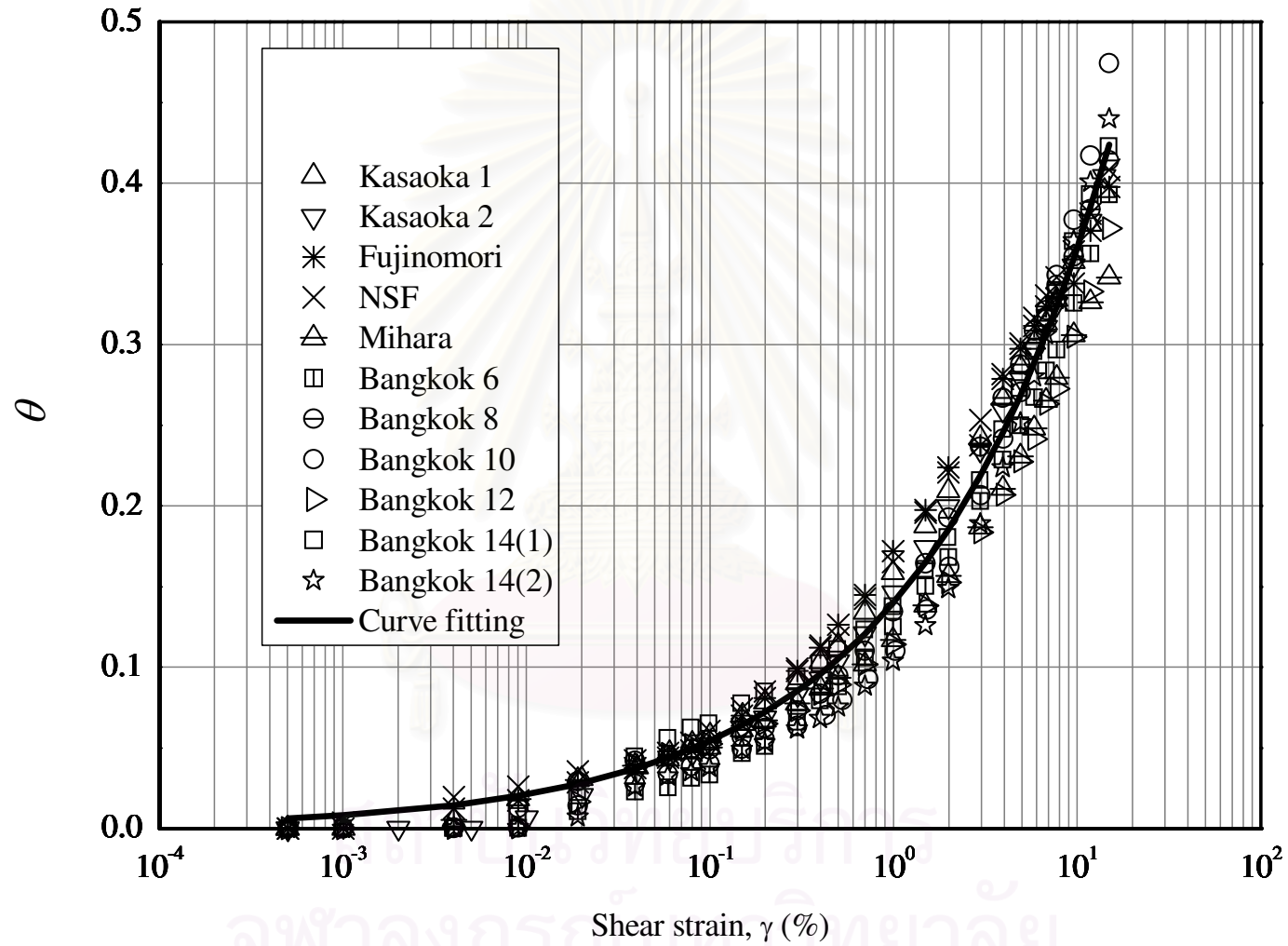
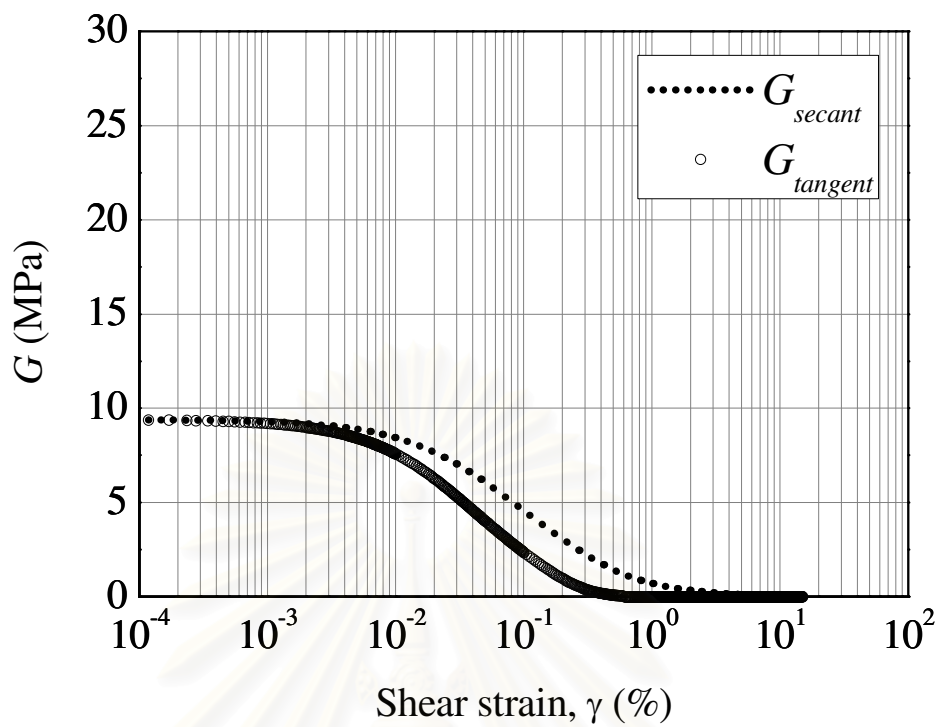
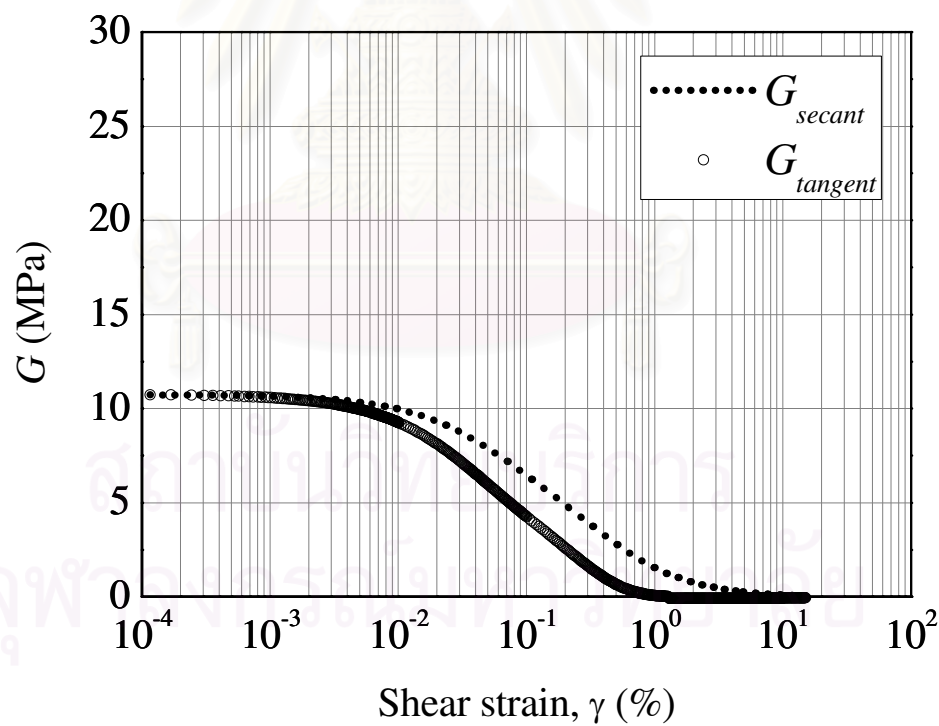


Figure 5.17 Curve fitting and the plot of θ versus γ .

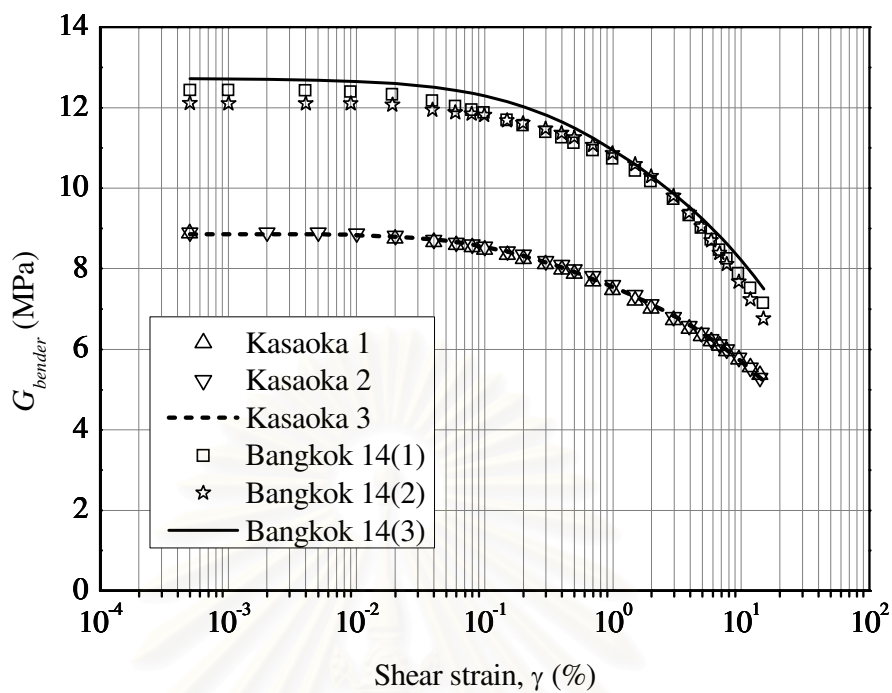


(a)

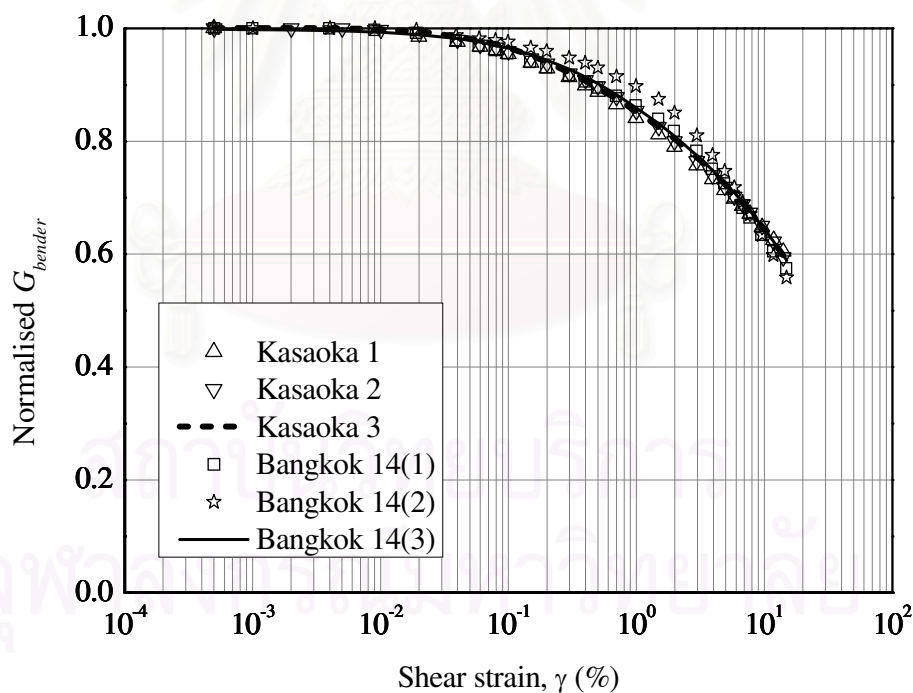


(b)

Figure 5.18 G degradation curves based on the calculation of G_{secant} and $G_{tangent}$ for (a) Kasaoka 3, (b) Bangkok 14(3).

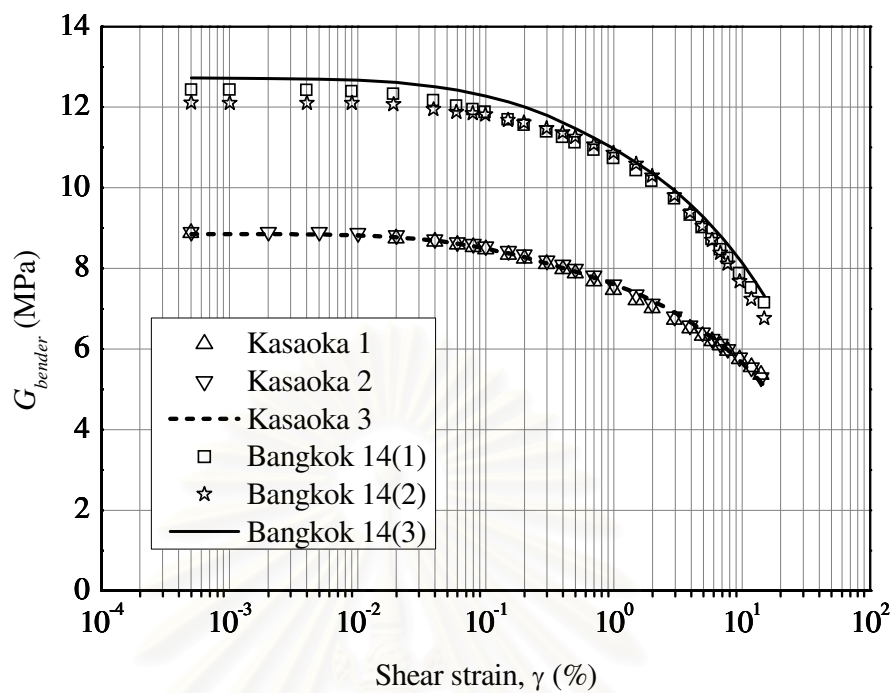


(a)

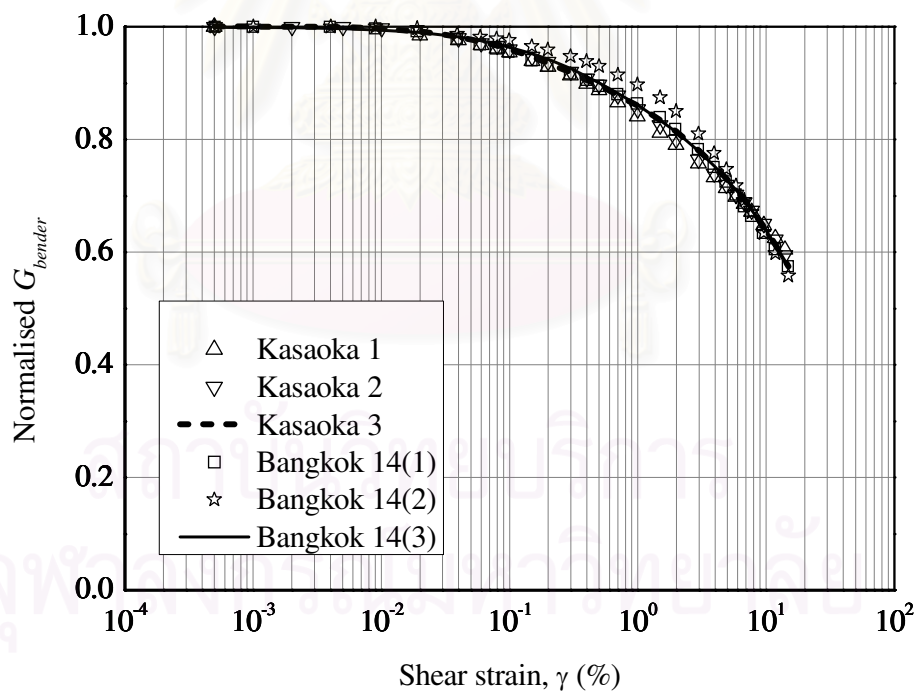


(b)

Figure 5.19 Plot of calculated G_{bender} for Kasaoka 3 and Bangkok 14(3) based on G_{secant} (a) G_{bender} versus γ curve, (b) normalised G_{bender} degradation curve.



(a)



(b)

Figure 5.20 Plot of calculated G_{bender} for Kasaoka 3 and Bangkok 14(3) based on $G_{tangent}$ (a) G_{bender} versus γ curve, (b) normalised G_{bender} degradation curve.

5.8 Summary

A testing methodology to identify the degradation curve for G calculated based on the BEs test, G_{bender} , is presented. The results of G_{bender} degradation curve are compared with G_{secant} and $G_{tangent}$. G_{secant} and $G_{tangent}$ are computed from a conventional triaxial test. This study yields the following major findings, namely,

1. The proposed testing methodology provides consistent results.
2. The stress path of the sample is not influenced by the proposed methodology.
3. The normalised G_{bender} degradation curve is not influenced by the types of samples such as reconstituted or undisturbed samples. Besides, the shape of the normalised G_{bender} degradation curve is not affected by the plasticity indices of the samples ranging from 25 to 52.
4. Normalised G_{bender} shows a relationship with γ . By applying this relationship, the G_{bender} degradation curve can be constructed when the $G_{max,bender}$ is obtained.
5. G_{max} for G_{secant} and $G_{tangent}$ are lower than the maximum value of G_{bender} because the test to determine the maximum value of G_{bender} is free from disturbance effects. Hence, the maximum value of G_{bender} can be referred as the G at very small strains and is suitable to be adopted in the finite element analysis.
6. G_{bender} shows a relationship with $G_{max,bender}$, G_{secant} and $G_{max,bender}$, $G_{tangent}$. These relationships are strain dependency and can be employed to cut short the proposed methodology to obtain the G_{bender} degradation curve.

CHAPTER VI

CONCLUSIONS

The G degradation curve can be constructed from the G_{max} determined either in field or laboratory. The down-hole test, cross-hole test and seismic cone penetration test are most common methods for field tests. For laboratory tests, BEs test, cyclic triaxial test, resonant column test, torsional shear test, conventional triaxial testing and local axial displacement gauge can be employed. For cohesive soil, the plasticity index of the soil controls the threshold of the normalised G degradation curve.

Phase Velocity of Shear Wave

The variable-path length method using continuous sinusoidal wave is used to determine phase velocity of shear wave in a clay sample. The combination of the proposed method and the conventional time domain method gives the explicit picture of the relationship between phase and group velocities. The uncertainty caused by the distance measurement can be avoided in the proposed method. The adapted continuous signal yields high signal recovery which is preferable for highly damped soil and in a noisy environment. Since the proposed method can determine v_{phase} at arbitrary frequency, this method should be able to be adopted for studying the frequency dependency of the V_s .

The Effects of the BE Installation on Shear Wave Velocity Measurement

The penetration tests performed by varying the rate of penetration, size of sample and isotropic consolidation pressure reveal that the installations of BEs into the clay sample generate almost no disturbance. Hence, the BEs tests can be easily carried out for clay samples in the laboratory and in the field with nearly no effect of the BEs installation. The testing results also confirm the findings yielded from previous research that the wave propagates from the tip of transmitter to the tip of receiver BEs.

Magnitude of the Shear Strain Generated by the BEs Test

A laser displacement gauge and self-monitoring circuit are used in the calibration process to circumvent the effect of epoxy coating and soil stiffness. Few conclusions can be made:

1. The magnitude of induced γ is not affected by the isotropic consolidation pressure.
2. The maximum γ near the transmitter and receiver are $10^{-1}\%$ and $10^{-4}\%$, respectively.
3. The V_s is relatively constant even when the magnitude of induced γ increases.
4. The ratios between shear strains near the transmitter and receiver are almost constant for all the input voltages with the corresponding frequency and isotropic consolidation pressure.
5. The magnitude of γ for BEs tests shall be represented by the maximum γ near the receiver BE which is $10^{-4}\%$.

Shear Wave Velocity Determination By the Swept Signal

From the validation process, it is found that the V_s determined by using $t_{(swept)}$ is close to the travel time reported by previous researchers. Therefore, the finding demonstrates that the swept signal can be used as an alternative signal for the measurement of V_s . In a noisy environment, the cross-correlation technique can transform the weak and long stimulating swept signal into a clear maximum peak for easy determination of the travel time.

Regeneration of Received Signal Based on the BEs Test by Using the Swept Signal

A technique for identifying frequency response of the BEs testing system based on the linear system theory is demonstrated. Frequency responses for several different testing systems involving conditions of specimens and dimensions of BEs are experimentally identified using the swept signal and applied to compute the received waveforms for arbitrary transmitted wave. Calculated received waveforms are compared with experimental data. The main observations from this study are as follows:

1. Received waveforms of the BEs test can be regenerated by frequency response

of the testing system obtained by swept signals. Two types of swept signals (TSP and LSSP) designed by different formula are tested. Calculated received waveforms are in good agreement with the observed ones irrespective of the types of swept signals or frequencies.

2. This method for received wave regeneration can be applied irrespective of a testing system. Test results which examine the influence of the testing system using different samples, different testing apparatus and different dimensions of specimen and BEs do not affect the applicability of this technique.
3. The shape of frequency response changes depending on testing system. In particular, change in resonant frequency is reasonably explained by change of soil stiffness and density.
4. Shear wave velocities obtained from calculated and observed received waves show good agreement in any testing system. Difference of shear wave velocities is less than 8%.

Strain Dependency of Shear Modulus

A testing methodology to identify the degradation curve for G calculated based on the BEs test, G_{bender} , is presented. The results of G_{bender} degradation curve are compared with G_{secant} and $G_{tangent}$. G_{secant} and $G_{tangent}$ are computed from a conventional test. This study yields the following major findings, namely,

1. The proposed testing methodology provides consistent results.
2. The stress path of the sample is not influenced by the proposed methodology.
3. The normalised G_{bender} degradation curve is not influenced by the types of samples such as reconstituted or undisturbed samples. Besides, the shape of the normalised G_{bender} degradation curve is not affected by the plasticity indices of the samples ranging from 25 to 52.
4. Normalised G_{bender} shows a relationship with γ . By applying this relationship, the G_{bender} degradation curve can be constructed when the $G_{max,bender}$ is obtained.
5. G_{max} for G_{secant} and $G_{tangent}$ are lower than the maximum value of G_{bender} because the test to determine the maximum value of G_{bender} is free from disturbance effects. Hence, the maximum value of G_{bender} can be referred as the G at very small strains and is suitable to be adopted in the finite element analysis.

6. G_{bender} shows a relationship with $G_{max,bender}$, G_{secant} and $G_{max,bender}$, $G_{tangent}$. These relationships are strain dependency and can be employed to cut short the proposed methodology to obtain the G_{bender} degradation curve.



สถาบันวิทยบริการ
จุฬาลงกรณ์มหาวิทยาลัย

REFERENCES

- Aoshima, N. (1981). Computer-generated pulse signal applied for sound measurement. **Journal of the Acoustical Society of America** 69 : 1484-1488.
- Arroyo, M., Wood, D. M. and Greening, P. D. (2003). Source near-field effects and pulse tests in soil samples. **Geotechnique** 53 (3) : 337-345.
- Arulnathan, R., Boulanger, R. W. and Riemer, M. F. (1998). Analysis of bender element tests. **Geotechnical Testing Journal** 21 (2) : 120-131.
- Atkinson, J. H. (1993). **An introduction to the mechanics of soils and foundations through critical state soil mechanics**. London: McGraw-Hill.
- Atkinson, J. H. (2000). Non-linear soil stiffness in routine design. **Geotechnique** 50 (5) : 487-508.
- Atkinson, J. H. and Salfors, G. (1991). Experimental determination of stress-strain-time characteristics in laboratory and In-situ tests. **Proc. 10th Eur. Conf. Soil Mech.**, 915-956. Florence.
- Blewett, J., Blewett, I. J. and Woodward, P. K. (1999). Measurement of shear-wave velocity using phase-sensitive detection techniques. **Canadian Geotechnical Journal** 36 : 934-939.
- Blewett, J., Blewett, I. J. and Woodward, P. K. (2000). Phase and amplitude responses associated with the measurement of shear-wave velocity in sand by bender elements. **Canadian Geotechnical Journal** 37 : 1348-1357.
- Boonyatee, T. and Chan, K. H. (2006). Determination of shear wave velocity using bender elements and chirp signal. **The Nineteenth KKCNN Symposium on Civil Engineering**, 321-324. Kyoto.
- Brignoli, E. G. M., Gotti, M. and Stokoe, K. H. (1996). Measurement of shear waves in laboratory specimens by means of piezoelectric transducers. **Geotechnical Testing Journal** 19 (4) : 384-397.
- Brillouin, L. (1960). **Wave propagation and group velocity**. New York: Academic Press.
- Burland, J. B. (1979). Contribution to discussion on Session 4. **Proc 7th European Conf. SMFE**, 137. Brighton.
- Butcher, A. P. and Powell, J. J. M. (1996). Discussion on evaluation of in situ anisotropy from crosshole and downhole shear wave velocity measurements by Sully, J. P. and Campanella, R. G. **Geotechnique** 46 (3) : 565-569.

- Chan, K. H. and Boonyatee, T. (2005). Determination of shear wave velocity using continuous wave method. **The Eighteenth KKCNN Symposium on Civil Engineering**, 55-60. Kaohsiung.
- Chan, K. H. and Boonyatee, T. (2006). Study of strain dependency of shear wave velocity using bender elements. **The Nineteenth KKCNN Symposium on Civil Engineering**, 389-392. Kyoto.
- Chan, K. H., Boonyatee, T. and Mitachi, T. (2007). A study of bender element installation in clay sample. **The Twentieth KKCNN Symposium on Civil Engineering**, 350-353. Jeju.
- Chang, H. P. N. (2005). **The relationship between void ratio and shear wave velocity of gold tailings**. M. Eng. Thesis, Faculty of Engineering, Build Environment and Information Technology, University of Pretoria.
- Costa Filho, L. de M. (1985). Measurement of axial strains in triaxial tests on London clay. **Geotechnical Testing Journal** 8 (1) : 3-13.
- Cuccovillo, T. and Coop, M. R. (1997). The measurement of local axial strains in triaxial tests using LVDTs. **Geotechnique** 47 (1) : 167-171.
- Drnevich, V. P. (1972). Undrained cyclic shear of saturated sand. **Journal of Soil Mechanics and Foundations Division**, ASCE, 98 (8) : 807-825.
- Dyvik, R. and Madshus, C. (1985). Lab measurements of G_{max} using bender elements. **Proceedings ASCE Annual Convention: Advances in the Art of Testing Soils under Cyclic Conditions**, 186-197. Detroit.
- Fam, M. and Santamarina, J. C. (1997). A study of consolidation using mechanical and electromagnetic waves. **Geotechnique** 47 (2) : 203-219.
- Fioravante, V. and Capoferri, R. (2001). On the use of multi-directional piezoelectric transducers in triaxial testing. **Geotechnical Testing Journal** 24 (3) : 243-255.
- Goto, S., Tatsuoka, F., Shibuya, S., Kim, Y. S. and Sato, T. (1991). A simple gauge for local small strain measurements in the laboratory. **Soils and Foundations** 31 (1) : 169-180.
- Greening, P. D. and Nash, D. F. T. (2004). Frequency domain determination of G_0 using bender elements. **Geotechnical Testing Journal** 27 (3) : 288-294.
- Hardin, B. O. and Drnevich, V. P. (1972 a). Shear modulus and damping in soils: measurement and parameter effects. **Journal of Soil Mechanics and Foundations Division**, ASCE, 98 (6) : 603-624.

- Hardin, B. O. and Drnevich, V. P. (1972 b). Shear modulus and damping of soils: design equation and curves. **Journal of Soil Mechanics and Foundations Division**, ASCE, 98 (7) : 667-692.
- Hight, D. W., Bennell, J. D., Chana, B., Davis, P. D., Jardine, R. J. and Porovic, E. (1997). Wave velocity and stiffness measurements of the Crag and Lower London Tertiaries at Sizewell. **Geotechnique** 47 (3) : 451-474.
- Hope, V. S. (1996). Discussion on evaluation of in situ anisotropy from crosshole and downhole shear wave velocity measurements by Sully, J. P. and Campanella, R. G. **Geotechnique** 46 (3) : 565-569.
- Hwang, S. C., Mitachi, T., Shibuya, S. and Tateichi, K. (1998). Stress-strain characteristics in the wide strain range from small strain to failure state and undrained shear strength of natural clays. **Journal of JSCE** 3 (42) : 305-319 (in Japanese).
- Ishihara, K. (1996). **Soil behaviour in earthquake geotechnics**. Oxford: Oxford University Press.
- Ishihara, K. and Towhata, I. (1983). Sand response to cyclic rotation of principal stress directions as induced by wave loads. **Soils and Foundations** 23 (4) : 11-26.
- Jamiolkowski, M., Lancellotta, R. and Lo Presti, D. C. F. (1995). Remarks on the stiffness at small strains of six Italian clays. In Shibuya, S. et al. (eds.), **Pre-failure deformation of geomaterials**, 817-836. Sapporo: Balkema.
- Jardine, R. J., Symes, M. J. and Burland, J. B. (1984). The measurement of soil stiffness in the triaxial apparatus. **Geotechnique** 34 (3) : 323-340.
- JGS-0523-2000. **Japanese Geotechnical Standards**.
- Jovicic, V., Coop, M. R. and Simic, M. (1996). Objective criteria for determining G_{max} from bender element tests. **Geotechnique** 46 (2) : 357-362.
- Kawaguchi, T. (2007). **Personal communication**.
- Kawaguchi, T., Mitachi, T and Shibuya, S. (2001). Evaluation of shear wave travel time in laboratory bender element test. **Proceedings 15th International Conference on Soil Mechanics and Geotechnical Engineering**, 155-158.
- Kim, Y. S., Tatsuoka, F and Ochi, K. (1994). Deformation characteristics at small strains of sedimentary soft rocks by triaxial compression tests. **Geotechnique** 44 (3) : 461-478.

- Kokusho, T. (1980). Cyclic triaxial test of dynamic soil properties for wide strain range. **Soils and Foundations** 20 (2) : 45-60.
- Kokusho, T. (2004). Nonlinear site response and strain-dependent soil properties. **CURRENT SCIENCE** 87 (10) : 1363-1369.
- Kokusho, T., Yoshida, Y. and Esashi, Y. (1982). Dynamic properties of soft clay for wide strain range. **Soils and Foundations** 22 (4) : 1-18.
- Kuribayashi, E., Iwasaki, T., Tatsuoka, F. and Horiuchi, S. (1974). **Dynamic deformation characteristics of soils – measurements by the resonant column test device**. Report of the Public Works Research Institute. Japan (in Japanese).
- Landon, M. M., DeGroot, D. J. and Sheahan, T. C. (2007). Nondestructive sample quality assessment of a soft clay using shear wave velocity. **Journal of Geotechnical and Geoenvironmental Engineering**, ASCE, 133 (4) : 424-432.
- Lee, J. S. and Santamarina, J. C. (2005). Bender elements: Performance and signal interpretation. **Journal of Geotechnical and Geoenvironmental Engineering**, ASCE, 131 (9) : 1063-1070.
- Leong, E. C., Yeo, S. H. and Rahardjo, H. (2005). Measuring shear wave velocity using bender elements. **Geotechnical Testing Journal** 28 (5) : 488-498.
- Lohani, T. N., Imai, G. and Shibuya, S. (1999). Determination of shear wave velocity in bender element test. In Seco e Pinto (eds.), **Proc. 2nd International Conference on Earthquake Geotechnical Engineering**, 101-106. Lisbon: Balkema.
- Luna, R. and Jadi, H. (2000). Determination of dynamic soil properties using geophysical methods. **Proc. of the First Int. Conf. on the App. of Geophysical and NDT Methodologies to Trans. Facilities and Infrastructure**. St. Louis.
- Lynnworth, L. C., Rea, W. R. and Papadakis, E. P. (1981). Continuous wave transmission techniques for measuring ultrasonic phase and group velocities in dispersive materials and composites. **Journal of the Acoustical Society of America** 70 (6) : 1699-1703.
- Mair, R. J. (1993). Developments in geotechnical engineering research: application to tunnels and deep excavations. **Proc. Instn. Civ. Engrs**, 27-41. London.
- Nishio, S. and Hotta, H. (2000). Applicability of self-monitoring bender element. **Proc. Japanese Geotechnical Society**, 261-262. Gifu (in Japanese).

- Ogino, T., Mitachi, T., Chan, K. H., Oikawa, H. and Tsushima, M. (2008). A method for received waveform reconstruction based on bender element test using frequency-swept signal. **Soils and Foundations** 48 (2) (in printing).
- Ogino, T., Oikawa, H., Mitachi, T., Tsushima, M. and Nishida, K. (2006). Shear wave velocity by TSP applied bender element test in sand. **Journal of JSCE** 62 (1) : 169-174 (in Japanese).
- Pain, H. J. (1999). **The physics of vibrations and waves**. 5th edition. England: John Wiley & Sons Ltd.
- Pennington, D. S., Nash, D. F. T. and Lings, M. L. (1997). Anisotropy of G_0 shear stiffness in Gault clay. **Geotechnique** 47 (3) : 391-398.
- Pennington, D. S., Nash, D. F. T. and Lings, M. L. (2001). Horizontally mounted bender elements for measuring anisotropic shear moduli in triaxial clay specimens. **Geotechnical Testing Journal** 24 (2) : 133-144.
- Piezo Systems, Inc. (2004). **Application data**. <http://www.piezo.com/>
- Prakash, S. (1981). **Soil dynamics**. New York: McGraw-Hill Book Co.
- Sachse, W. and Pao, Y-H (1978). On the determination of phase and group velocities of dispersive waves in solids. **Journal of Applied Physics** 49 (8) : 4320-4327.
- Salgado, R. and Drnevich, V. P., Ashmawy, A., Grant, W. P. and Vallenias, P. (1997). Interpretation of large-strain seismic cross-hole tests. **Journal of Geotechnical and Geoenvironmental Engineering**, ASCE, 123 (4) : 382-388.
- Sanchez-Salinerio, I., Roesset, J. M. and Stokoe, K. H. (1986). **Analytical studies of body wave propagation and attenuation**. Report GR 86-15. University of Texas, Austin.
- Santamarina, J. C. and Fam, M. A. (1997). Discussion on interpretation of bender element tests by Viggiani, G. and Atkinson, J. H. **Geotechnique** 47 (4) : 873-877.
- Schultheiss, P. J. (1982). **Influence of packing structure on seismic wave velocities in sediments**. PhD. thesis, University College of North Wales.
- Seed, H. B. and Idriss, I. M. (1970). **Soil moduli and damping factors for dynamic response analyses**. Report No. ERRC 70-10. Earthquake Engineering Research Center, University of California at Berkeley.
- Shannon, W. L., Yamane, G. and Dietrich, R. J. (1959). Dynamic triaxial tests on sand. **Proceedings of the 1st Panamerican Conference on Soil Mechanics and Foundation Engineering**, 473-486. Mexico City.

- Shibuya, S. (2001). **Quasi-elastic stiffness in the behaviour of soft clay**. D. Eng. thesis, Graduate School of Engineering, University of Tokyo.
- Shibuya, S., Hwang, S. C. and Mitachi, T. (1997). Elastic shear modulus of soft clays from shear wave velocity measurement. **Geotechnique** 47 (3) : 593-601.
- Shibuya, S. and Mitachi, T. (1997). Development of a fully digitized triaxial apparatus for testing soils and soft rocks. **Geotechnical Engineering Journal** 28 (2) : 183-207.
- Shibuya, S. and Tamrakar, S. B. (2003). Engineering properties of Bangkok clay. In Tan, T. S. et al. (eds.), **Characterisation and Engineering Properties of Natural Soils**, 645-692. Singapore.
- Shirley, D. J. and Hampton, L. D. (1978). Shear-wave measurements in laboratory sediments. **Journal of the Acoustical Society of America** 63 (2) : 607-613.
- Smith, S. W. (1999). **The Scientist and Engineer's Guide to Digital Signal Processing**. 2nd edition. San Diego: California Technical Publishing.
- Stokoe, II, K. H. and Woods, R. D. (1972). In situ shear wave velocity by cross-hole method. **Journal of Soil Mechanics and Foundations Division**, ASCE, 98 (5) : 443-460.
- Sully, J. P. and Campanella, R. G. (1995). Evaluation of in situ anisotropy from crosshole and downhole shear wave velocity measurements. **Geotechnique** 45 (2) : 267-282.
- Sun, J. I., Golesorkhi, R. and Seed, H. B. (1988). **Dynamic moduli and damping ratios for cohesive soils**. Report No. EERC-88/15. Earthquake Engineering Research Center, University of California at Berkeley.
- Tanaka, H., Tanaka, M. and Iguchi, H. (1994). Shear modulus of soft clay measured by various kinds of test. In Shibuya, S. et al. (eds.), **Pre-failure deformation of geomaterials**, 235-240. Sapporo: Balkema.
- Tamrakar, S. B. (2001). **Design parameters for elasto-plastic FE analysis of soft clay ground**. D. Eng. thesis, Research Group of Geo-environmental Engineering, Graduate School of Engineering, Hokkaido University.
- Tatsuoka, F., Kohata, Y., Mizumoto, K., Kim, Y. S., Ochi, K. and Shi, D. (1993). Measuring small strain stiffness of soft rocks. In Anagnostopoulos (eds), **Geotechnical Engineering of Hard Soils-Soft Rocks**, 809-816. Athens : Balkema.

- Tatsuoka, F. and Shibuya, S. (1991). Deformation characteristics of soils and rocks from field and laboratory tests. **Proceedings of the 9th Asian Regional Conference on Soil Mechanics and Foundation Engineering**, 101-177. Bangkok.
- Teachavorasinskun, S. and Akkarakun, T. (2004). Paths of elastic shear modulus of clays. **Geotechnique** 54 (5) : 331-333.
- Teachavorasinskun, S. and Amornwithayalax, T. (2002). Elastic shear modulus of Bangkok clay during undrained triaxial compression. **Geotechnique** 52 (7) : 537-540.
- Timoshenko, S. P. and Goodier, J. N. (1970). **Theory of elasticity**. 3rd edition. New York : McGraw-Hill.
- Towhata, I. and Ishihara, K. (1985). Undrained strength of sand undergoing cyclic rotation of principal stress axes. **Soils and Foundations** 25 (2) : 135-147.
- Viggiani, G. and Atkinson, J. H. (1995). Interpretation of bender element tests. **Geotechnique** 45 (1) : 149-154.
- Vucetic, M. and Dobry, R. (1991). Effect of soil plasticity on cyclic response. **Geotechnical Engineering Journal** 117 (1) : 89-107.
- White, J. E. (1965). **Seismic waves: radiation, transmission and attenuation**. New York: McGraw-Hill, Inc.
- Wroth, C. P. (1975). In situ measurement of initial stresses and deformation characteristics. **Proc. Geot. Engng Div. Specialty Conf. on In Situ Measurement of Soil Properties**, ASCE, 181-230. North Carolina State University.
- Zeng, X. and Grolewski, B. (2005). Measurement of G_{max} and estimation of K_0 of saturated clay using bender elements in an oedometer. **Geotechnical Testing Journal** 28 (3) : 264-274.
- Zeng, X. and Ni, B. (1999). Stress-induced anisotropic G_{max} of sands and its measurement. **Journal of Geotechnical and Geoenvironmental Engineering**, ASCE, 125 (9) : 741-749.



APPENDICES

สถาบันวิทยบริการ
จุฬาลงกรณ์มหาวิทยาลัย

APPENDIX A

BENDER ELEMENT PREPARATION



1. Solder and lead solder are used in the connection process.



2. Soldering paste.

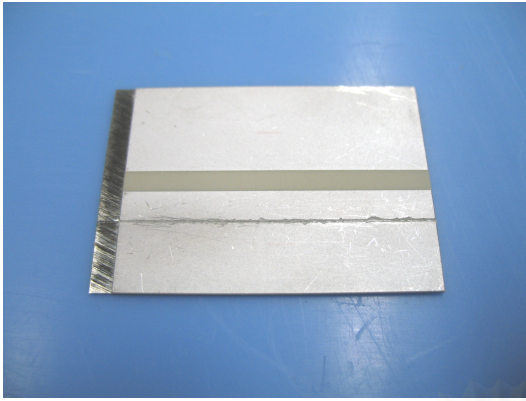


3. Digital multimeter is used to check short circuit after cutting the BE and connection process.

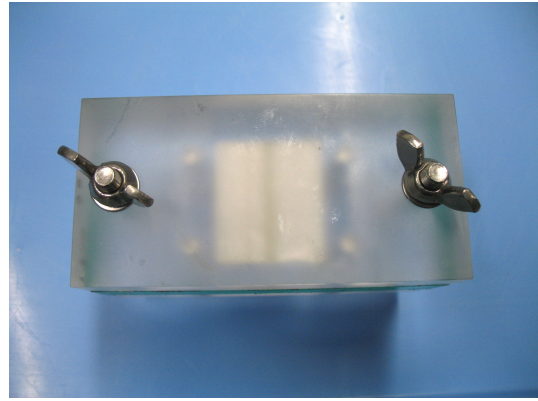


4. Epoxy.

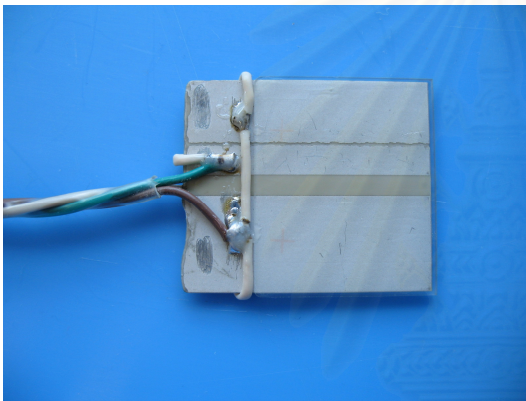
Figure A.1 Equipment and material used for preparing a waterproof BE transducer.



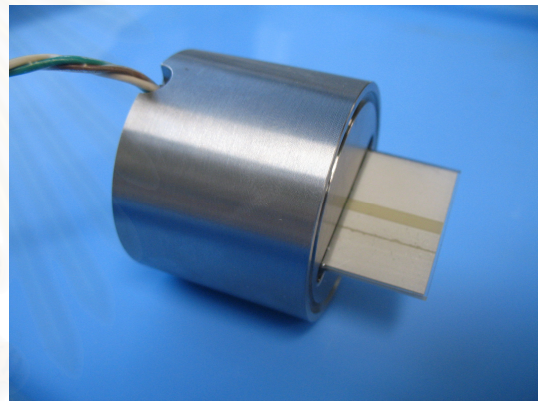
1. BE is cut on both sides of the electrode surfaces to provide a self-monitoring circuit.



2. BE is placed in a mould and coated using epoxy. 10 mm of the length is uncoated.



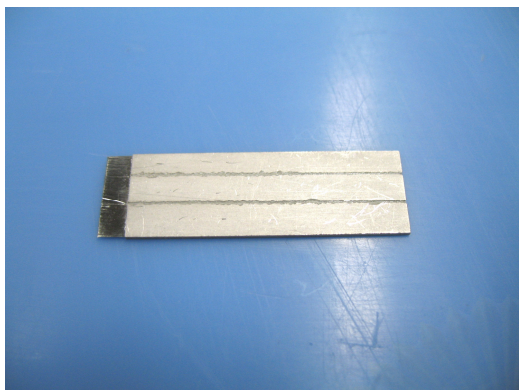
3. After coating, cables are connected to the BE.



4. BE completed with coating and cables is fixed at the top cap by using epoxy.

สถาบันวิทยบริการ
จุฬาลงกรณ์มหาวิทยาลัย

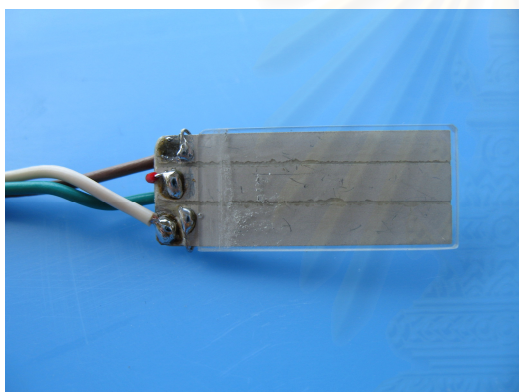
Figure A.2 Preparation of transmitter BE at the top cap.



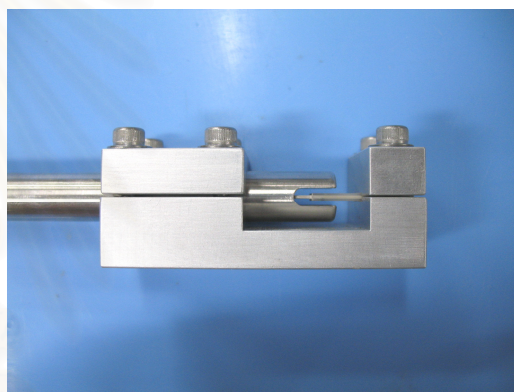
1. BE is cut on both sides of the electrode surfaces to provide a self-monitoring circuit.



2. BE is placed in a mould and coated using epoxy. 5 mm of the length is uncoated.



3. After coating, cables are connected to the BE.



4. BE completed with coating and cables is fixed at the penetration rod by using epoxy. The process is done by utilising a guide apparatus to make sure that the BE is well aligned.



5. Receiver BE installation completed.

Figure A.3 Preparation of receiver BE at the penetration rod.

APPENDIX B

TESTING EQUIPMENT

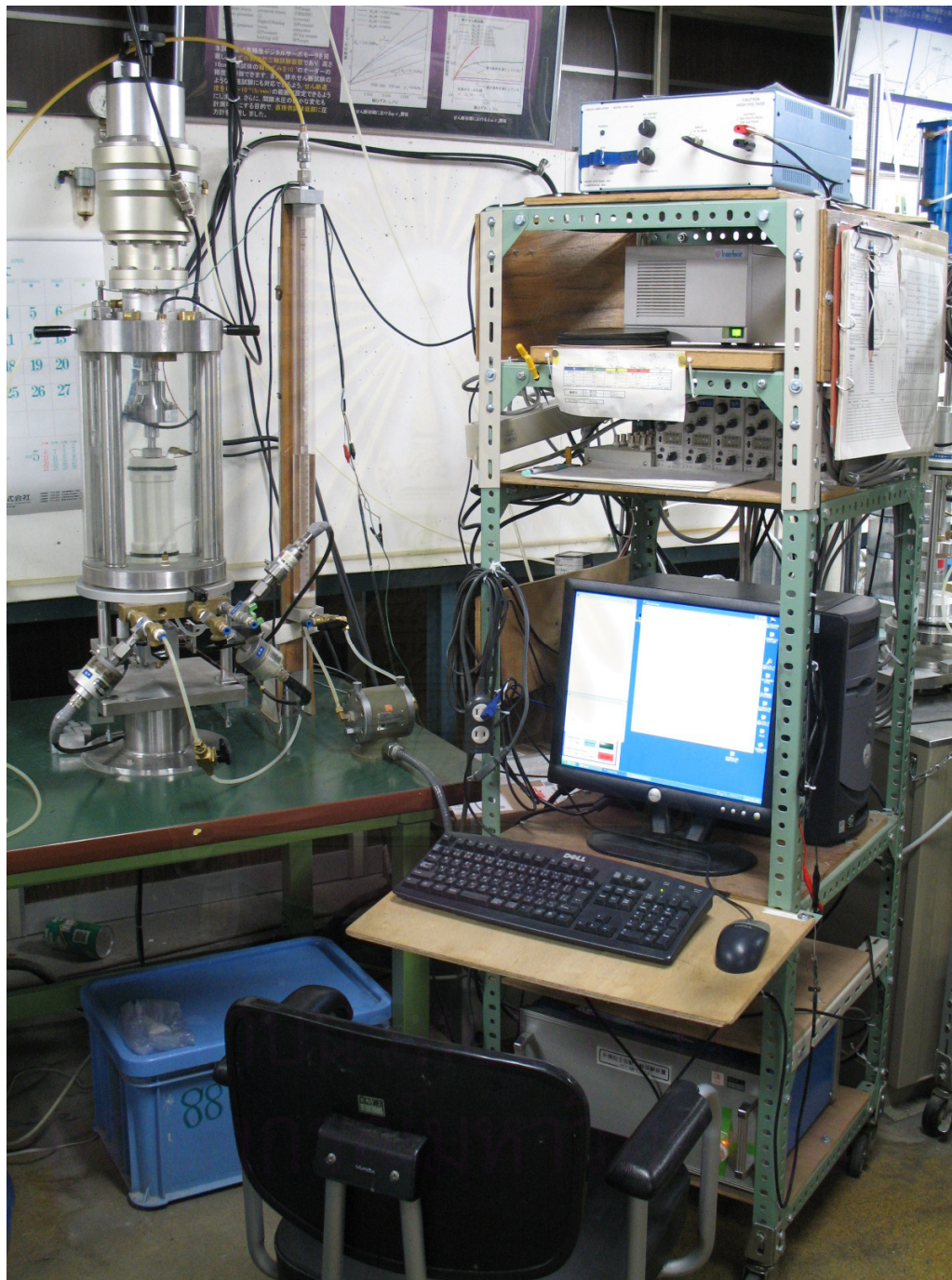


Figure B.1 Testing equipment.

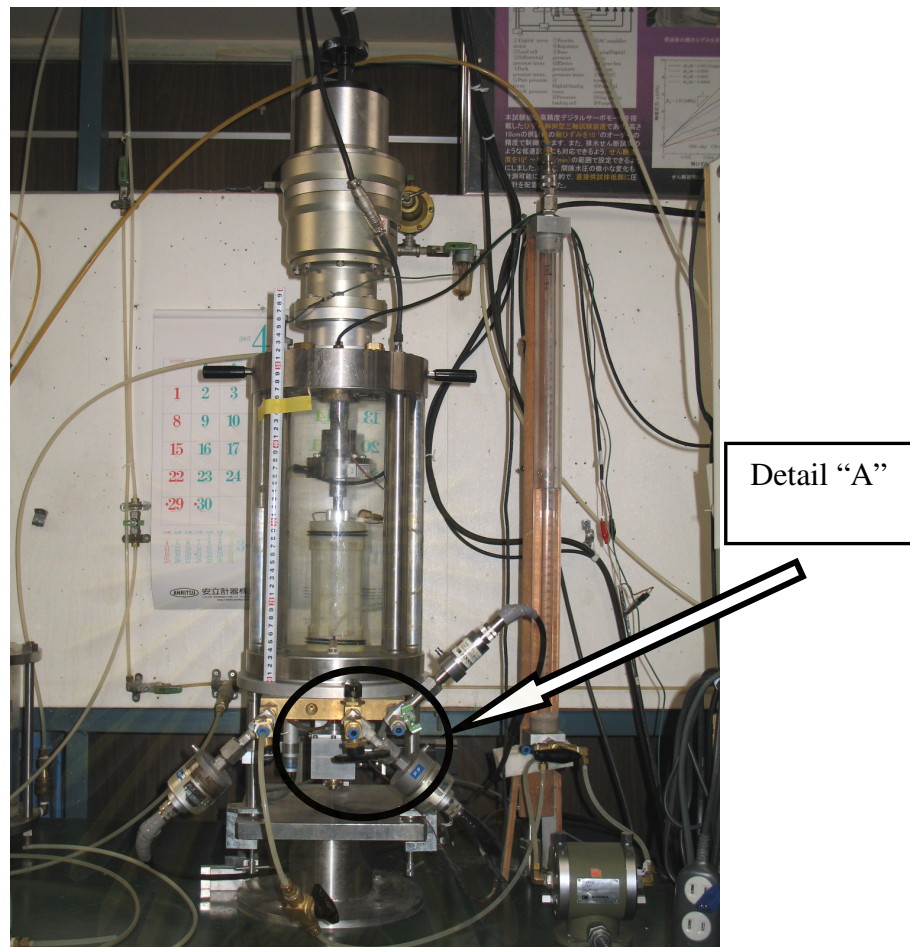


Figure B.2 Modified triaxial apparatus.

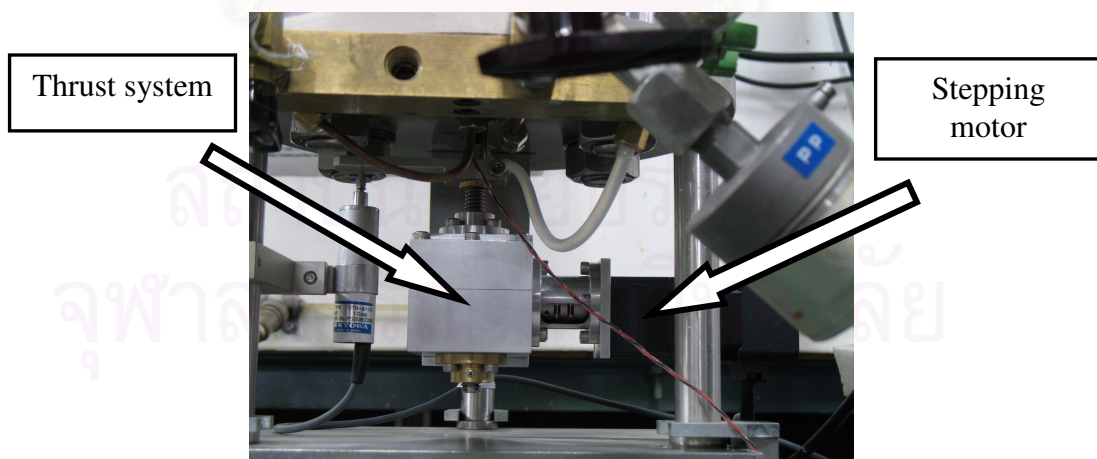


Figure B.3 Detail "A" - Thrust system completed with stepping motor.

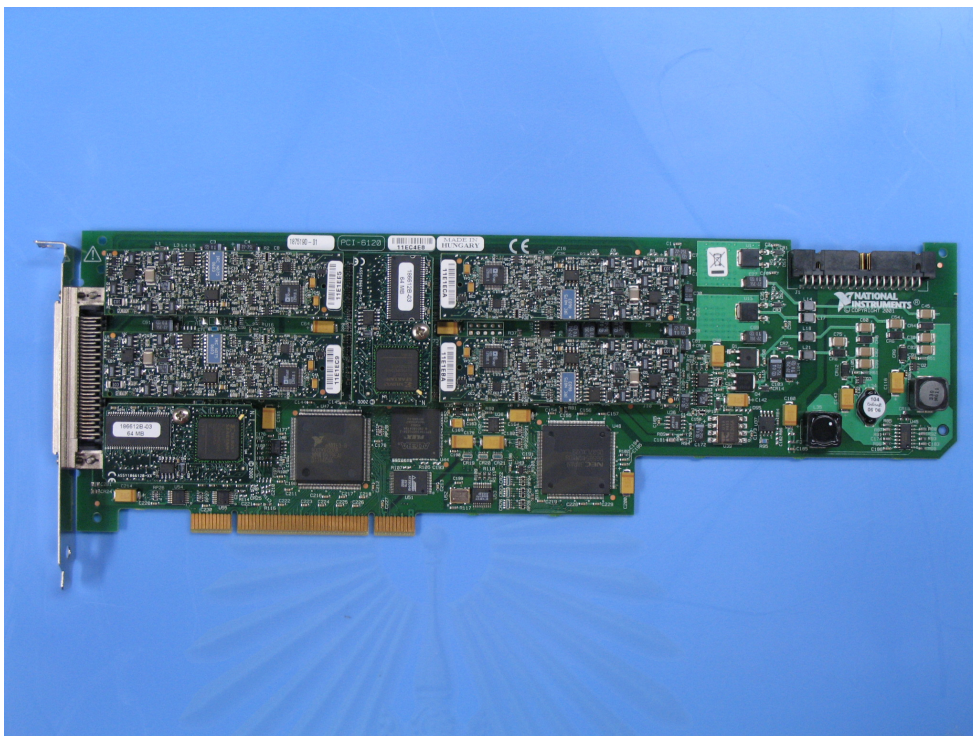


Figure B.4 National Instruments NI 6120 card.



Figure B.5 Connection cable and box.

APPENDIX C

CONSOLIDATION AND SWELLING TESTS RESULTS

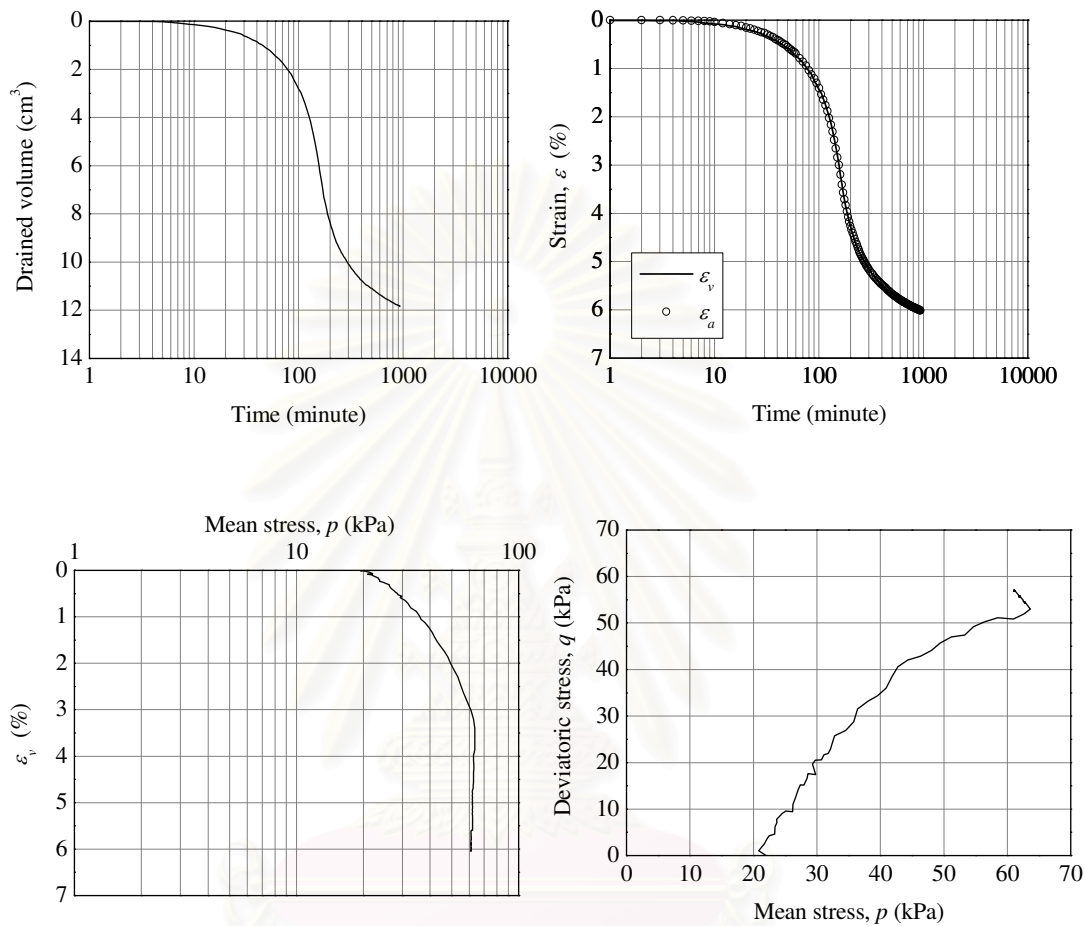


Figure C.1 Results of consolidation test for (Kasaoka 1) sample.

สถาบันวิทยบริการ
จุฬาลงกรณ์มหาวิทยาลัย

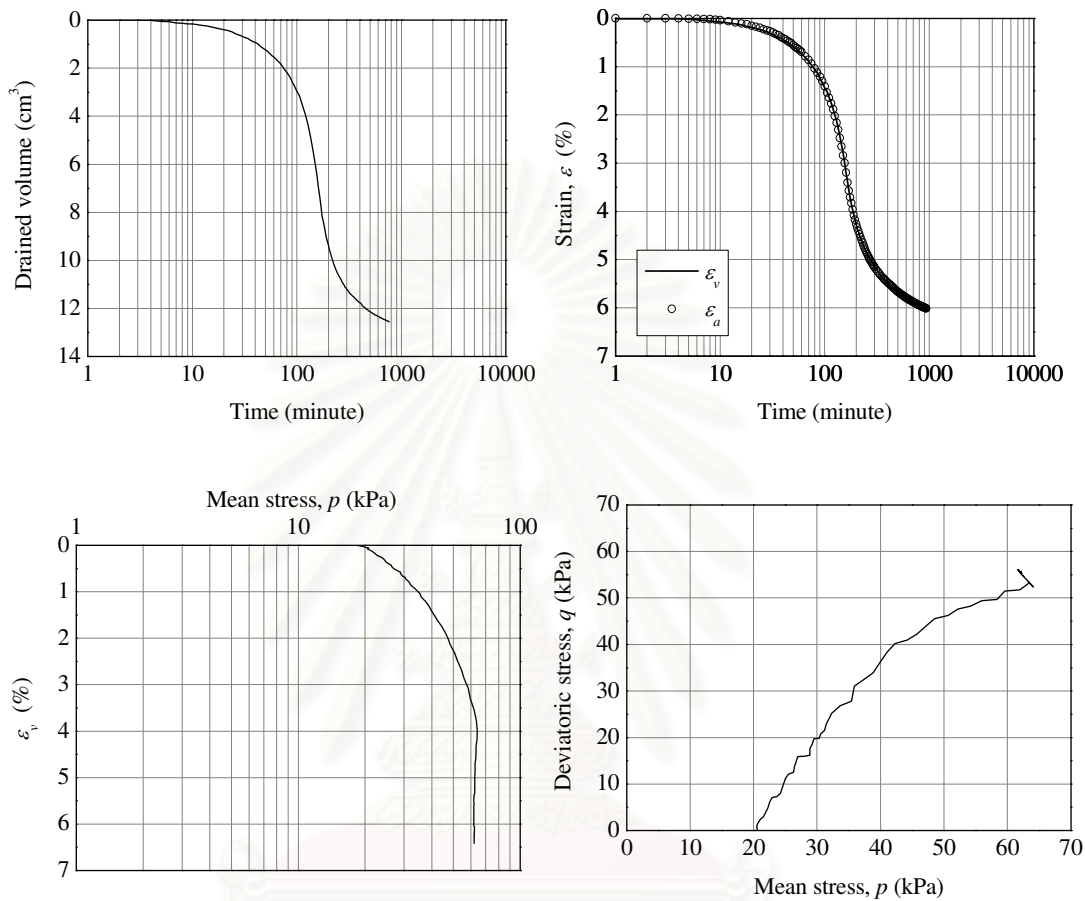


Figure C.2 Results of consolidation test for (Kasaoka 2) sample.

สถาบันวิทยบริการ
จุฬาลงกรณ์มหาวิทยาลัย

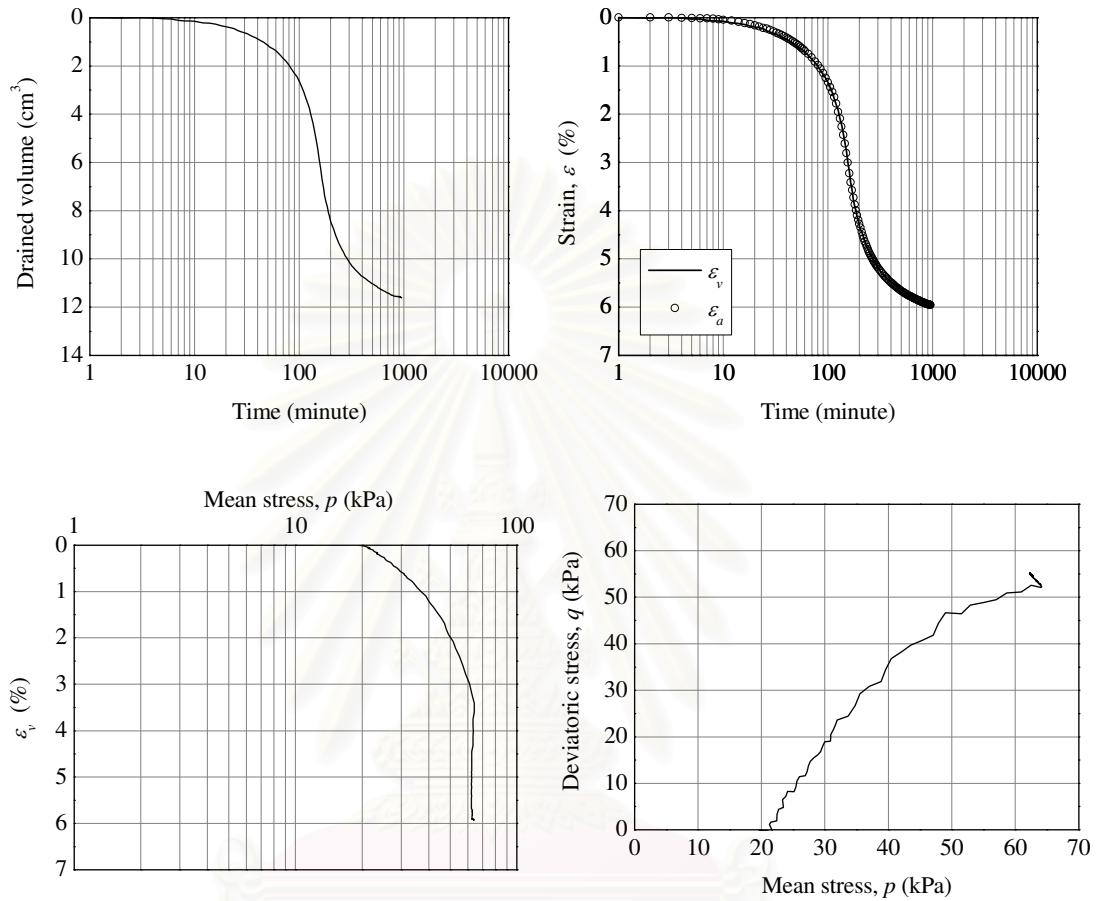


Figure C.3 Results of consolidation test for (Kasaoka 3) sample.

สถาบันวิทยบริการ
จุฬาลงกรณ์มหาวิทยาลัย

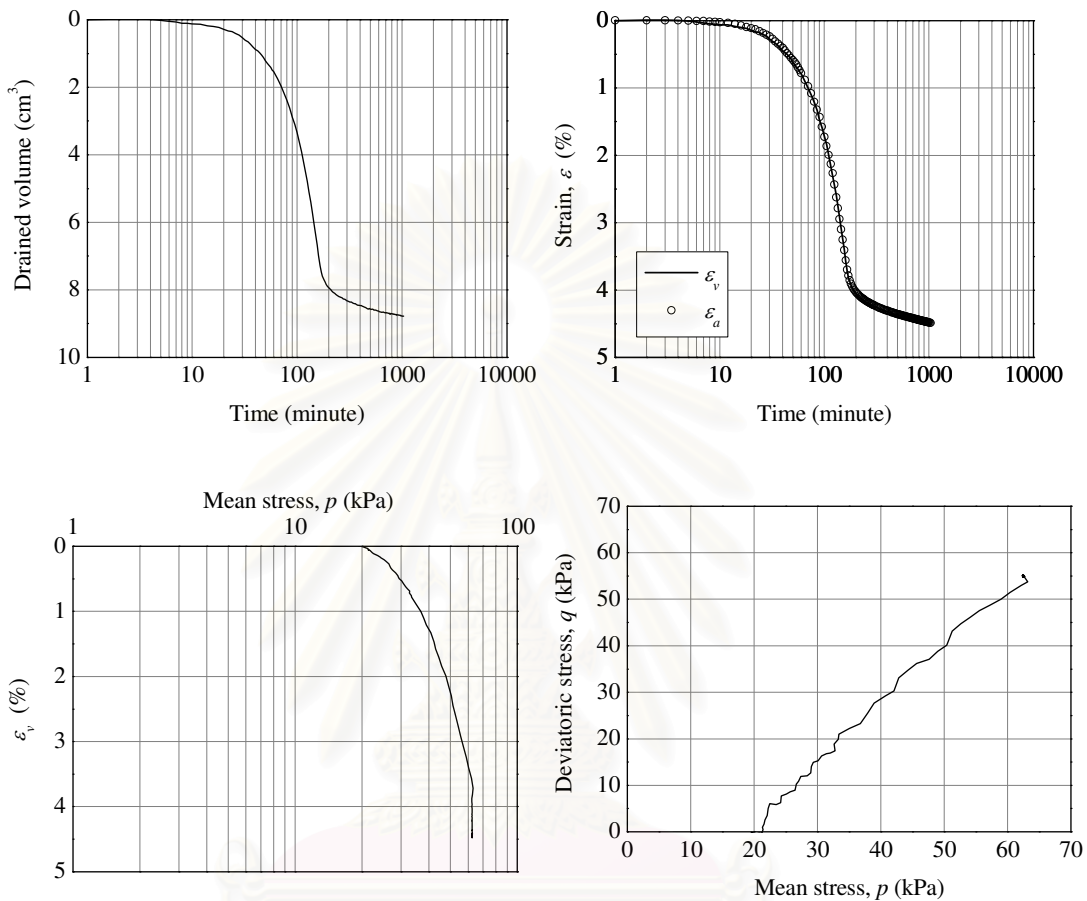


Figure C.4 Results of consolidation test for Fujinomori sample.

สถาบันวิทยบริการ
จุฬาลงกรณ์มหาวิทยาลัย

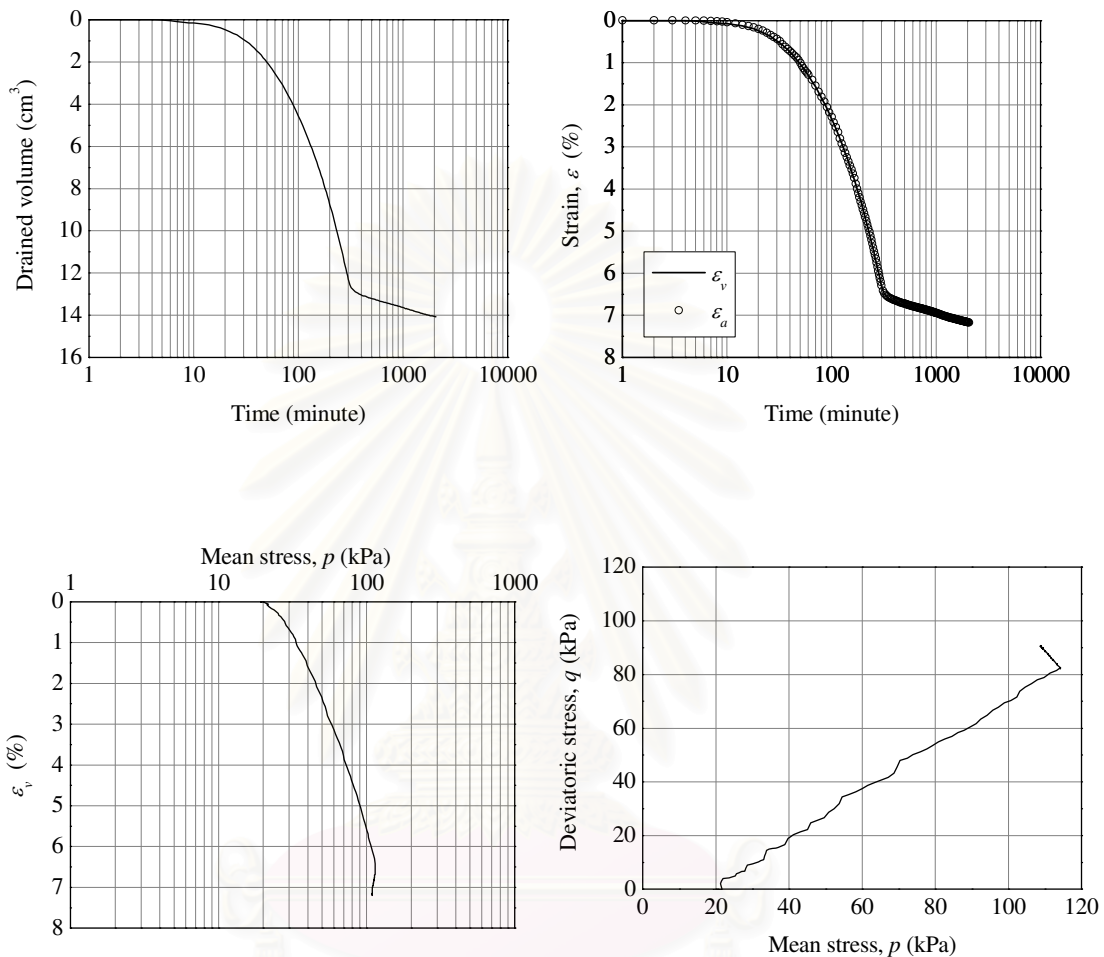


Figure C.5 Results of consolidation test for NSF sample.

สถาบันวิทยบริการ
จุฬาลงกรณ์มหาวิทยาลัย

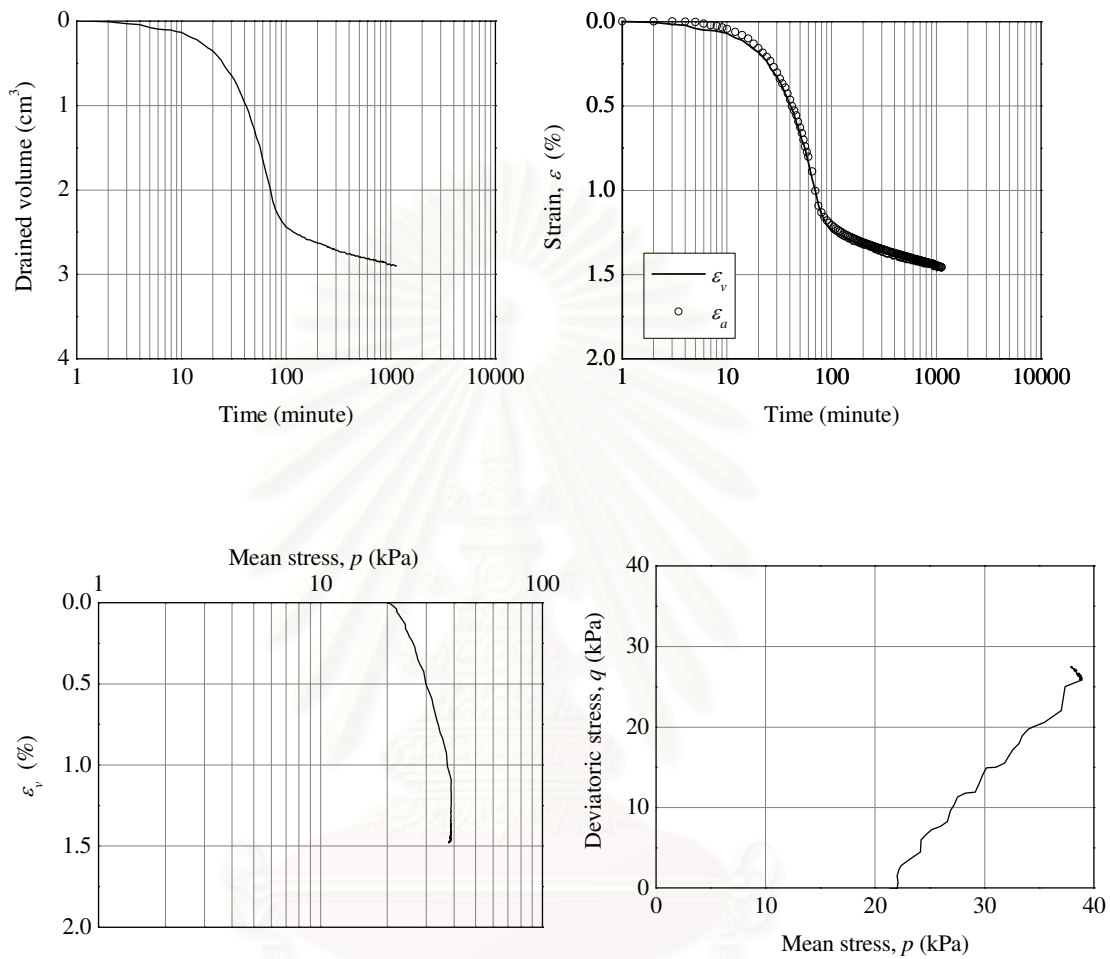


Figure C.6 Results of consolidation test for Mihara sample.

สถาบันวิทยบริการ
จุฬาลงกรณ์มหาวิทยาลัย

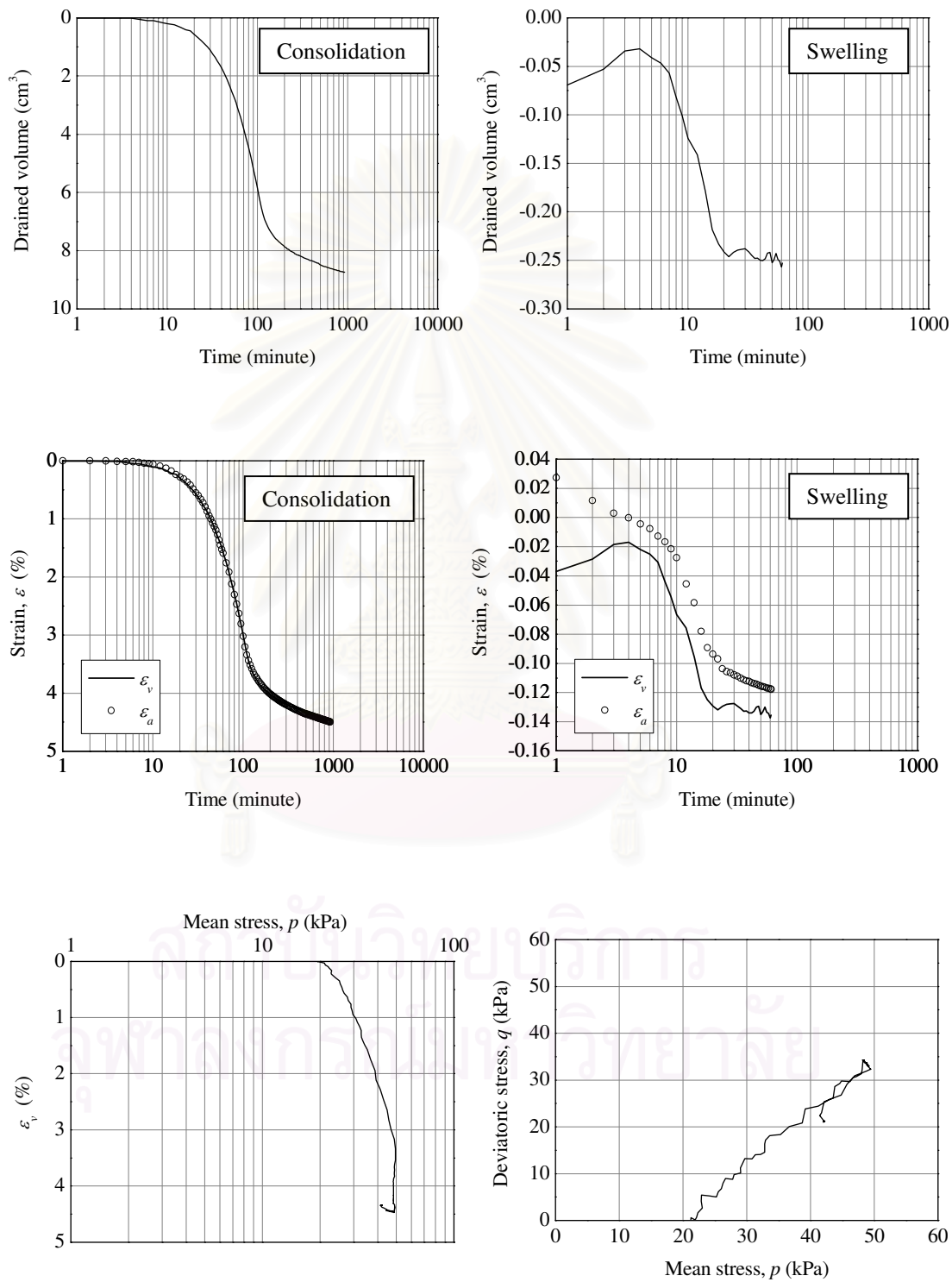


Figure C.7 Results of consolidation and swelling tests for (Bangkok 6) sample.

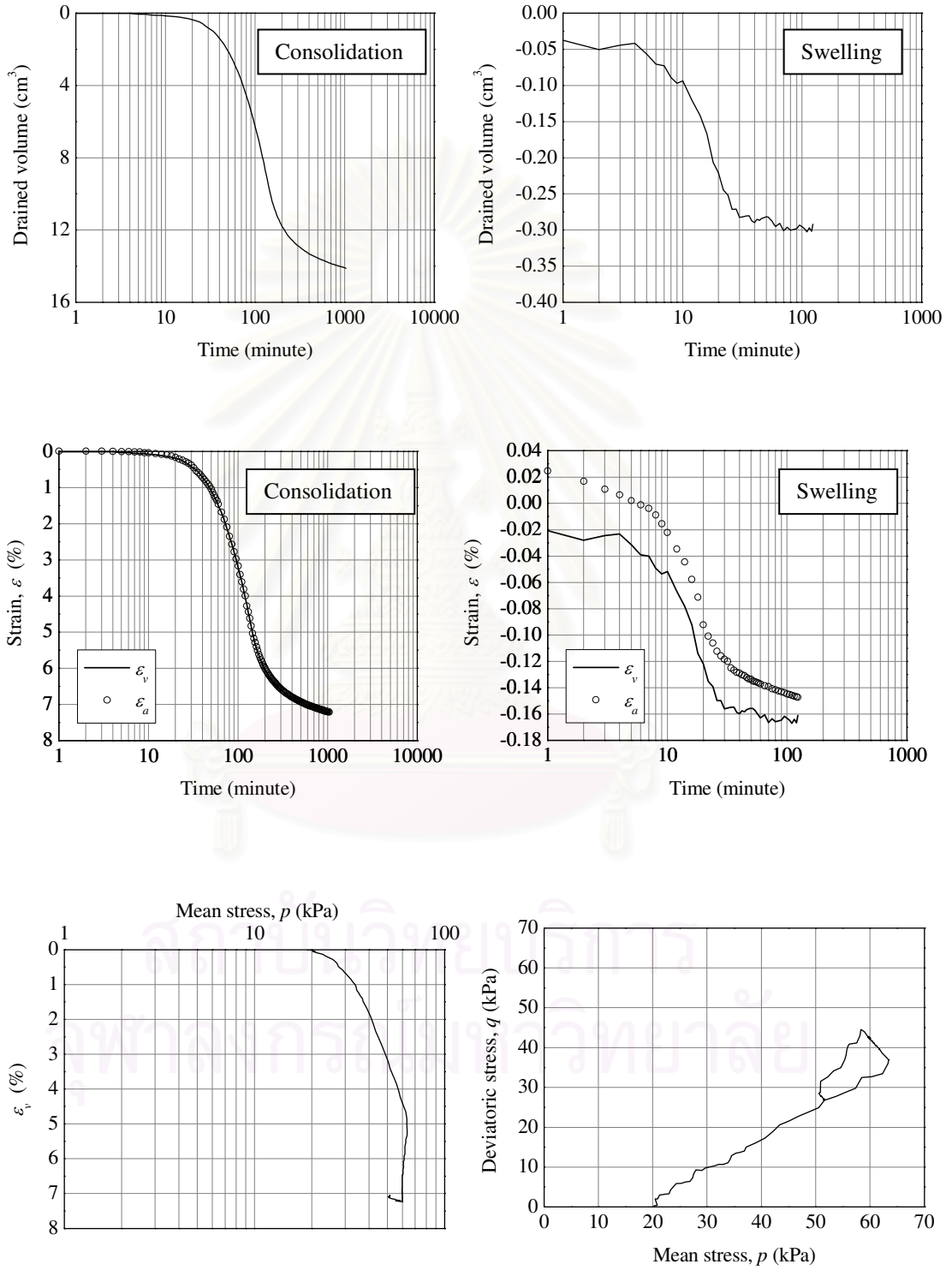


Figure C.8 Results of consolidation and swelling tests for (Bangkok 8) sample.

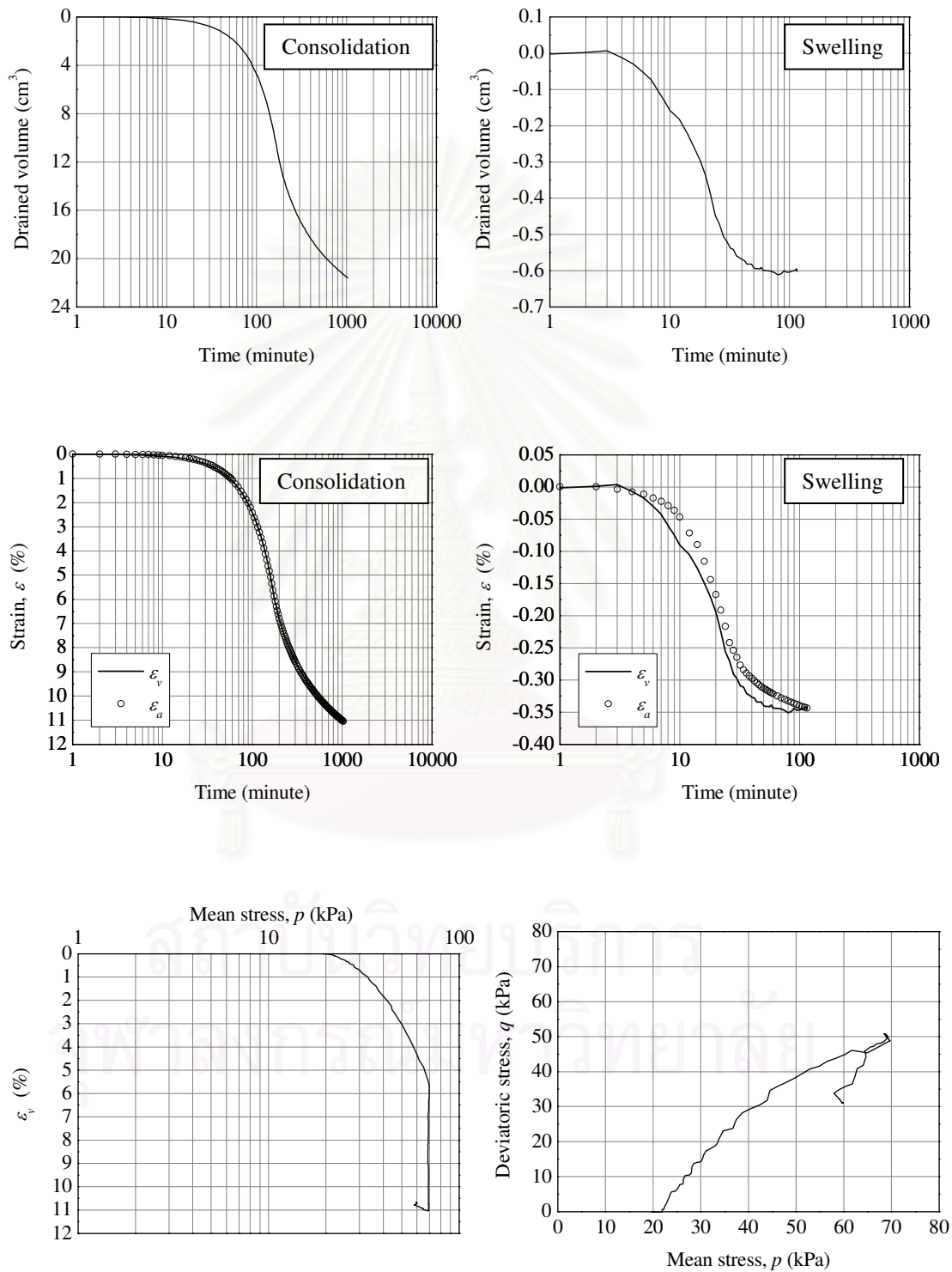


Figure C.9 Results of consolidation and swelling tests for (Bangkok 10) sample.

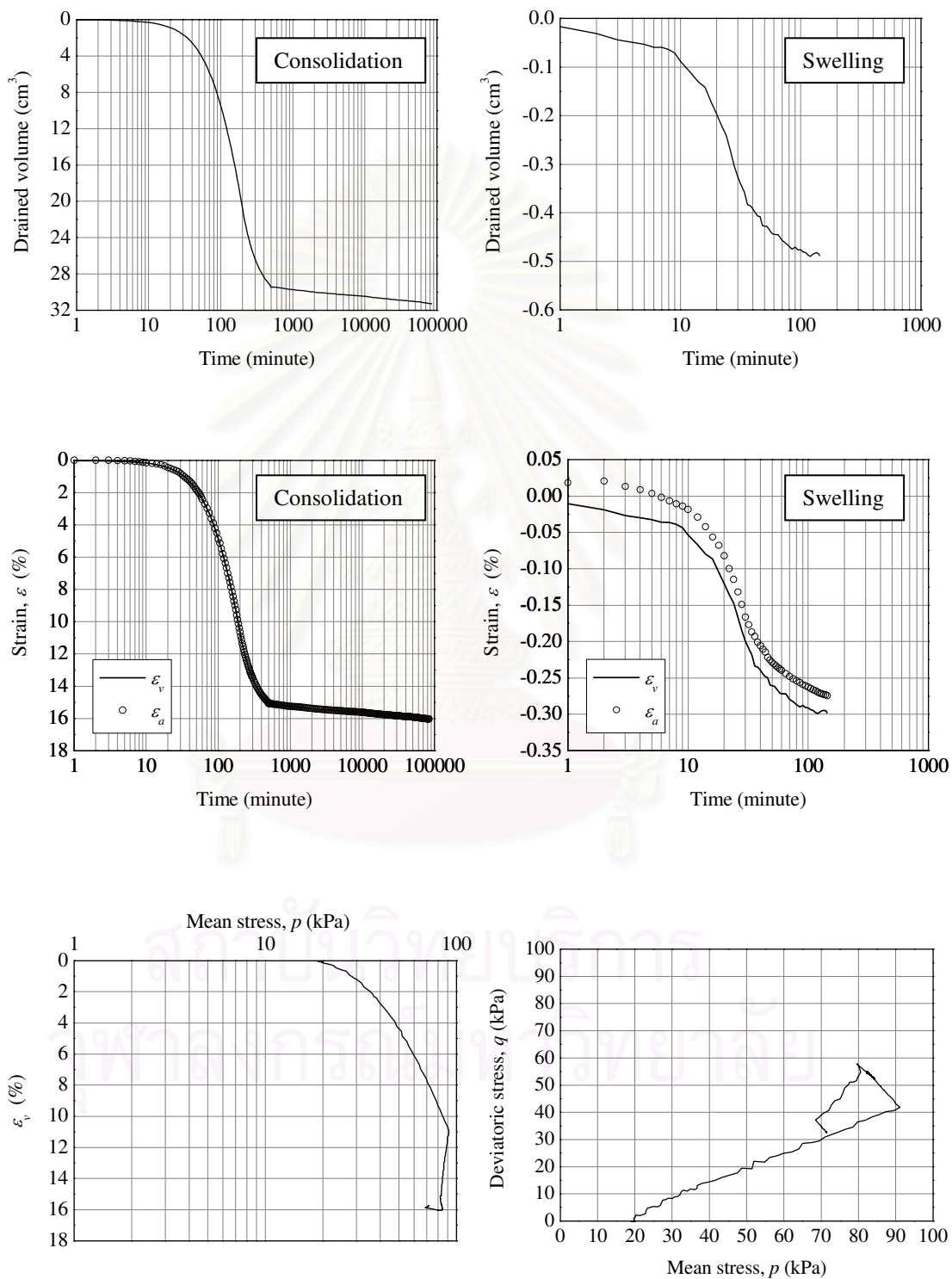


Figure C.10 Results of consolidation and swelling tests for (Bangkok 12) sample.

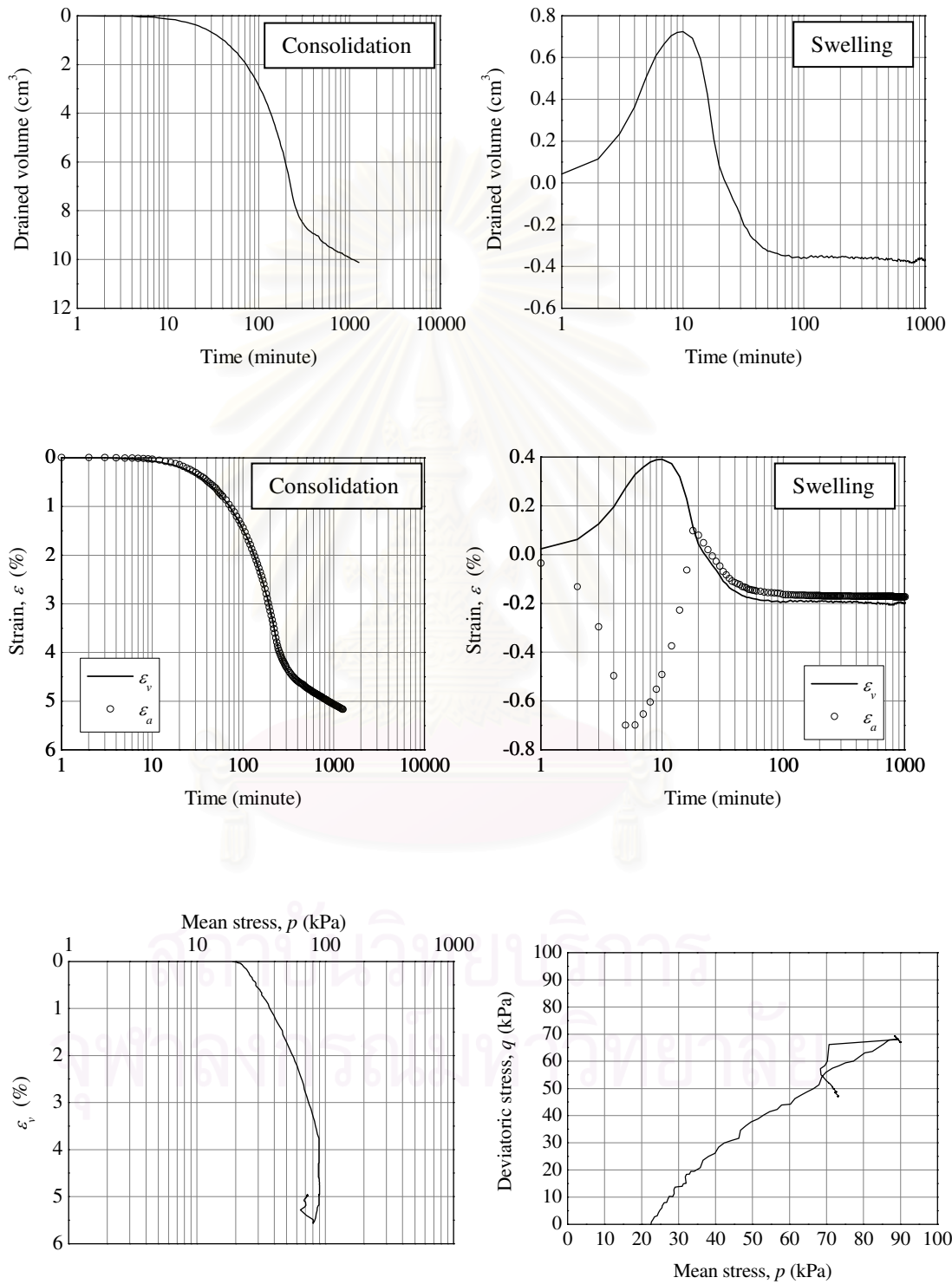


Figure C.11 Results of consolidation and swelling tests for (Bangkok 14(1)) sample.

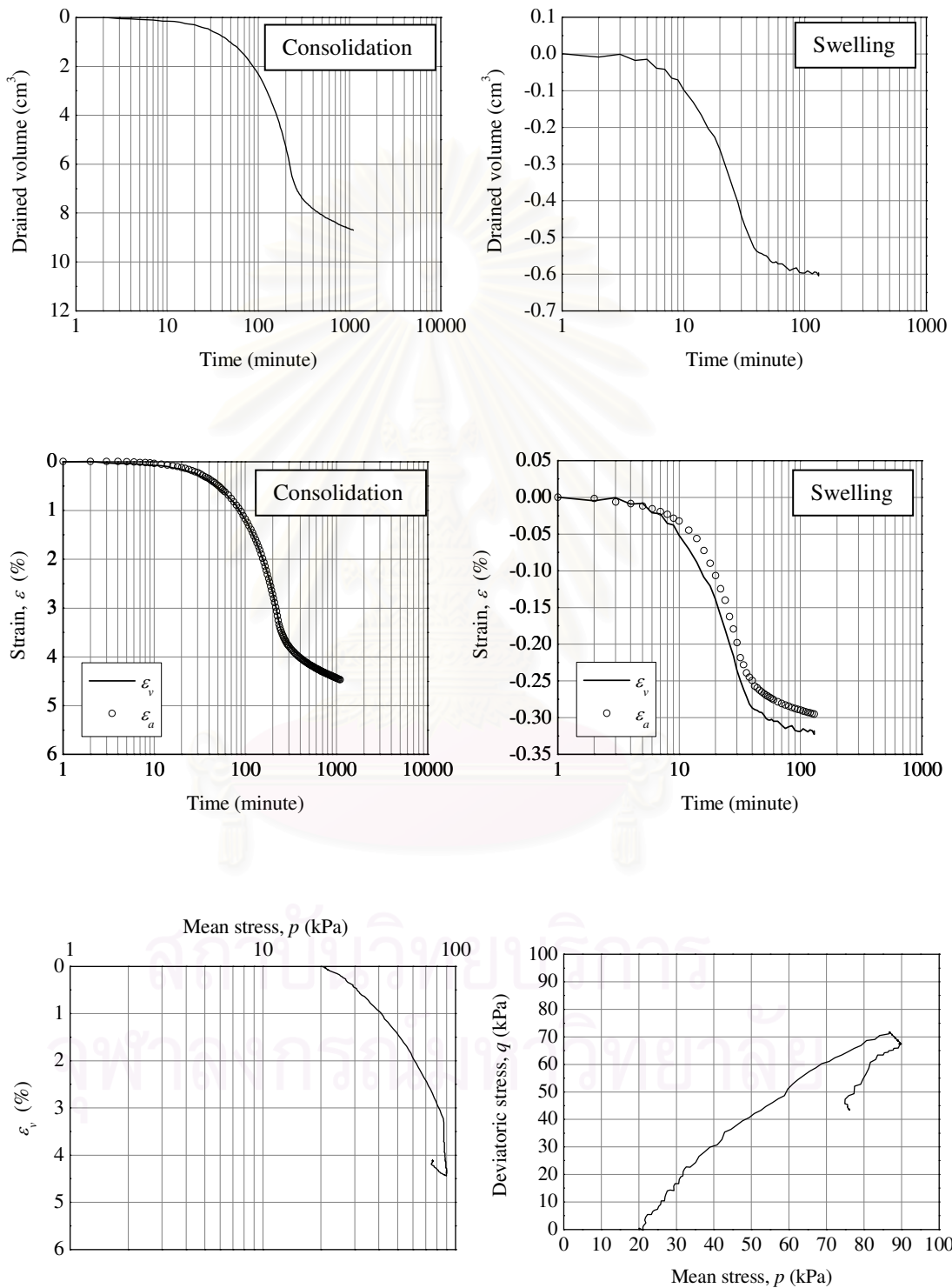


Figure C.12 Results of consolidation and swelling tests for (Bangkok 14(2)) sample.

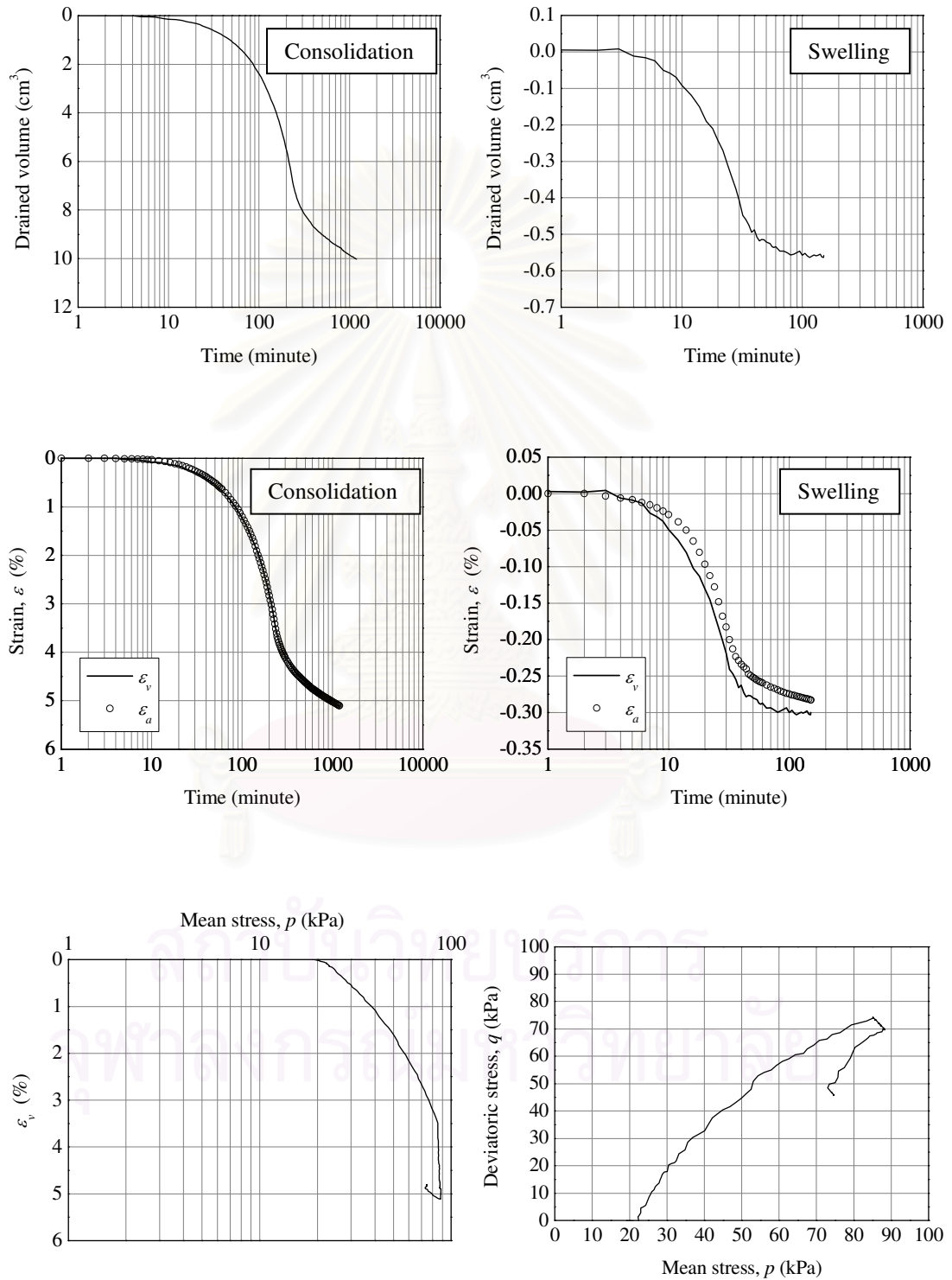


Figure C.13 Results of consolidation and swelling tests for (Bangkok 14(3)) sample.

APPENDIX D

STRESS PATH AND STRESS STRAIN CURVES

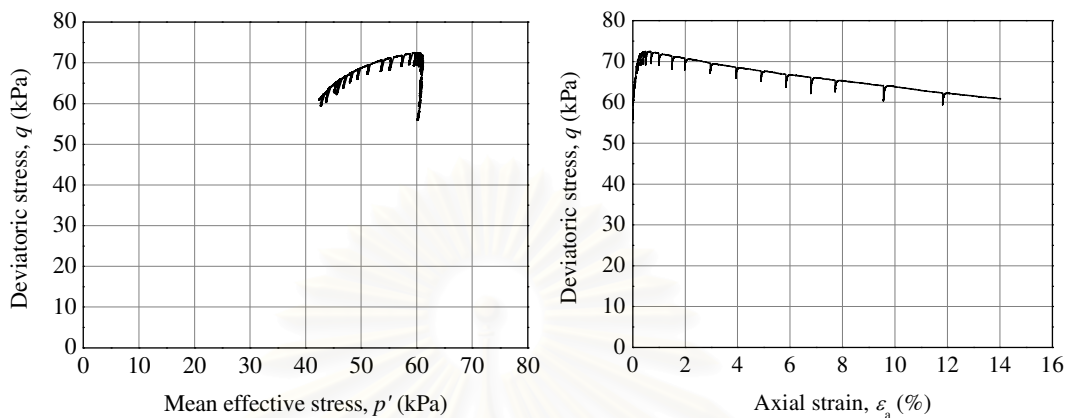


Figure D.1 Stress path and stress strain curves for (Kasaoka 1) sample.

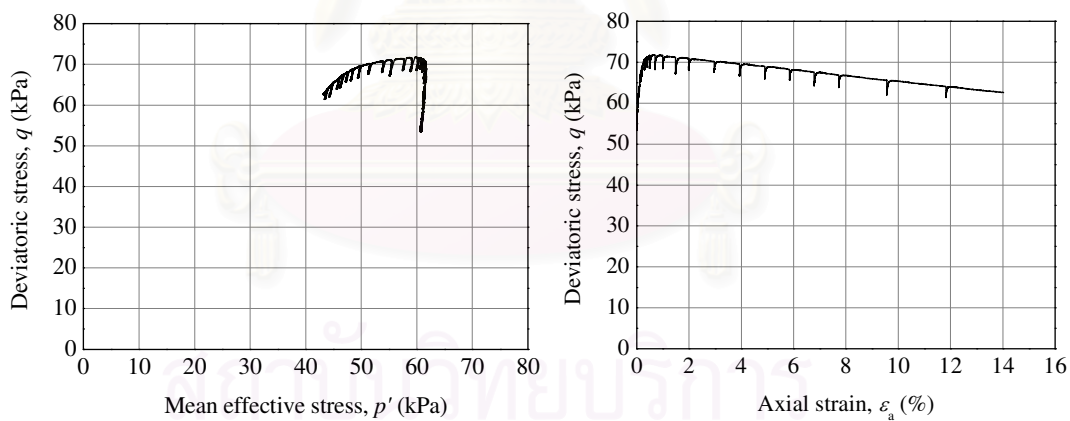


Figure D.2 Stress path and stress strain curves for (Kasaoka 2) sample.

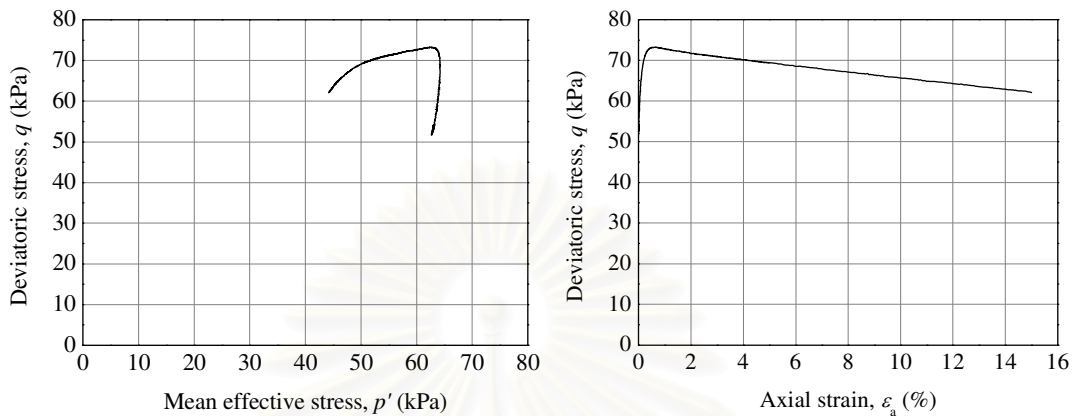


Figure D.3 Stress path and stress strain curves for (Kasaoka 3) sample.

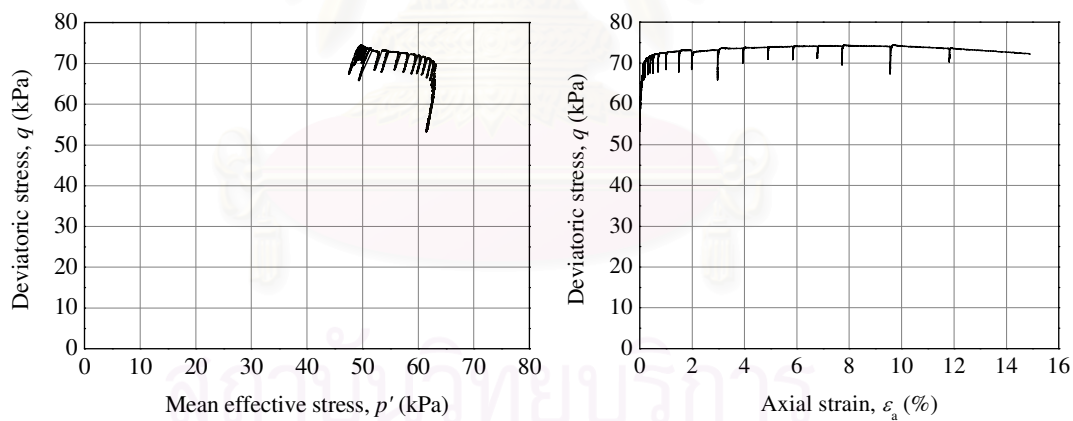


Figure D.4 Stress path and stress strain curves for Fujinomori sample.

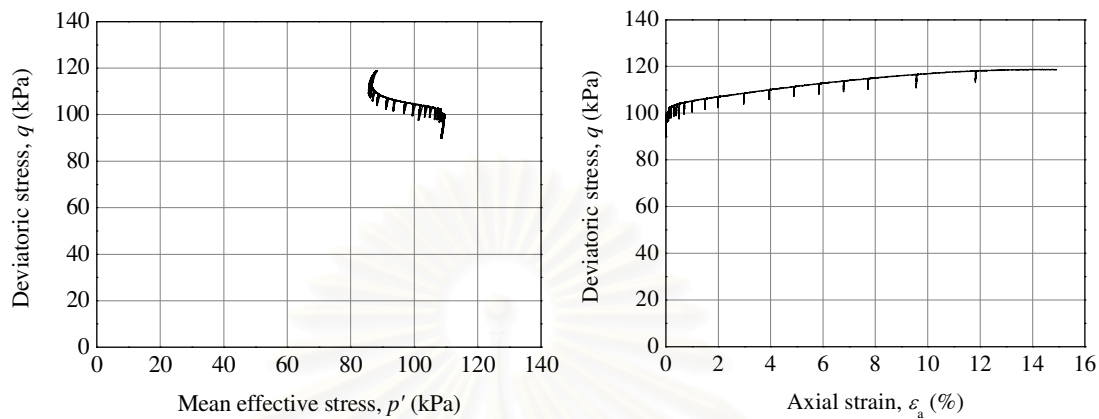


Figure D.5 Stress path and stress strain curves for NSF sample.

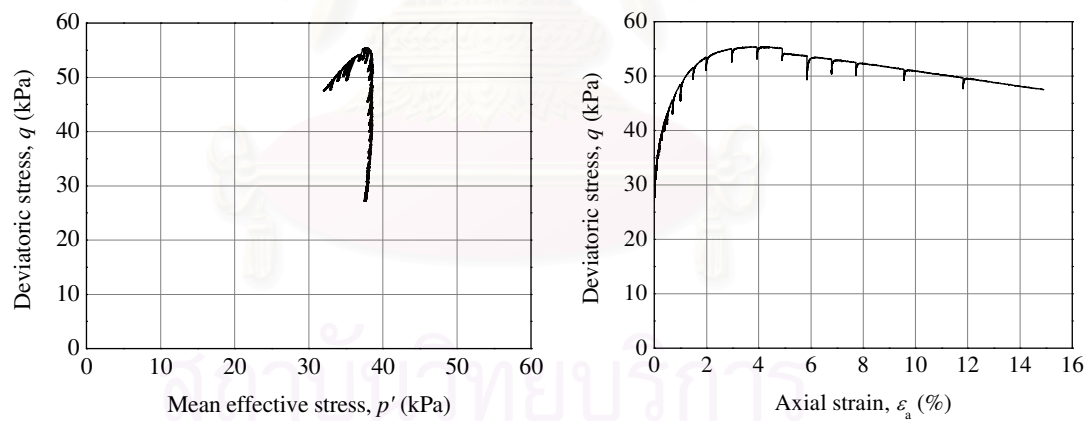


Figure D.6 Stress path and stress strain curves for Mihara sample.

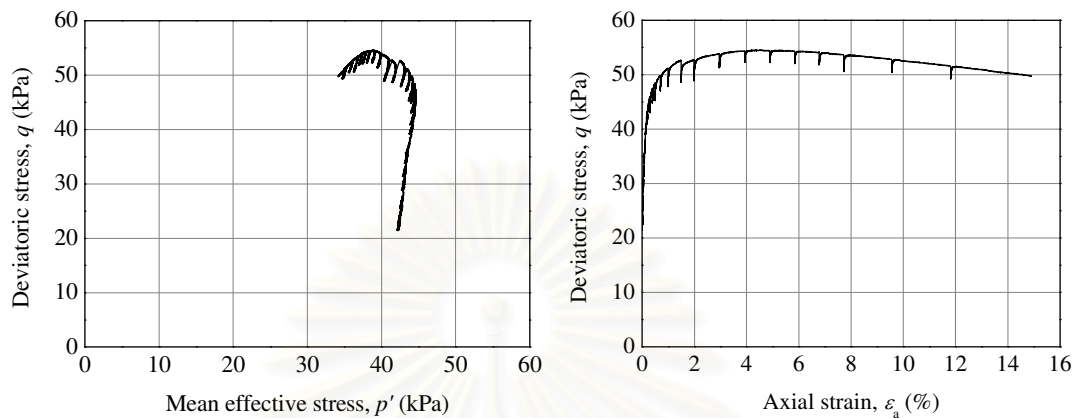


Figure D.7 Stress path and stress strain curves for (Bangkok 6) sample.

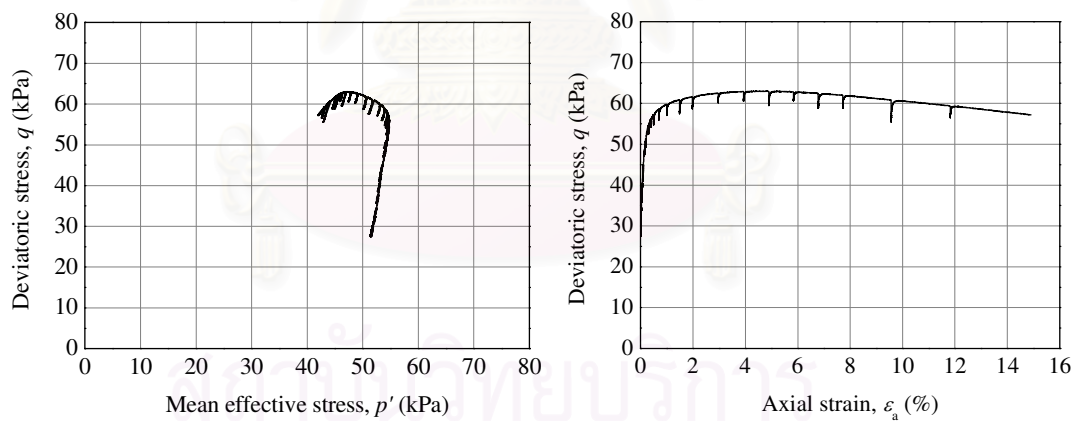


Figure D.8 Stress path and stress strain curves for (Bangkok 8) sample.

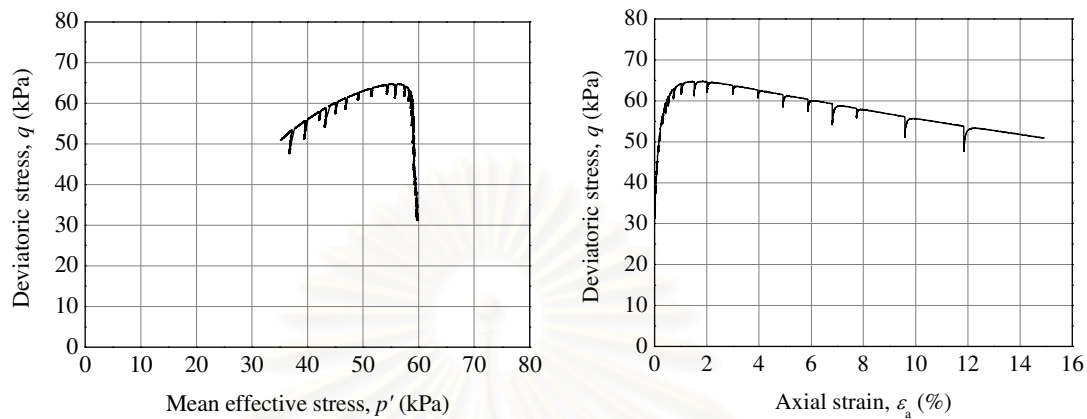


Figure D.9 Stress path and stress strain curves for (Bangkok 10) sample.

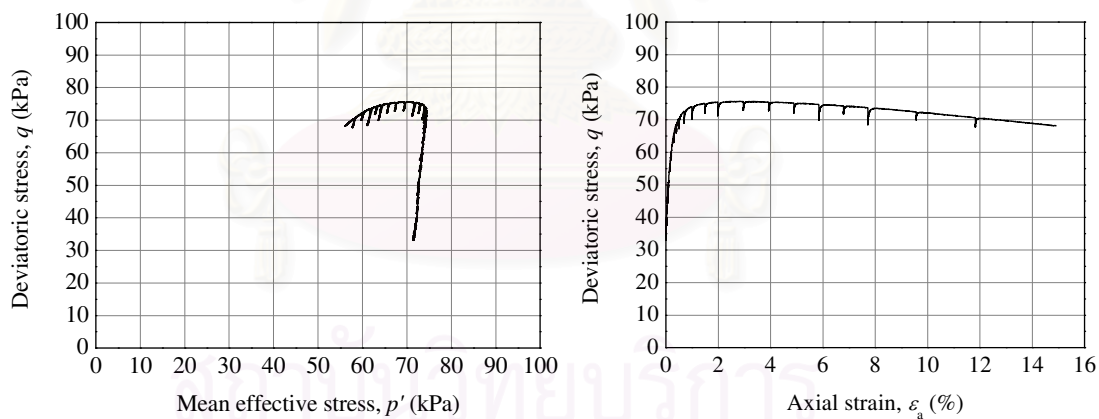


Figure D.10 Stress path and stress strain curves for (Bangkok 12) sample.

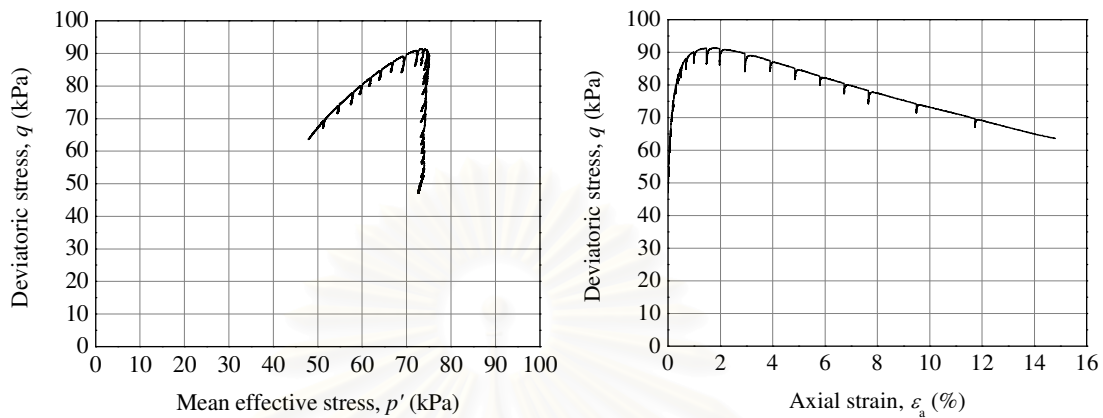


Figure D.11 Stress path and stress strain curves for (Bangkok 14(1)) sample.

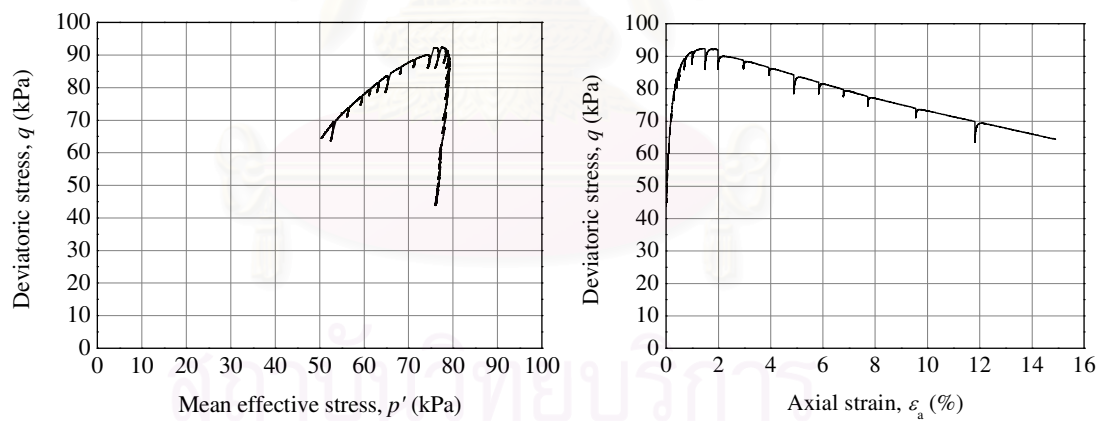


Figure D.12 Stress path and stress strain curves for (Bangkok 14(2)) sample.

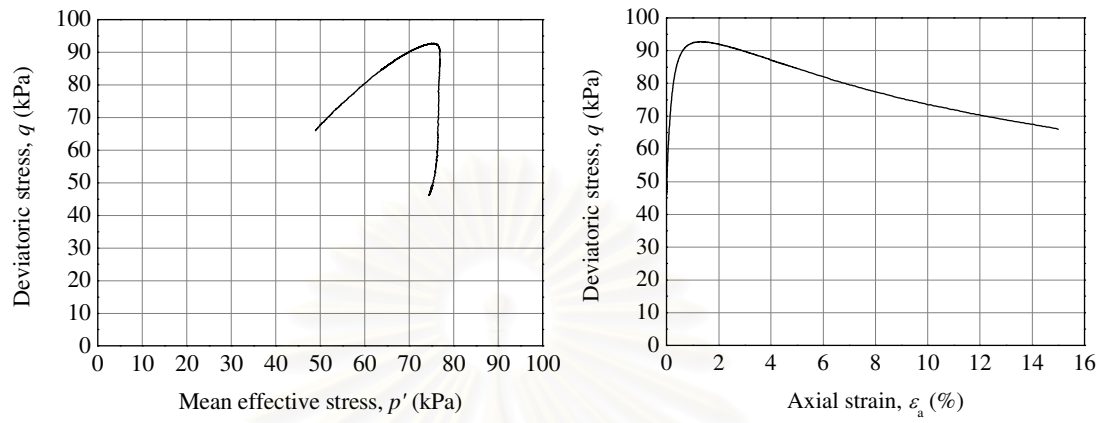


Figure D.13 Stress path and stress strain curves for (Bangkok 14(3)) sample.

สถาบันวิทยบริการ
จุฬาลงกรณ์มหาวิทยาลัย

BIOGRAPHY

Mr. Kok-Hooi Chan was born in Teluk Intan, Perak, Malaysia on 24th May 1977. He attained his Bachelor of Engineering (Honours) in Civil Engineering from the University Science of Malaysia in 2000. Then he furthered his study to earn a Master of Science in Geotechnic Engineering from the same university in 2001. In May 2001, he started working as a design engineer in Geotechnical and Dam Division at SMHB Consulting Engineers. After having worked for 17 months at this consulting firm, he moved on to work for a bridge contractor firm as a project engineer for 21 months. As a project engineer, he managed and supervised the construction of balance cantilever box girder bridge. In the year 2005, he applied for a scholarship to ASEAN University Network / Southeast Asia Engineering Education Development Network (AUN/SEED-Net JICA) to study a PhD sandwich programme at the Department of Civil Engineering, Chulalongkorn University. His advisor and co-advisor were Associate Professor Tirawat Boonyatee (Chulalongkorn University) and Professor Toshiyuki Mitachi (Hokkaido University), respectively. His main research theme was to determine the strain dependency of shear modulus of soft clays by using bender element. He also received a research grant from the 90th Years Anniversary of Chulalongkorn University (Ratchadphiseksomphot Endowment Fund) for his research study. During his doctoral study, he was also a teaching assistant of the Department of Civil Engineering and researcher of the Center of Excellence in Earthquake Engineering and Vibration. He also spent 11 months of his PhD sandwich program in soil mechanic laboratory at Hokkaido University as a researcher. He has already submitted 1, 2 and 1 papers to The Eighteenth, Nineteenth and Twentieth KKCNN Symposia on Civil Engineering, respectively. His paper submitted to Soils and Foundations journal was accepted for publication.